# MODELING GRASSLAND PRODUCTIVITY THROUGH REMOTE SENSING PRODUCTS

A Thesis Submitted to the College of

Graduate Studies and Research

in Partial Fulfillment of the Requirements

for the Degree of Doctor of Philosophy

in the Department of Geography

University of Saskatchewan

Saskatoon

By

YUHONG HE

Keywords: mixed grassland, ecosystem modeling, remote sensing data, spatially distributed productivity

PERMISSION TO USE

In presenting this thesis in partial fulfillment of the requirements for a Postgraduate degree from the University of Saskatchewan, I agree that the Libraries of the University may make it freely available for inspection. I further agree that permission for copying of this thesis in any manner, in whole or in part, for scholarly purposes may be granted by the professors who supervised my thesis work or, in their absence, by the Head of the Department or the Dean of the College in which my thesis work was completed. It is understood that any copying or publication of use of this thesis or parts thereof for financial gain shall not be allowed without my written permission. It is also understood that due recognition shall be given to me and to the University of Saskatchewan in any scholarly use which may be made of any material in my thesis.

Requests for permission to copy or to make any other use of the material in this thesis in whole or in part should be addressed to:

Head of the Department of Geography

University of Saskatchewan

Saskatoon, Saskatchewan, S7N 5A5, Canada

ABSTRACT

Mixed grasslands in south Canada serve a variety of economic, environmental and ecological purposes. Numerical modeling has become a major method used to identify potential grassland ecosystem responses to environment changes and human activities. In recent years, the focus has been on process models because of their high accuracy and ability to describe the interactions among different environmental components and the ecological processes. At present, two commonly-used process models (CENTURY and BIOME-BGC) have significantly improved our understanding of the possible consequences and responses of terrestrial ecosystems under different environmental conditions. However, problems with these models include only using site-based parameters and adopting different assumptions on interactions between plant, environmental conditions and human activities in simulating such complex phenomenon. In light of this shortfall, the overall objective of this research is to integrate remote sensing products into ecosystem process model in order to simulate productivity for the mixed grassland ecosystem in the landscape level. Data used includes 4-years of field measurements and diverse satellite data (System Pour l'Observation de la Terre (SPOT) 4 and 5, Landsat TM and ETM, Advanced Very High Resolution Radiometer (AVHRR) imagery).

Using wavelet analyses, the study first detects that the dominant spatial scale is controlled by topography and thus determines that 20-30 m is the optimum resolution to capture the vegetation spatial variation for the study area. Second, the performance of the RDVI (Renormalized Difference Vegetation Index), ATSAVI (Adjusted Transformed Soil-Adjusted Vegetation Index), and MCARI2 (Modified Chlorophyll Absorption Ratio Index 2) are slightly better than the other VIs in the groups of ratio-based, soil-line-related, and chlorophyll-corrected VIs, respectively. By incorporating CAI (Cellulose Absorption Index) as a litter factor in ATSAVI, a new VI is

developed (L-ATSAVI) and it improves LAI estimation capability by about 10%. Third, vegetation maps are derived from a SPOT 4 image based on the significant relationship between LAI and ATSAVI to aid spatial modeling. Fourth, object-oriented classifier is determined as the best approach, providing ecosystem models with an accurate land cover map. Fifth, the phenology parameters are identified for the study area using 22-year AVHRR data, providing the input variables for spatial modeling. Finally, the performance of popular ecosystem models in simulating grassland vegetation productivity is evaluated using site-based field data, AVHRR NDVI data, and climate data. A new model frame, which integrates remote sensing data with site-based BIOME-BGC model, is developed for the mixed grassland prairie. The developed remote sensing-based process model is able to simulate ecosystem processes at the landscape level and can simulate productivity distribution with 71% accuracy for 2005.

ACKNOWLEDGEMENTS

First and foremost, I would like to thank Dr. Xulin Guo for years of invaluable guidance, mentoring, and encouragement. She is a superior researcher, teacher, advisor, and friend, whose brilliant insights and generous support have constantly inspired me throughout my Ph.D. studies. Without her help, I could never have completed this dissertation. I am grateful to my committee members, Dr. Dirk de Boer, Dr. Steven Franklin, Dr. Bram Noble, and Bing Cheng Si, for their assistance and guidance and for devoting their valuable time to serve on my Ph.D. program. I would like to thank specially Dr. Bing Cheng Si, Dr. John Wilmshurst, Dr. Chunhua Zhang, and Dr. Huiping Xu, Dr. Youfei Zheng for their valuable advice and help in my research.

I wish to express my gratitude to Chunhua Zhang, Selena Black, Yunpei Lu, Robert Sissons, Mike Nilson, Jesse Nielsen, Doug Reed, Weidong Zhou, and Xiaoyong Xu for their essential help in collecting, processing, and interpreting field data. Many thanks go to my friends in the department and in Saskatoon for their help in my research as well as my life. I owe so much to many friends and I greatly appreciate the friendship of Selena Black, Angela Daigneault, Josi Hauschild, Rui Li, Yan Luo, Zhaoqin Li, Zimu Yu, and Yanan Xing. They are part of my life in Saskatoon when I am away from my family.

Finally I am deeply grateful to my parents, Haiyun Cheng and Shiping He and my three sisters, Ying, Yudan, and Lei. Without their love, support and encouragement, none of my achievements would have been possible. Special thanks are given to my husband, Xiaoyong Xu, for his unconditional support in countless aspects. He is the best blessing in my life.

TABLE OF CONTENTS

page

LIST OF TABLES

LIST OF FIGURES

Figure page

# CHAPTER 1 – INTRODUCTION

## 1.1 Research Background

One fifth of the Earth's land surface is grassland (Ojima et al., 1996; Parton et al., 1996). There are approximately 24 M ha of mixed grassland in south Canada serving a variety of economic, environmental and ecological purposes. In recent years, however, grassland degradation has become a worldwide problem due to intense human activities and climate change (Li and Ji, 2002) and the mixed grassland in south Canada is no exception (Mitchell and Csillag, 2001). Pressures from human impact and resource use, including soil erosion, fire management, as well as species extinction and invasion, emphasize the need to understand grassland ecology and ecosystem processes (Mitchell, 2003). This research concentrates on developing methods to assess and monitor spatial grassland productivity, in order to interpret how weather, land management (i.e. grazing), and landscape features influence grassland vegetation.

Due to the expense and the time-consuming nature of conventional ground-based monitoring, the model approach has become a major method in identifying potential ecosystem responses to environmental change and human activities. This is because models are able to synthesize information in a quantitative fashion (Rastetter, 1996) and can serve as an efficient and cost effective alternative to field experimentation. Further, models can provide a sound framework for planning changes in land use and management thereby anticipating and better

managing potentially adverse environmental impacts in the future. During the past 30 years several models have been developed to assess the impacts of climate change and human activities on grasslands (Campbell, et al., 1999; Huntchings and Gardon, 2001; Nouvellon et al., 2000). However, the choice of an appropriate model for the particular grassland system is not always obvious. Different input parameters of space and time can alter or mask processes of interest, and the assumptions used in the model development may not be applicable in all potential application areas of study (Mitchell and Csillag, 2001). Therefore the main purpose of this research is to develop a remote sensing data-based model frame, which will more effectively utilize physical and biological layers to simulate grassland ecosystem dynamics in south Canada. This raises a number of important questions concerning the current state in modeling grassland productivity, notably:

- What are the uncertainties of model processes and how do these uncertainties relate to model predictions?
- Which class of model developed in mixed grassland will improve predictive accuracy?
- What kinds of input parameters, which are required by current models, are more persuasive and more feasible for the mixed grassland?
- What lessons can be learned from current models to improve further model design?

The following review will survey current productivity models to further explore the above-mentioned questions. The purpose of the review is threefold: 1) identify the importance of grassland productivity, 2) briefly describe ecosystem process models and review their strengths and weaknesses; and 3) discuss the feasibility of remote sensing data-based process models.

### 1.1.1 Grassland Productivity

Globally, grasslands are important in the study of terrestrial ecosystems as they cover nearly 20% of the Earth's surface (Lieth, 1978), contain about 30% of global carbon stocks (Ojima et al., 1996; Parton et al., 1996), and store at least 10% of the global soil organic matter (SOM, Eswaran et al., 1993). Grasslands are also economically important, containing much of the worlds grazing capacity (Burke et al., 1989). The mixed grasslands of south Canada are a critical component of the global ecosystem as a pool of carbon dioxide and also a gene pool for wildlife and vegetation (Hall et al., 2000). In recent years, a number of researchers (e.g. Mitchell and Csillag, 2001; Peat, 1997) have focused their attention on Grassland National Park (GNP), located in the northern portion of the mixed prairie. This region represents the northern edge of the continental distribution of vegetation that uses the C4 photosynthetic pathway. It is important to determine relative affinities of C3 and C4 plants to expected climate and atmospheric changes in order to evaluate potential impacts on species distributions, and global carbon and nitrogen budgets (Peat, 1997). Such work helps answer questions about functional group dynamics in landscape level such as the North American Great Plains as a whole, as well as addressing important issues specific to regions experiencing changes in vegetation communities, such as GNP.

Human activities and climate variability influence the physical processes of the grassland ecosystem. Therefore the budget of energy, water, and carbon in grasslands is altered (Li and Ji, 2002). As a result, degradation and desertification of the grassland are very common phenomena, and mixed grasslands have frequently been associated with fluctuating, and unreliable productivity (Curll et al., 1985a, b; Evans et al., 1990; Orr et al., 1990; Fothergill et al., 2000; Laws and Newton, 1992; Schwinning and Parsons, 1996a, b). Therefore, it is pressing to study the processes of plant eco-physiology, land surface physics, and human disturbance by estimating grassland productivity.

Grassland productivity can be studied either through experiments, or by using ecological models. To date most experimental studies have mainly focused on the level of production. The effects of single management factors on short-term grassland performance have been well studied (e.g. Barthram et al., 1992; Curll et al., 1985a,b; Evans et al., 1990; Evans et al., 1992; Frame, 1990; Grant et al., 1985; Gilliland, 1996; Nassiri, 1998; Orr et al., 1990; Parsons et al., 1991a). Unfortunately, due to the expense and the time-consuming nature of conventional ground-based monitoring, both the duration and scale of these experiments are commonly limited to a maximum of 4 or 5 years and to community level, which results in difficulty in analyzing the stability of productivity (Mitchell and Csillag, 2001). Therefore, in field experiments the identification of the processes and interactions has been complicated by environmental variables (Schulte, 2003).

Grassland productivity has received considerable attention in theoretical ecological studies, in which the behavior of ecosystems is analyzed using mechanistic models. Recently, increasing computer capability has enabled the development of increasingly complex dynamic simulation models, in which pasture processes are simulated over time (e.g. Brereton and McGilloway, 1999; Grenfell, 1988; Parsons et al., 1991b; Schwinning and Parsons, 1996a,b; Thornley and Verberne, 1989; Thornley et al., 1995). These models can simulate numerous possible ecosystems in various hypothetical environments, thus allowing a mechanistic analysis of the processes regulating ecosystem stability.

### 1.1.2 Ecosystem Models

Ecosystem models offer a feasible approach to estimating grassland net primary productivity (NPP). Over the past 30 years, with the development of computational capacity, models proposed to calculate vegetation productivity are quite diverse. At one end of the

spectrum is the simple, remote sensing data-based model, which empirically derives the correlation of productivity with remote sensing products, such as light use efficiency (LUE) model (Montieth, 1972). At the other end of the spectrum is the process model, which simulates biochemistry property of ecosystem in detail, such as BIOME-BGC (Running and Hunt, 1993), CENTURY4.0 (Parton et al., 1993), and TEM4.0 (McGuire et al., 1995).

Each model approach is based on simplifying assumptions about the structure of an ecosystem, and how vegetation may respond to changes in the environment. Different models use different simplifying assumptions and different environmental variables, leading to different estimates of productivity (Cramer et al., 1999). Remote sensing data-based models have limitations in ecological processing and are hard to transfer from one ecosystem to another with different sets of climate conditions. Process models, the focus of this study, also referred to as physically based models, can describe a process based on well-understood and established concepts.

The utility of process ecosystem models for research has been recognized in the last decade, with BIOME-BGC and CENTURY being used for forest and grassland ecosystems, respectively. In this section, the commonly-used process models (CENTURY and BIOME-BGC), which have significantly improved our understanding of the possible consequences and responses of terrestrial ecosystems under different environmental conditions (Christopher et al., 1995; Cramer et al., 1999; Song and Woodcock, 2003), are briefly introduced and their development status and existing problems are analyzed.

#### 1.1.2.1 Brief Introduction of Process Models

The sources, features and main inputs and outputs of both process models are presented in Table 1.1. The models have the ability to simulate seasonal biogeochemical fluxes using

climate and soil information as driving input variables. Mechanistic relationships of these models are used to describe the fluxes of CO2, water, and nutrients between the different compartments of vegetation, soil, and atmosphere.

Table 1.1 The characteristics of the process models (Cramer, 1999)

| Item | | | Biome-BGC4.0 | CENTURY |
|---|---|---|---|---|
| **Source** | | Full name | Biome BioGeochemical Cycles model | |
| | | Host Institution | School of Forestry, University of Montana, Missoula, MT, USA | University of Colorado, Fort Collins, Colorado, USA |
| | | Key reference | Running & Hunt 1993 | Parton *et al.* 1993 |
| **Features** | | Spatial resolution of NPP | 0.5° x 0.5° | 0.5° x 0.5° |
| | | Temporal resolution of NPP | 1 day | 1 month |
| | | NPP calculated as: | GPP-RA | NPP |
| | | Influenced by | GPP = f(SRad, LAI, Temp, SW, VPD, CO 2, LeafN) | NPP = f(VegC, Dead, N, P,SW,Temp, Prec, PET, S) |
| | | | RA = f(VegC, Temp) | |
| | | No. of VEGC pools | 4 | 8 |
| **Input Variables** | Veg.Type | Map | P(me) | P(me) |
| | | Climate | | |
| | Soil | Type/texture | %text[FAO] | %text[FAO] |
| | | r.depth | F(veg) | |
| | | WHC | F(text) | F(text,veg) |
| | Elev. | | | X |
| | Atm. | $CO_2$ | 340 | 340 |
| | Climate | Mean T | | M[CL] |
| | | ΔT | M[CL] | |
| | | Precipitation | M[CL] | M[CL] |
| | | Humidity | | |
| | | Radiation | | M(λ,c(CL) |
| **Selected Outputs** | | | Biogeochemical fluxes (LAI) | Distribution Biogeochemical fluxes |

CENTURY is the pioneer mechanistic ecosystem model and arose from a background that explicitly considered soil carbon and nitrogen pool turnover rates over widely differing time-scales. CENTURY used a vegetation map (see Melillo et al., 1993) which was derived from

a number of sources (e.g. Matthews, 1983), to initialize structural and functional model parameters. BIOME-BGC derives several output variables by flux integration over the canopy. This model is fundamentally different from other models in three ways (Churkina, et al., 1995). First, the hydrological cycle is considered a key process and the BIOME-BGC model estimates the maximum sustainable LAI from water balance model-fluxes of water and CO2 and is mechanistically coupled through canopy conductance using the Penman-Monteith equation. Daily feedbacks between the water and carbon cycle drive estimated gross primary productivity (GPP), therefore canopy conductance (and hence, assimilation of photosynthates) could be controlled by changes in evapotranspiration. Second, the seasonality of canopy phenology is not climatically driven. Third, no production data are used to calibrate these models. The parameterization of processes is dependent on vegetation classes which distinguish plant functional types (e.g., evergreen vs. deciduous, broad-leaved vs. needle-leaved, C3 vs. C4) rather than the biome classes considered in other biogeochemical models.

#### 1.1.2.2 Model Application and Limitations

It has been claimed that both models can be used to examine the influence of climate change and/or doubled CO2 on NPP (Melillo et al., 1993). However, recent research depicts somewhat dissatisfying results. The grassland version of CENTURY was tested using observed data from 11 temperate and tropical grasslands around the world by Breymeyer (1996). It was found that 40% of aboveground plant productivity values which are simulated had errors of more than ±25% of the observed plant production (Parton, et al., 1996). The Vegetation-Ecosystem Modeling Analysis Project (VEMAP) compared the NPP estimates of the conterminous United States for contemporary climate and three climate change scenarios between CENTURY and Biome-BGC. Although both models estimated similar NPP for the conterminous United States

under contemporary conditions, the response of NPP to climate change varied between the models. Both models estimated increases in NPP with climate change and showed correlations among water use, nitrogen availability, and primary production, but the models simulated spatial variability in ecosystem processes in substantially different ways (VEMAP Members, 1995).

Considering the unsatisfactory modeling results, several gaps in these models are identified. First, though process models are based on current knowledge of major ecological/biophysical processes, they suffer from detailed parameters which are frequently not available, making the task of operating and validating process-models difficult. Second, these models have assumed homogeneity within the ecosystem, using lumped (averaged) parameters (Fitz, et al., 1996). Due to the inherent heterogeneity in natural systems, more recent research has emphasized the need for general ecological models that can be re-parameterized and applied to different ecosystems for distributed simulation (Band et al., 1991; Costanza et al., 1990; Costanza and Maxwell, 1991). Third, these models simply describe functional changes within particular vegetation types. They can not estimate changes in vegetation distribution as a result of climate change (Chutkins, 1995).

### 1.1.3 Feasibility of Using Remote Sensing Data in the Process Models

The above analysis of the limitations in process models demonstrates the importance of the quality and availability of input parameters (detail parameters, average parameters and vegetation distribution parameters). These parameters are crucial to the accuracy of the final productivity estimation. However, it is often very difficult to obtain such high-quality input parameters at the landscape level, due to the lack of fine-resolution observation data in space and time. With the development of remote sensing techniques, much information (e.g. LAI and land cover type) has been estimated with satellite data at various spatial and temporal resolutions

(Hansen et al., 2000; Loveland et al.,2000; Myneni et al., 1997b; Olson, 1994). It is also generally accepted that monitoring vegetation activity in the landscape level should be necessarily carried out with remote sensing techniques, as direct measurements are difficult in the mixed grassland due to its nature of high diversity and heterogeneity.

Originally, remote sensing data are mainly used in a LUE model to model productivity by determining the temporal behavior of the photosynthetically active tissue. Further, considering the gaps of the LUE model in ecological processing, some process models (e.g. BIOME-BGC) now use satellite data as well, but only for calibration or prescription of certain limited processes (Churkina et al., 1995). In recent years, an alternative approach (Mougin, 1995) has been taken into account. In this approach, the ecosystem process models not only use satellite data as input variables like LUE model, but integrate satellite data in an explicit formulation of the main processes. In this way, a close analysis of the relationships between different processes (photosynthesis, C transpiration, etc.) described by the process models and satellite data can be carried out. However, very few studies have used this alternative approach to simulate vegetation productivity for the mixed grassland.

### 1.1.4 Summary of Research Gaps

As a result (Figure 1.1), it is necessary to study grassland productivity. There are two types of models in the study of grassland ecosystem. The first is based on experimental research. Unfortunately, experimental models are limited because they are dependent on both internal system properties and environmental factors. The second type of model is based on theoretical ecological studies. They can analyze the underlying processes of grassland ecosystems in isolation of their environment. Nevertheless, their output must still be treated cautiously unless their complex input values can be obtained for the heterogeneous ecosystems. Some research has

used remote sensing products as input variables of ecosystem models. However, very few studies have determined the appropriate inputs and parameters for modeling vegetation productivity in the landscape level.

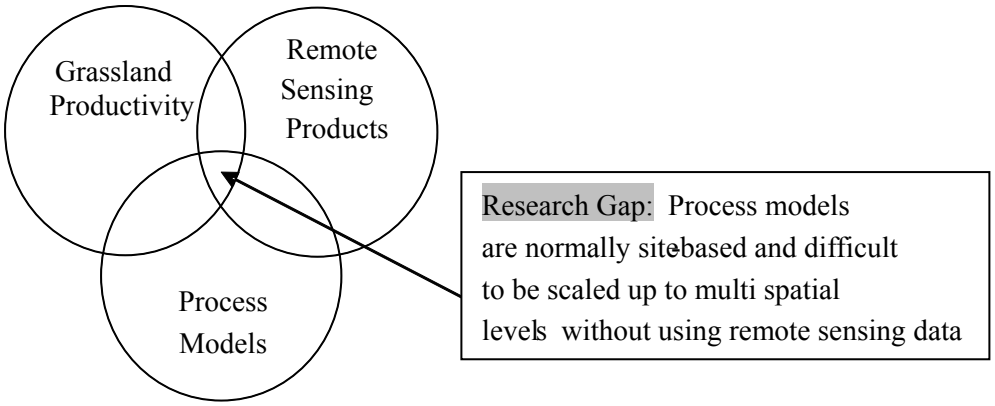


Figure 1.1 The diagram of the research gap

## 1.2 Research Objectives

### 1.2.1 Research Goals

In order to address these research gaps, the aims of this study are to:

- Examine how environmental factors affect spatial variation of biophysical properties in the mixed grassland ecosystem and determine the optimum pixel size for studying northern mixed grasslands in order to aid in the selection of satellite images,
- Determine the best indicators (remote sensing indicator and phenological indicator) which are highly related to mixed grassland development and could be used to derive vegetation biophysical maps to aid spatial modeling,
- Investigate the appropriate classification approach for the mixed grassland and

develop land cover map for the study area as model's input, and

- Evaluate the output (productivity) of the popular ecosystem process models (CENTURY and BIOME-BGC) and develop an ecosystem process model framework for the mixed grassland ecosystem that will make up the shortcoming in the popular process models and integrate satellite data into the model in order to simulate vegetation productivity for the mixed grassland functioning at the landscape scale.

### 1.2.2 Research Hypothesis

The overall hypothesis of this research is that remote sensing data can provide ecosystem processing models with spatially distributed inputs and parameters (Figure 1.2).

More specifically,

- Remote sensing data, with different resolutions, can increase grassland productivity prediction accuracy at different levels.
- Remote sensing data, with mixed information in each pixel, can provide ecosystem processing models with input parameters.
- Remote sensing data can be more effective in heterogeneous landscapes because of continuous data acquisition in the coverage.
- Remote sensing data can be used to monitor ecosystem dynamics through process models because of the high temporal resolution.

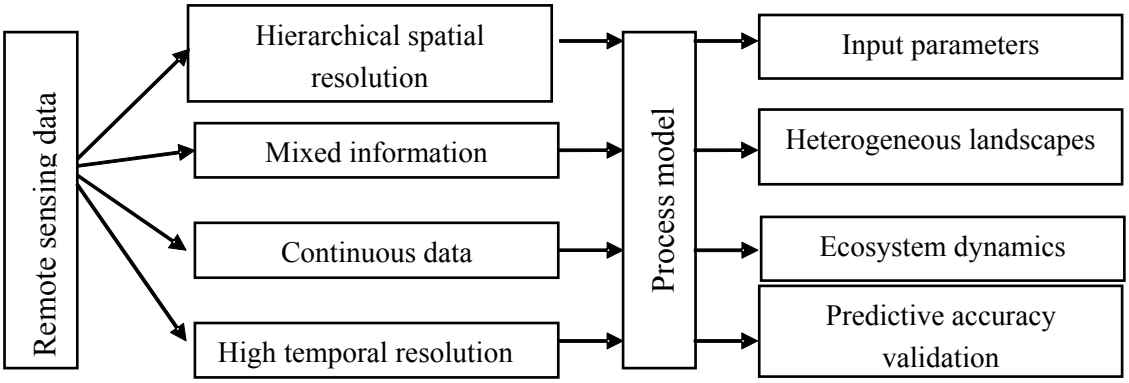


Figure 1.2 The flowchart of the research hypothesis

## 1.3. Study Area

The field study was conducted at Grasslands National Park (GNP, Figure 1.3), in southwest Saskatchewan, Canada (N 49° 12’, W 107° 24’). This area falls within the mixed-grass prairie biome of the northern Great Plains, and is characterized by semi-arid climate, open landscape, and large areas dominated by herbaceous plant communities (Coupland, 1993). The park is approximately 906.5 km2 in area located in two discontinuous blocks, west and east. The first land was acquired for the park in 1984 and the legal agreement signed by Canada and Saskatchewan in 1988 marked the formation of the park. Most areas of the park have been under protection from livestock grazing for over 20 years.

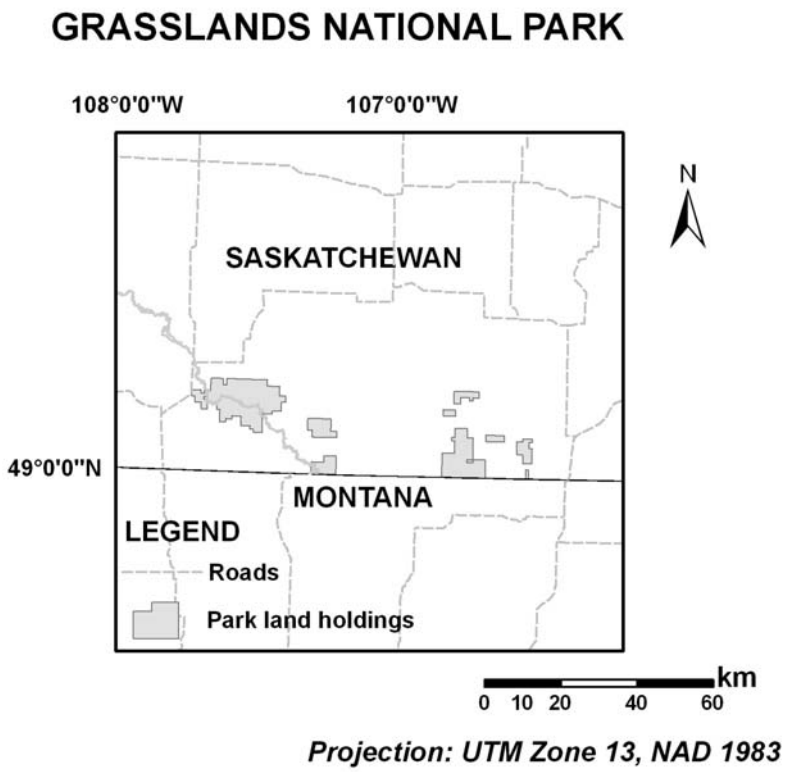


Figure 1.3 The location map of Grassland National Park

The dominant native grass species found in the study area are needle-and-thread grass (Hesperostipa comata (Trin. & Rupr.) Barkworth), blue grama (Bouteloua gracilis (Willd. ex Kunth) Lag. ex Griffiths), and western wheat grass (Pascopyrum smithii (Rydb.) A. Löve). Other prominent invasive or introduced species includes smooth brome (Bromus inermis Leyss) and crested wheat grass (Agropyron cristatum(L.) Gaertn) (Figure 1.4). The forbs and shrubs are only 5.2 to 15.5 percent of the mean basal cover in the mixed grassland (Coupland, 1950), mainly found along the Frenchman River. The GNP area has average temperatures ranging from -12.4 $^{o}$C in January to 18.3 $^{o}$C in July, and a total precipitation of 350 mm per year (Environment Canada, 2000). The soils in the study area are brown Chernozemic clay loam soils (Saskatchewan Soil Survey, 1992).

Sloped and Upland Grasslands

Valley Grasslands

Eroded Communities

Shrub Communities

Figure 1.4 Stratification of the landscape in the GNP area

## 1.4 Thesis Structure

There are seven chapters in this thesis (Figure 1.5). Chapter 1 is the introduction where a general review of pertinent literature is presented, as well as the research objectives, study area, and the thesis structure. The literature review gives an overview of why and how study grassland productivity, and emphasizes that the models, integrating remote sensing data, offer a feasible approach to estimating grassland productivity in the landscape level.

Chapter 2 addresses the first research objective, that is, examines the environmental factors that affect spatial variation of biophysical properties and determines the optimum pixel size for studying the mixed grassland ecosystem. This manuscript provides a more detailed review of the literature regarding why it is important to investigate the spatial variation of grassland biophysical properties and why it is critical to select the optimal pixel size of remotely sensed data for the landscape level study. Using a wavelet technique, the chapter estimates the dominant scale of spatial variation in both field data and remote sensing data (ground hyperspectral data and satellite data) for the mixed grass ecosystem. Therefore, the most optimal pixel size for studying the mixed grass ecosystem is identified and evaluated.

Chapters 3, 4, and 5 examine suitable vegetation indeces, develop vegetation biophysical maps, detect phenology variables, and derive land cover maps for modeling the mixed grassland ecosystem. These chapters address the second research objective: to explore remote sensing tools and their ability to estimate grassland biophysical properties.

Chapter 6 uses 5-year field data, 20-year AVHRR NDVI data, and climate data to evaluate outputs (vegetation productivity) of the popular process models (CENTURY and BIOME-BGC) and introduces an ecosystem process model framework for mixed grassland ecosystem that integrates satellite products (developed from chapter 2 & 3) into the process model in order to simulate vegetation productivity for the mixed grassland at the landscape scale.

In chapter 7, the results and conclusions of each manuscript are summarized. As well, the limitations of the present research are discussed, and a recommendation for future work relating to this thesis is given.

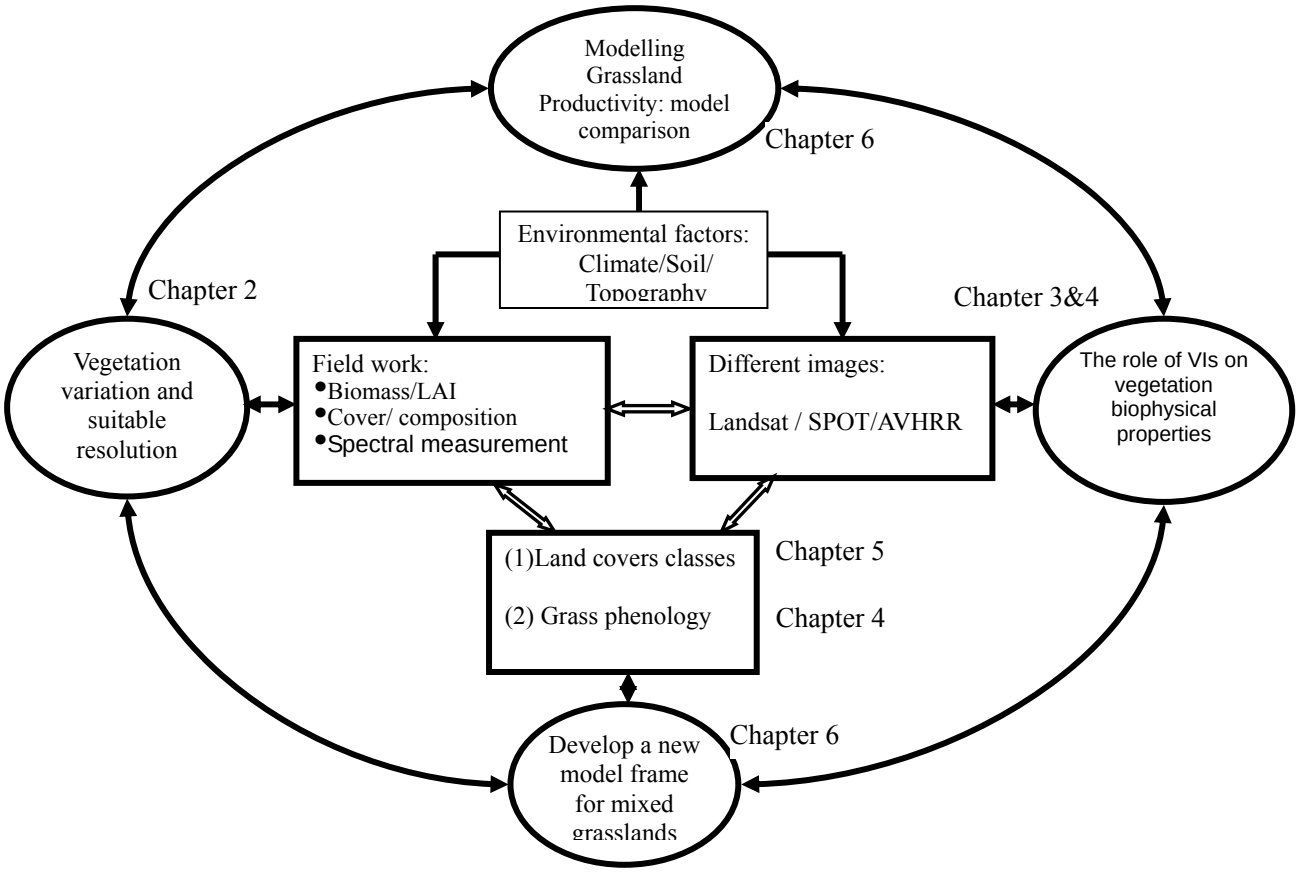


Figure 1.5 Methodology framework of the thesis

## 1.5 References

Band, L.E., Peterson, D.L., Running, S.W., Coughlan, J., Lammers, R., Dungan, J., and Nemani, R. 1991. Forest ecosystem processes at the watershed scale: basis for distributed simulation. Ecological Modelling. 56, 171-196.

Barthram, G. T., Grant, S.A., and Elston, D.A. 1992. The effects of sward height and nitrogen fertilizer application on changes in sward composition, white clover growth and the stock carrying capacity of an upland perennial ryegrass/white clover sward grazed by sheep for 4 years. Grass and Forage Science. 47, 326-341.

Brereton, A.J., and McGilloway, D.A. 1999. Sward factors and herbage intake. In: Pasture Ecology and Animal Intake. EU Concerted Action AIR3 CT93 0947. Occasional Publication No 3, Dublin, pp. 144-162.

Burke, I.C., Yonker, C.M., Parton, W.J., Cole, C.V., Flach, K., and Schimel, D.S. 1989. Texture, climate, and cultivation effects on soil organic matter content in US grassland sites. Soil Science Society of America Journal 53, 800–850.

Campbell, B.D., Smith, D.M.S, and Ash, A.J. 1999. A rule-based model for the functional analysis of vegetation change in Australian grasslands, Journal of Vegetation Science. 10, 723-730.

Churkina, G., Colinet, G., Collatz, J., Emanuel, W., Esser G., Field, G., Fischer, A., A. Friend, A. Haxeltine, M. Heimann, J. Hoffstadt, C. Justice, J. Kaduk, L. Kergoat, D. Kicklighter, W. Knorr,

G. Kohlmaier, B. Lurin, P. Maisongrande, P. Martin, R. McKeown, B. Meeson, B. Moore, R. Olson, R. Otto, W. Parton, M. Pleochl, S. Prince, J. Randerson, I. Rasool, B. Rizzo, A. Ruimy, S. Running, D. Sahagian, B. Saugier, A. Schloss, J. Scurlock, W. Steffen, P. Warnant, and U. Wittenberg, 1995: GBP/GAIM REPORT SERIES REPORT #5. NET PRIMARY PRODUCTIVITY MODEL INTERCOMPARISON ACTIVITY (NPP), available at http://gaim.unh.edu/Products/Reports/Report_5/index.html.

Christopher, B.F., Randerson, J.T., and Malmstrom, C.M. 1995. Global net primary production: Combining ecology and remote sensing. Remote Sensing of Enviornment. 51, 74-88.

Costanza, R., and Maxwell, T. 1991. Spatial ecosystem modeling using parallel processors. Ecological Modelling. 58, 159-183.

Costanza, R., Sklar, F.H. and White, M.L. 1990. Modeling coastal landscape dynamics. BioScience. 40, 91-107.

Coupland, R.T. 1950. Ecology of mixed prairie in Canada. Ecological Monographs. 20, 271–315.

Coupland R.T. (ed), 1993. Ecosystems of the world 8A, 8B: natural grasslands. Elsevier, Amsterdam.

Cramer, W., Kicklighter, D.W., Bondeau, A., Moore, B., Churkina, C., Nemry, B., Ruimy, A., and Schloss, A.L. 1999. Comparing global models of terrestrial net primary productivity (NPP): overview and key results. Global Change Biology. 5, 1-15.

Cramer, W., and C. B. Field, 1999: Comparing global models of terrestrial net primary

productivity (NPP). Global Change Biology, 5, 16-24.

Curll, M.J., Wilkins, R.J., Snaydon, R.W., and Shanmugalingam, V.S. 1985a. The effects of stocking rate and nitrogen fertiliser on a perennial ryegrass-white clover sward: 1. Sward and sheep performance. Grass and Forage Science. 40, 129-140.

Curll, M.J., Wilkins, R.J., Snaydon, R.W., and Shanmugalingam, V.S. 1985b. The effects of stocking rate and nitrogen fertilizer on a perennial ryegrass-white clover sward: 2. Subsequent sward and sheep performance. Grass and Forage Science. 40, 141-149.

Eswaran, H., van den Berg, E., and Reich, P. 1993. Organic carbon in soils of the world. Soil Science Society of America Journal. 57, 192–194.

Evans, D.R., Williams, T.A., and Mason, S.A. 1990. Contribution of white clover varieties to total sward production under typical farm management. Grass and Forage Science. 45, 129-134.

Evans, D.R., Williams, T.A., and Evans, S.A. 1992. Evaluation of white clover varieties under grazing and their role in farm systems. Grass and Forage Science. 47, 342-352.

Fitz, H.C., DeBellevue, E.B., Costanza, R., Boumans, R., Maxwell, T., Wainger, L., and Sklar, F.H. 1996. Development of a general ecosystem model for a range of scales and ecosystems. Ecological Modelling. 88, 263-295.

Fothergill, M., Davies, D.A., and Morgan, C.T. 2000. Sheep grazing and white clover. A rest is best? In: Rook, A.J., Penning, P.D. (Eds.), Grazing Management. Occasional Symposium No. 34. Harrogate, 29 February-2 March, The British Grassland Society, pp. 27-32.

Frame, J. 1990. Herbage productivity of a range of grass species in association with clover.

Grass and Forage Science. 45, 57-64.

Gilliland, T.J. 1996. Assessment of perennial ryegrass variety compatibility with white clover under grazing. Plant Varieties and Seeds. 9, 65-75.

Grant, S.A., Suckling, D.E., Smith, H.K., Torvell, L., Forbes, T.D.A, and Hodgson, J. 1985. Comparative studies of diet selection by sheep and cattle: the hill grasslands. Journal of Ecology. 73, 987-1004.

Grenfell, B.T. 1988. Gastrointestinal nematode parasites and the stability and productivity of intensive ruminant grazing systems. Philosophical Transactions of the Royal Society of London. B 321, 541-563.

Hall B.M. 2000. GLCM texture: A tutorial. http://www.ucalgary.ca/~mhallbey/texture/texture_tutorial.html.

Huntchings, N.J., and Gordon, I.J. 2001. A dynamic model of herbivore-plant interactions on grassland, Ecological Modelling. 136, 209-222.

Laws, J.A., and Newton, E. 1992. The grazing management of sheep on grass white clover permanent pasture. Irish Journal of Agricultural and Food Research. 31, 143-156.

Li, Y.P., and Ji, J.J. 2002. Framework of a Regional Impacts Assessment Model and Its Application on Arid/Semi-Arid Region. http://www.iemss.org/iemss2002/proceedings/pdf/volume%20due/140_li.pdf.

Lieth, H.F.H. (Ed.), 1978. Patterns of Primary Productivity in the Biosphere. Hutchinson Ross, Stroudsberg, PA . pp. 342.

Matthews, E. 1983. Global vegetation and land use: New high resolution data bases for climate studies. Journal of Climatology and Applied Meteorology. 22, 474-487

McGuire, A., Melillo, J., and Kicklighter, D. 1995. Equilibrium responses of soil carbon to climate change - empirical and process based estimates, Journal of Biogeography. 22, 785-796.

Melillo, J.M., McGuire, A.D., Kicklighter, D.W., Moore III, B., Vorosmarty, C.J., and Schloss, A.L. 1993. Global climate change and terrestrial net primary production. Nature. 363, 234-240.

Melillo, J.M., Hall, D.O., and Ågren, G.I. Executive summary. I n: Hall, D.O., Breymeyer, A.I., Melillo, J.M., Argen, G.I.(Eds.), 1996. Global Change: Effects on Coniferous Forests and Grasslands. Wiley, London, pp. 1.

Mitchell, S.W., and Csillag, F. 2001. Assessing the stability and uncertainty of predicted vegetation growth under climatic variability: northern mixed grass prairie. Ecological Modelling. 139, 101-121.

Mitchell, S.W. 2003. Does Pattern Matter? Spatio-temporal modeling strategies to predict grassland productivity dynamics, grassland national park, Saskatchewan. Ph.D. Thesis, Graduate department of geography, University of Toronto.

Montieth, J.L. 1972. Solar radiation and production in tropical ecosystems. Journal of Applied Ecology. 9, 747–766.

Mougin, E., Seen, D.L., Rambal, S., Gaston, A., and Hiernaux, P. 1995. A regional sahelian grassland model to be coupled with multipectral satellite data. I: model description and

validation. Remote Sensing of Environment. 52, 181-193.

Nassiri, M. 1998. Modelling interactions in grass/clover mixtures. Ph.D. Thesis. Wageningen Agricultural University, Wageningen, The Netherlands, pp. 165.

Nouvellon, Y., Rambal, S., Seen, D.L., Moran, M.S., Lhomme, J.P., Begue, A., Chehbouni, A.G., and Keer, Y. 2000. Modelling of daily fluxes of water and carbon from shortgrass steppes, Agricultural and Forest Meteorology. 100, 137-153.

Ojima, D.S., Parton, W. J., Coughenor, M.B., Scurlock, J.M.O., Kircherner, T.B., Kittel T.G.F., Hall, D.O., Schimel, D.S., Moya, E.G., Gilmanov, T.G., Seastedt, T.R., Kamnalrut, A., Kinyamario, J.I., Long, S.P., Menaut, J.-C., Sala, O.E., Scholes, R.J., Veen, J.A,v., 1996. Impact of climate and atmospheric carbon dioxide changes on grasslands of the world. In: Hall, D.O., Breymeyer, A.I., Melillo, J.M., Argen, G.I.(Eds.), Global Change: Effects on Coniferous Forests and Grasslands. Wiley, London, pp. 271-311.

Orr, R.J., Parsons, A.J., Penning, P.D., and Treacher, T.T. 1990. Sward composition, animal performance and the potential of grass/white clover swards continuously stocked with sheep. Grass and Forage Science. 45, 325-336.

Parton, W., Scurlock, J., and Ojima, D. 1993. Observations and modelling of biomass and soil organic matter dynamics for the grassland biome worldwide, Global Biogeochemical Cycles. 7, 785-809.

Parton, W.J., Coughenor, M.B., Scurlock, J.M.O., Ojima, D.S., Gilmanov, T.G., Kircherner, T.B., Menaut, J.-C., Seastedt, T.R., Moya, E.G., Kamnalrut, A., Kinyamario, J.I., Hall, D.O., 1996. Global grassland ecosystem modeling: development and test of ecosystem models for grassland

system. I n: Hall, D.O., Breymeyer, A.I., Melillo, J.M., Argen, G.I.(Eds.), Global Change: Effects on Coniferous Forests and Grasslands. Wiley, London, pp. 229-269.

Parsons, A.J., Harvey, A., and Woledge, J. 1991a. Plant-animal interactions in a continuously grazed system. I. Differences in the physiology of leaf expansion and the fate of leaves of grass and clover. Journal of Applied Ecology. 28, 619-634.

Parsons, A.J., Harvey, A., and Johnson, I.R. 1991b. Plant_/animal interactions in a continuously grazed system. II. The role of differences in the physiology of plant growth and of selective grazing on the performance and stability of species in a mixture. Journal of Applied Ecology. 28, 635-658.

Peat, H.C.L. 1997. Dynamics of C3 and C4 productivity in northern mixed grass prairie. M.Sc. Thesis, University of Toronto, Toronto, pp. 163

Rastetter, E. B. 1996. Validating models of ecosystem response to global change. Bioscience. 46, 190-198.

Running, S.W., and Hunt, E.R. Generalization of a forest ecosystem process model for other biomes, BIOME-BGC and an application for global-scale models, in Scaling Physiological Processes: Leaf to Globe, J. Ehleringer, and C. Field, pp. 1410158, Academic Press, San Diego, 1993.

Schulte, R.P.O., Lantinga, E.A., and Struik, P.C. 2002. Analysis of the production stability of mixed grasslands. I: A conceptual framework for the qualification of production stability of grassland ecosystems. Companion paper.

Schulte, R.P.O. 2003. Analysis of the production stability of mixed grasslands II: A mathematical framework for the quantification of production stability in grassland ecosystems. Ecological Modelling. 159, 71-99.

Schwinning, S., and Parsons, A.J. 1996a. Analysis of the coexistence mechanisms for grasses and legumes in grazing systems. Journal of Ecology. 84, 799-813.

Schwinning, S., and Parsons, A.J. 1996b. A spatially explicit population model of stoloniferous N-fixing legumes in mixed pastures with grass. Journal of Ecology. 84, 815-826.

Song C.H., and Woodcock, E.C. 2003. A regional forest ecosystem carbon budget model: Impacts of forest age structure and landuse history. Ecological Modelling. 164, 33–47.

Thornley, J.H.M., and Verberne, E.L.J. 1989. A model of nitrogen flows in grassland. Plant, Cell and Environment. 12, 863-886.

Thornley, J.H.M., Bergelson, J., and Parsons, A.J. 1995. Complex dynamics in a carbon nitrogen model of a grass legume pasture. Annals of Botany. 75, 79-94.

VEMAP Members. 1995. Vegetation/Ecosystem Modeling and Analysis Project: Comparing biogeography and biogeochemistry models in a continental-scale study of terrestrial ecosystem responses to climate change and $CO_2$ doubling. Global Biogeochemcal+ Cycles. 9.

# CHAPTER 2 – DETECTING GRASSLAND SPATIAL VARIATION AND DETERMINING OPTIMUM PIXEL SIZE FOR STUDYING THE MIXED GRASSLAND ECOSYSTEM

## 2.1 Abstract

Insight into the spatial variation of an ecosystem can provide better understanding of ecological processes and patterns in different scales. Detecting these multiple scales of spatial variation in grassland landscapes is valuable for selecting suitable resolutions of remote sensing products, determining management options, and designing proper sampling regimes. The objective of this study is to examine how environmental factors affect spatial variation of mixed grassland biophysical properties and what is the suitable spatial resolution for studying the mixed grassland ecosystem. Field leaf area index (LAI), soil moisture, and topographical parameters (relative elevation, upslope length, and a wetness index) were obtained in three parallel transects of a grassland ecosystem in Saskatchewan, Canada in 2004. One 20 m resolution SPOT 4 (HRVIR) image was acquired at the same period of the growing season but in the following year. Normalized Difference Vegetation Index (NDVI) was calculated from the satellite image of the center 381 m transect and two extensive 2560 m perpendicular transects. A wavelet approach was used to identify the scales of variations. Statistical results showed that LAI is significantly correlated to the wetness index ($r^2$ = 0.37) and soil moisture ($r^2$ = 0.43). The wetness index is better than relative elevation and upslope length in demonstrating the effect of topography on grassland vegetation. The variation of soil moisture is significant at two small scales of about 20 m and 40 m, and that of the wetness index is at the large scale of 120 m. The variation of

grassland LAI is significant at three scales (20 m, 40 m and 120 m), which indicates that the spatial variation of LAI might be controlled by both topography and soil moisture, though the 120 m is the dominant scale of variation in LAI. NDVI significantly correlated with grassland LAI along the centre transect. The effect of topography on grassland LAI is also proven by the significant relationships between NDVI and the wetness index. The wavelet analysis identified the variation of two extensive transects at the scale of about 120 m, which is similar to the dominant variation scale of grassland LAI. These results confirmed that the effect of topography on spatial variation can be identified from the appropriate satellite image. The results demonstrated that the 20 to 30 m (one fourth of a period, 120 m) would be an optimum pixel size to detect potentially important patterns associated with topography in our study area. This study suggested that the spatial scales of soil and topographic data aid in the selection of appropriate satellite image resolution for monitoring and managing ecosystem.

## 2.2 Introduction

Spatial variation is one of the most important and widely applicable concepts in grassland ecology (Armesto et al., 1991). The mixed grassland of North America has been described as inherently heterogeneous due to its composition, productivity, and diversity varying across multiple scales (Ludwig and Tongway, 1995). Insight into the spatial variation of grassland can provide better understanding of ecological processes and patterns in different scales. Detecting these multiple-scales of spatial variation in grassland landscapes is valuable for selecting suitable resolutions when remote sensing products are applied to ecosystem models, determining management options, and designing proper sampling regimes for monitoring ecosystem heterogeneity and biodiversity.

A number of recent studies have effectively demonstrated that the spatial pattern of grasslands ecosystem is apparently scale dependent (Nellis and Briggs, 1989). Large-scale patterns can be determined by variation in topography or climate condition. Lobo et al. (1998) and Sebastian (2004) determined spatial structure of grassland by topography; Dennis et al. (2002) identified the spatial distribution of upland beetles in relation to landform; and Reed et al. (1993) found that the state of an environmental variable (e.g. soil nutrient elements) affected plant community composition. Small-scale heterogeneity may result from a combination of biotic and abiotic factors. The variation of vegetation at small scales is affected by soil heterogeneity (Reynolds et al., 1997), but it is also influenced by biotic factors such as grazing animals (Mitchley, 1994), unpalatable and spiny plants (Callaway et al., 2000), shrubs and trees (Söderström et al., 2001), ant mounds (Blomqvist et al., 2000), and dung and urine patches (Shiyomi et al., 1998).

Researchers have currently adopted different data collection methods to determine either large- or small-scale spatial variations of grasslands. Fine resolution data that can be obtained from field measurements are commonly used for small-scale spatial pattern analysis. Considering that field measurements are rarely obtained to a broad extent, related variables derived from satellite imagery covering a broad extent become a valuable source of data in characterizing spatial dependence in ecological systems (Lobo et al., 1998). Recently, numerous studies have used remote sensing imagery for estimating vegetation variability across space (Marceau and Hay, 1999). In grassland ecosystems, Griffiths et al. (2000) measured grassland species diversity based on 30 m Landsat Thematic Mapper (TM) imagery; Lobo et al. (1998) analyzed the spatial pattern of grassland landscape variables using fine resolution maps; Schmidtlein and Sassin (2004) modeled floristic gradients of meadows based on 2 m resolution hyperspectral airborne imagery; and Ji and Peters (2003) determined the response of grassland

vegetation to moisture availability through 1 km resolution Advanced Very High Resolution Radiometer (AVHRR) data. All these studies demonstrated that remote sensing data with diverse resolutions are efficient in detecting the spatial variation of grassland ecosystems.

However, what has been largely missing is a general comparison between spatial patterns obtained from field measurements and those gained via remote sensing data. Few studies have examined both large- and small-scale spatial variation within mixed grassland ecosystems in North America. This shortfall in previous studies may be a result of a lack of appropriate data with fine resolution across a broad area (Brosofske et al., 1999). Without investigating the spatial scales of research objects based on field measurements, scientists may be constrained by the predetermined spatial resolution (i.e. the pixel size) when using satellite-based remotely sensed data (Rahman et al. 2003). To choose satellite imagery with an appropriate resolution, studies have suggested that different pixel sizes should be adopted for different grassland ecosystems (Rahman et al., 2003; Gamon et al. 1993, Davidson and Csillag, 2001). Therefore, this study will combine the fine resolution ground measurements with a wide-extent satellite image to determine the spatial pattern and appropriate resolution for a mixed grassland ecosystem.

Approaches that quantify the spatial characteristics of biotic or abiotic variables have recently been developed. These methods include geostatisics (Miller et al., 1988), lacunarity (Plotnick et al., 1993), spectral analysis (Turner et al., 1991), state-space methods (Wendroth et al., 1992), and G statistic (Dennis et al., 2002). These methods, however, could not evaluate features that existed over a series of multiple scales (Si and Farrell, 2004). Because grassland ecosystems generally have trends in spatial domain (i.e. non-stationary spatial series), and these trends may indicate important soil, topographic, and ecological processes that affect grassland production, a different method has to be adopted to analyze the data from grassland ecosystems.

The wavelet approach has been proposed to detect various features of non-stationary data due to its three abilities which may be overlooked by other methods: .1) aggregating patterns along transects at different scales (Mehlum et al., 1999); 2) analyzing non-stationary or non-sinusoidal multi-frequency data (Bradshaw and Spies, 1992; Bradshaw and McIntosh, 1994; Saunders et al., 2005); and 3) providing diverse wavelet functions to examine the different types of data and hypothesized patterns.

The applications of wavelet analysis on vegetation ecology have grown considerably over the past two decades. For example, this technique has been used to explore multi-scale patterns in ecological data (Saunders et al., 2002), microclimate along transects (Redding et al., 2003), soil variability (Lark and Webster, 1999), plant productivity (Csillag and Kabos, 2002), crop biomass production and topographical parameters (Si and Farrell, 2004), and ground cover (Dale and Mah, 1998). However, few studies have applied the wavelet approach in the analysis of mixed grassland biophysical data and environmental information (Mi et al., 2005).

Therefore, the overall objectives of this manuscript are to 1) examine how much of the variation in vegetation biophysical property is accounted for by soil moisture and topographic parameters (relative elevation, upslope length, and wetness index), 2) examine if the significant scale of variations in vegetation biophysical properties can be identified from topographic indices and soil moisture, 3) examine the relationship between satellite-derived data and topographical indices and test the spatial variation of two extensive transects, and 4) identify and evaluate the most optimal pixel size for studying the mixed grass ecosystem. Since geographic data generally exhibit certain non-stationary features (large scale trend and localized features), we chose wavelet analysis as a tool for identifying the dominant scales of variations. We used leaf area index (LAI) as the grassland biophysical parameter to study vegetation variation of the mixed grassland ecosystem, for the reason that LAI is the best parameter to represent the

biophysical properties in the mixed grassland (Zhang, 2006) and LAI is an important parameter in the ecosystem models (Liu et al., 1997).

## 2.3 Materials and Methods

### 2.3.1 Field Study Sites

The study was conducted in Grasslands National Park (GNP), Saskatchewan, Canada (49° 15’ N, 107° 09’ W). GNP was established in 1984 to preserve a representative portion of the Canadian mixed grass prairie ecosystem. This area is characterized as having a semi-arid climate, with an annual precipitation of approximately 340 mm, mainly accumulating as rainfall in the growing season (May - September). The mean annual temperature in this region is 3.4° C. The growing season is relatively short (170 days on average) and is often further shortened by the lack of moisture (Csillag et al., 2001).

GNP consists of upland, slopeland, and valley grasslands. Considering that upland grasslands dominate the mixed grassland ecosystem in North America, we located our sampling site in upland native grassland (Figure 2.1). We chose this site because it was situated along a typical rolling terrain with a soil moisture gradient. The dominant soil type is a nutrient poor, shallow, clay-loam brown soil, but a wide variety of soil types (chernozems, solonetzes, regosols and gleysols) are present (Csillag et al., 2001). The dominant grass species included needle-and-thread grass (Stipa comata Trin. & Rupr.), blue grama grass (Bouteloua gracilis (HBK) Lang. ex Steud.), June grass (Koeleria macrantha (Ledeb) J.A. Schultes f.) and western wheatgrass (Agropyron smithii Rydb.).

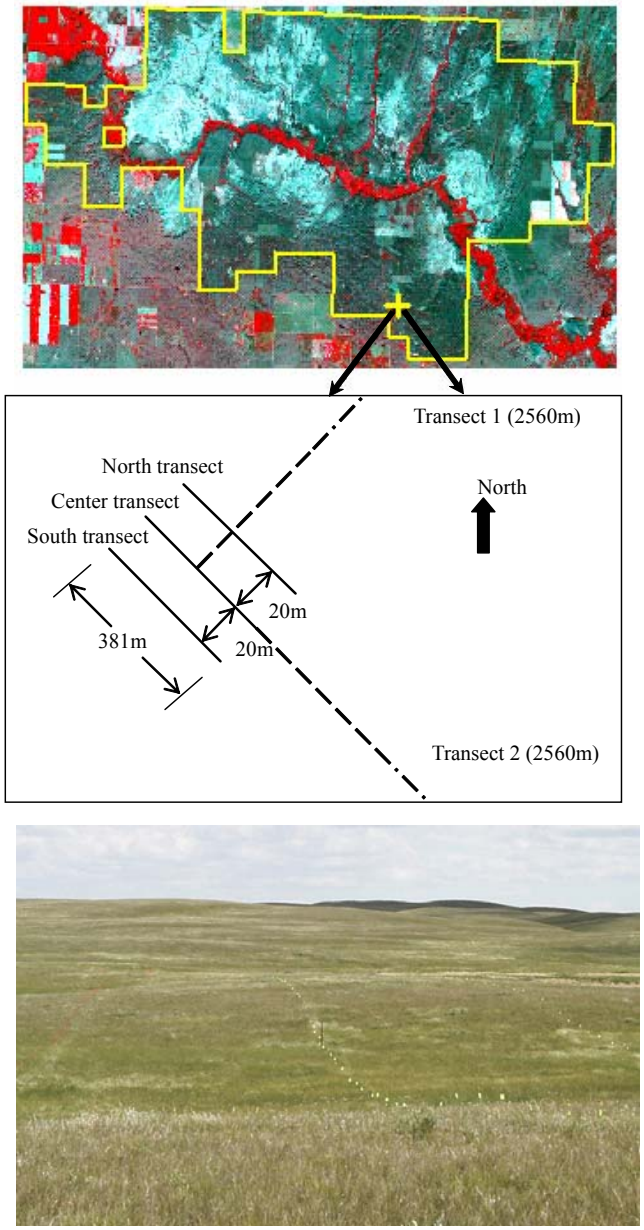


Figure 2.1 The field sites at Grassland National Park. The top image is a SPOT4 scene (20-m resolution) in a false color composite (RGB: NIR, Red, and Green bands). Therefore, the red color in this image indicates high vegetation cover. The yellow box within the image is the park holding boundary. The yellow cross sign in the image is the centre of the study location, which located at typical upland grassland with the representative rolling terrain and moisture gradient. The graph in the middle illustrates all transects used in our study. Topographical parameters were collected

from the three parallel transects (north, centre, and south), and the LAI measurements from the centre transect. The broadband NDVI values were derived from the SPOT satellite image of transect 1 and transect 2. The bottom photo was taken from the study area.

### 2.3.2 Field Data

Field data collection was performed in the summer of 2004 along three 381-m parallel transects (South, Centre, and North), separated by a lateral distance of 20 m between transects. The LAI, soil and topographic samples were taken from quadrats located at 3 m intervals along the centre transect (128 locations), and from quadrats located at 6 m intervals along the other two transects (64 locations per transect). The size of the quadrat is 50×50 cm2. In all, a total of 256 points were measured within an area of 1.905 ha (i.e. 381 by 50 m).

LAI, soil moisture, relative elevation, slope, and distance were recorded at each quadrat. LAI (the projected area of all vegetation parts normalized by the subtending ground area) was measured using a LiCOR LAI-2000 Plant Canopy Analyzer (LI-COR Inc., Lincoln, Nebraska, USA). The LAI-2000 was shaded when measurements were being taken to reduce the effect of glazing from direct sunshine. At each plot, LAI is the average of four automatically calculated LAI values; each was the comparison result of one above canopy reading followed by 10 below canopy readings all completed within two minutes to avoid atmospheric variation. Soil moisture was measured using an Aquaterr Soil Moisture and Temperature Probe (Forestry Suppliers, Inc., Jackson, USA). A laser theodolite (ATT Metrology Services, Inc., California, USA) was used to measure relative elevation, angle and distance. These topographic measurements allow for precise calculation of slope percentage and upslope length at any point along transects.

Three topographical parameters, relative elevation, upslope length, and wetness index (WI), were calculated and used in this paper. Relative elevation was defined as the distance a point sits above or below the average elevation of the study area. Upslope length was calculated as the distance from the measurement point in the landscape to the highest relative elevation point along the local slope (Si and Farrell, 2004). The wetness index developed by Beven and Kirkby (1979) was calculated using the following equation.

$$WI = \ln(\frac{\gamma}{\tan\beta}) \quad (1)$$

Where γ is the upslope length and tan β is the local terrain slope of the landscape elements. We choose upslope length as a topographic index because upslope length is conceptually appealing for semi-arid zone where snowmelt runoff and snow redistribution are the water redistribution processes (Si and Farrell, 2004). We selected the wetness index because it is physically based and widely accepted.

### 2.3.3 Satellite Multispectral Imagery Acquisition

This study used a SPOT 4 HRVIR image with 20 m resolution, including four bands of green, red, near infrared (NIR), and short wave infrared (SWIR) (broadband data). This image covers the study area (Scene Centre Location: N049° 08' 51", W107° 29' 31") and was acquired on June 22, 2005, the same growth period in which ground data was collected in 2004 (Figure 2.1). Considering topography is relatively time-invariant, the dominant spatial variation of grassland associated with topography should be similar for both 2004 and 2005.

The SPOT image was processed for geometric and radiometric corrections in PCI Geomatica V.9.1 software. First, the geometric correction was done with 34 GCP’s (Ground

Control Points) and resulted in an accuracy of better than 0.3 pixel root mean square error (RMSE), representing approximately 6 meters or less error on the earth's surface. The road shape file provided from the GNP's GIS database further confirmed the geometric correction accuracy because easily identifiable objects, such as road intersections from the shape file corresponded well with those in the image. Distortions caused by variations in topography were corrected using a Digital Elevation Model (DEM), which was also obtained from the GNP's GIS database. Because this study involved analysis of biophysical parameters derived from the image, it was necessary to perform atmospheric and radiometric correction to convert digital numbers to radiance and, in turn, radiance to reflectance values. This atmospheric correction was done using the ATCOR 2 module within PCI Geomatica V.9.1 software. The algorithms used in this module were developed by DLR, German Aerospace Research Establishment based on information from the references (Ahern et al., 1977; Lanzl and Richter, 1991; Richter, 1990). The ATCOR 2 was run on parameters found within the image's metadata.

After preprocessing the image, the broadband NDVI (Rouse et al., 1974) was derived from the NIR and Red bands for estimating grassland biophysical properties in this study, as below:

$$NDVI = \frac{\rho_{NIR} - \rho_{\mathrm{Red}}}{\rho_{NIR} + \rho_{\mathrm{Red}}} \qquad (2)$$

NDVI was selected because it is known to highlight biophysical factors such as chlorophyll content and LAI (Deering et al., 1975; Huete et al., 2002). The NDVI values were extracted along the centre transects, which were geo-referenced in the field by taking GPS readings. Because the resolution of the image is 20 m, we can only extract data from 20 pixels for the

centre 381 m transect. In order to match the ground sampling with the resolution of remote sensing data, LAI and ground topographic data were smoothed with a 20 m moving window. Furthermore, in the interest of examining whether or not image data capture the same scale information as ground truth data, we also extracted the NDVI from two extensive 2560 m perpendicular transects (transect 1 and transect 2), which were located near the three afore-mentioned transects (Figure 2.1).

### 2.3.4 Statistical Analysis

A widely used empirical approach for modeling the relationship between two variables is regression analysis (Cohen et al., 2003). We applied regression models to evaluate the linear relationships among LAI, environmental factors (relative elevation, upslope length, wetness index, soil moisture), and NDVI from the centre transect at the 95% significance level. Although LAI and NDVI were from different years, the NDVI should be correlated with LAI because LAI variation depends, to a large extent, on the relatively time-invariant topography. RMSE, equation (3), has been calculated to evaluate the regression model’s accuracy.

$$RMSE = \sqrt{\frac{1}{n}\sum_{i=1}^{n}(x_i - \hat{x}_i)^2} \qquad (3)$$

### 2.3.5 Wavelet Approach

Since choice of wavelet function is crucial for spatial analysis, four commonly-used types of wavelet families (Haar, Daubechies Least Asymmetric, Mexican Hat, and Morlet) were tested to determine the best spatial analyzer for this study. The Morlet wavelet mother function (Equation (3): with dimensionless frequency, W0=6) were finally chosen, since it gives more

satisfying results for the scale analysis and provides a balance between time and frequency localization (Grinsted et al., 2004). The continuous wavelet transformation (Bradshaw and Spies 1992) was used to examine the spatial variability of the ground measurements (wetness index, soil moisture, and LAI) along the center transect and of satellite data (NDVI) along two extensive transects. As suggested by Si (2003), we first utilized exploratory analysis of the local wavelet spectrum to identify whether any patterns exist in the data. The local wavelet spectrum was also used to determine whether these patterns are repeated across the transect (a global event) or are restricted to only one, or few, localized regions across the transect (localized events). The periodicity of the repeated pattern is referred to as the ‘scale of variation’. If the pattern is global in scale, the wavelet variance is then analyzed to determine its statistical significance.

The Morlet wavelet mother function is scaled by a parameter of a and translated by a parameter of b to give:

$$\psi_{a,b}(t) = \frac{1}{\sqrt{a}}\psi(\frac{t-b}{a}) \tag{4}$$

The a parameter can be interpreted as a dilation (a>1) or contraction (a<1) factor of the wavelet function, corresponding to different scales of observation. The parameter, b, can be interpreted as a temporal or spatial translation or shift of the wavelet function (Si and Farrell, 2004). The continuous Morlet wavelet transform of a real signal f(x) where x is a real variable (Brunsell and Gillies, 2003) is defined as:

$$W_{(a,b)} = \frac{1}{\sqrt{a}}\int_{-\infty}^{+\infty} f_{(x)}\overline{\psi(\frac{x-b}{a})}dx \tag{5}$$

where W is the wavelet coefficients (i.e. local wavelet spectrum) and the overbar designates the

complex conjugate. The coefficient $1/\sqrt{a}$ is included to normalize the energy of the wavelets (Bruce et al., 2001). We used the Wavelet Toolbox in MATLAB (MathWorks, Inc) for calculating the wavelet transform over a continuous range of dilation scales of both field measurements and NDVI. Prior to the wavelet transform calculation, LAI, soil, topography, and NDVI variables were standardized by subtracting their mean from the measurements and dividing the difference by their standard deviation to facilitate comparison between local wavelet spectra.

In order to interpret the local wavelet spectrum, the wavelet (scale) variance (Dale and Mah, 1998, Saunder et al., 2005):

$$V_{(a)} = \frac{\sum_{i=1}^{n} W^2(a,b_i)}{n} \tag{6}$$

is calculated as an average of the wavelet energy to examine overall, 'global' structure (i.e. scales of pattern) within the data (Bradshaw and Spies, 1992). In equation (6), *n* is the number of data points in the spatial series. Large wavelet variance at a scale indicates that the variation at this scale is important for describing the spatial pattern along the transect. The significance test for the wavelet (scale) variance was performed against a red noise data series. A simple model for the red noise is the univariate lag-1 autoregressive progress (Torrence and Compo, 1998):

$$x_n = \alpha x_{n-1} + Z_n, \tag{7}$$

where $\alpha$ is the assumed lag-1 autocorrelation. The discrete Fourier power spectrum of a red noise with unit variance is (Torrence and Compo, 1998):

$$\phi_k = \frac{1 - r^2}{1 + r^2 - 2r\cos(2\pi k / N)} \tag{8}$$

where N is the number of locations, K=0,1,…,N/2 is the frequency index, and r is the first order autocorrelation coefficient (Shumway and Stoffer, 2000). Thus, by choosing an appropriate lag-1 autocorrelation, one can use (8) to model a red-noise spectrum. In this paper, if the actual global wavelet spectrum is significantly greater than the red noise spectrum at a confidence level of 95%, then it can be assumed to be a true feature or significant different from that of red noise with this confidence.

### 2.4 Results

#### 2.4.1 Statistical Analyses of the Correlations of LAI, Soil Moisture, Topographic Parameter, and NDVI

Figure 2.2 illustrated the measured relative elevation, soil moisture, and LAI, as well as the calculated upslope length and wetness index along the centre transect. There are three main depressions (centred at 87, 210, and 360 m) and a small depression centred at 270 m along the transect. The upslope length and wetness index showed a similar trend: large values in the depressions and small values on the knolls. The LAI curve along the transect showed a coarse trend which is similar to that of the topographical indices, as well as finer fluctuations that resemble the variations seen in soil moisture. In addition, LAI, upslope length, and wetness index increased sharply near the three large depressions. Clearly, spatial variations in LAI, soil moisture, and topography indices are non-stationary, exhibiting localized features and trends along the transect (Figure 2.2).

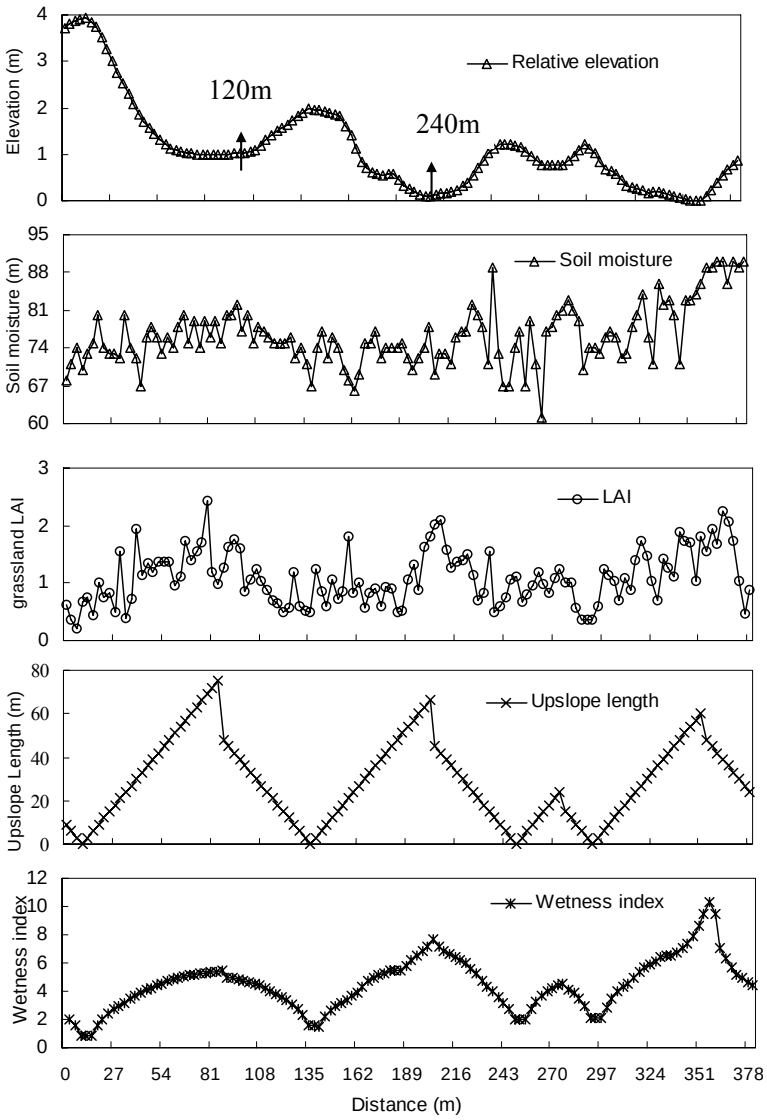


Figure 2.2 Measured grassland relative elevation, soil moisture, LAI, upslope length, and wetness index in 128 plots as a function of distance along the centre transect

Statistical analysis indicated that LAI is significantly correlated with both soil moisture and topographic parameters (i.e. relative elevation, upslope length, wetness index) (Table 2.1). The strongest correlation is found between LAI and soil moisture ($r^2$= 0.43, $p<0.001$). Among the three topographic indices, the wetness index has the strongest correlation with LAI ($r^2$= 0.37, $p<0.001$). The values of RMSE show the similar results as $r^2$ (Table 2.1).

Table 2.2 Statistics of LAI, soil moisture, and topography parameters obtained at 128 locations along the central sampling transect.

| Variable | Mean | SD[#] | Minimum | Maximum | RMSE | $r^{2\#\#}$ |
|---|---|---|---|---|---|---|
| LAI | 1.09 | 0.47 | 0.20 | 2.42 | | |
| Soil moisture (%) | 76 | 5.59 | 61 | 90 | 0.32 | $0.43^{***}$ |
| Wetness index | 4.48 | 1.84 | 0.83 | 10.27 | 0.37 | $0.37^{***}$ |
| Relative elevation (m) | 1.12 | 0.95 | 0.00 | 3.93 | 0.41 | $0.22^{***}$ |
| Upslope length (m) | 28.43 | 18.97 | 0.00 | 75 | 0.38 | $0.33^{***}$ |

[#] Standard Deviation

[##] Coefficient of determination between LAI and the corresponding variable in the first column.

[***] Significant at $P < 0.001$

NDVI is significantly correlated with LAI ($r^2 = 0.52$, Figure 2.3 A), and topographic parameters (i.e. relative elevation, upslope length, and wetness index, Figure 2.3 B) along the centre transect. When compared with upslope length and relative elevation, the wetness index showed the strongest correlation with the NDVI ($r^2 = 0.44$, Figure 2.3 B).

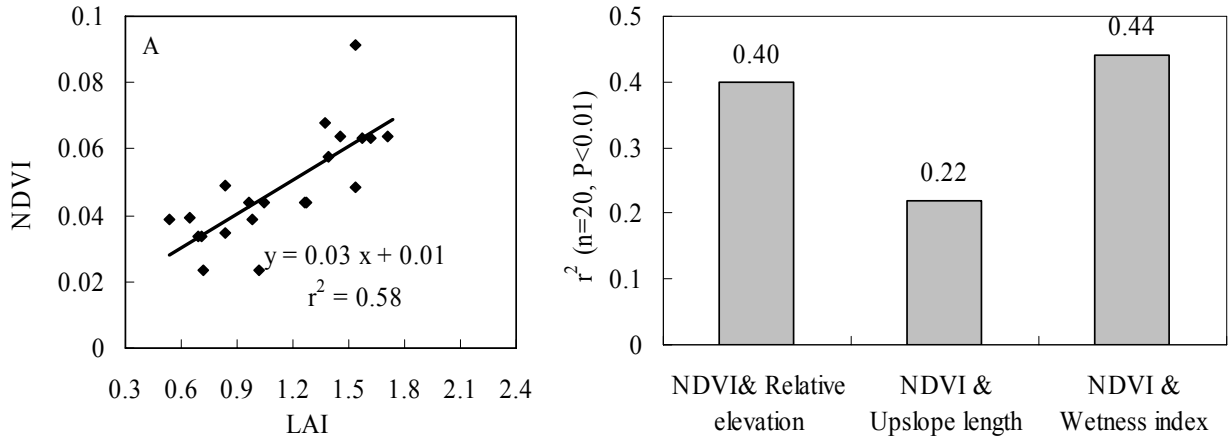


Figure 2.3 The results of regression analyses between NDVI and LAI (A), and between NDVI and topographical parameters (B) along the centre transect. The $r^2$ is the coefficient of determination

### 2.4.2 Wavelet Analyses of Ground Measurements (LAI, Soil Moisture, and Topography)

Visual inspection of the local wavelet spectrum for LAI (Figure 2.4 A1) revealed three scales of variation across the transect (0 to 20 m, 40 to 60 m, and 100 to 140 m). For the 0 to 20 m scale, the intensity of local wavelet spectra along the transect is relatively weak, indicating small-scale variance in the LAI is weak. For the 40 to 60 m scale, there are large variances compared to the 0 to 20 m scale. For the 100 to 140 m scale, regions are centred at 15, 80, 140, 210, 280, and 360m that are interlaced with the lowest and highest variances along the transect. These regions correspond to the locations of peaks (knolls) and troughs (depressions) across the transect, suggesting the effect of terrain on LAI. The statistical testing of the 'global' features indicated that the wavelet variances around 20 m, 40 m, and 120 m are significantly different from (or greater than) that of the red noise spectrum. Contribution of the wavelet variance at 120 m scale to the total variance is much more than that at the other two scales (Figure 2.4 A2). This indicated that LAI shows distinct spatial patterns at different scales, especially at 120 m, which corresponded well to the typical observed sizes of the topographic features.

Similar to those observed in LAI, the local wavelet spectrum of soil moisture (Figure 2.4 B1) exhibited three scales of variations at 0 to 20 m, 40 to 60 m, and 100 to 140 m. For the 40 to 60 m scale, regions of high variables also corresponded to the knolls and depressions occurring along the transect. The spatial variability of soil moisture is significantly different from that of red noises at 20 and 40 m scales, but not at 120 m (Figure 2.4 B2).

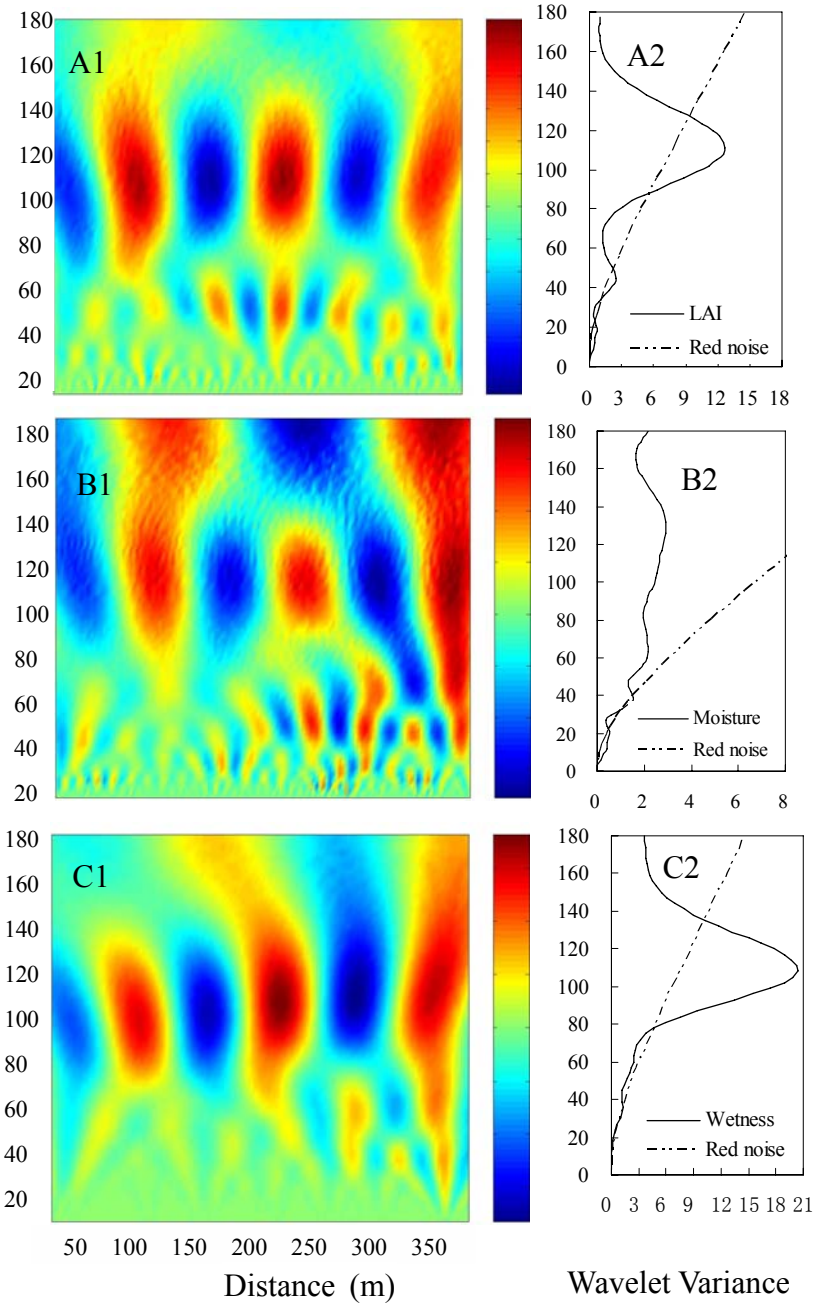


Figure 2.4 The local wavelet spectrum of LAI (A1), soil moisture (B1), and wetness index (C1). The wavelet variance of LAI (A2), soil moisture (B2), and wetness index (C2). The solid line in A2, B2, and C2 figures is wavelet variance. The dashed line is the power spectrum of a red noise at a confidence level of 95%.

The local wavelet spectrum of the wetness index (Figure 2.4 C1) exhibited three scales of variations at 0 to 80 m, 80 to 140 m, and greater than 140 m. For the 0 to 80 m scale, the local spectra are relatively uniform. The 80 to 140 scales are the regions showing the lowest and highest variances. Strong variances are centred at 15, 80, 140, 210, 280, and 360 m across the centre transect. Over 140 m, the local spectra are relatively weak again. 'Global' feature analysis (Figure 2.4 C2) revealed that the spatial variability of the wetness index is significantly different from that of the red noise spectrum at the 120 m scale which is similar to the dominant spatial pattern found in the LAI analysis.

### 2.4.3 Wavelet Analyses of Satellite Data (NDVI) For the Two Extensive Transects

The local spectrum of the NDVI in transect 1 (Figure 2.5 A1) exhibited two scales at 0 to 120 m, and over 120 m. For the 0 to 120 m scale, regions of high local spectra are mainly shown at the middle of the transect, which may correspond to the knolls and depressions occurring along the transect. At scales greater than 120 m, the local wavelet power spectrum increases. The 'global' feature analysis show the spatial variability associated with the broadband NDVI along transect 1 is significantly different at the scales of about 50 m and 120 m from that of the red-noise spectrum (Figure 2.4 A2).

The local spectrum of the NDVI in transect 2 (Figure 2.5 A2) exhibited different local patterns from that observed in transect 1(Figure 2.5 A1). The major difference is that the local spectrum of the NDVI along transect 2 is much stronger than that along transect 1, especially at scales larger than 120 m. The 'global' feature analysis (Figure 2.5 B2) revealed that spatial variability of the NDVI in transect 2 is significantly different from that of the red noise spectrum around the scales of 40 m, 120 m and 180 m. The 40 m and 120 m scales coincide with the

spatial variability of the NDVI in transect 1. However, both ‘global’ features along the two transects did not show spatial variation at the 20 m scale, which was identified by the ground measurements.

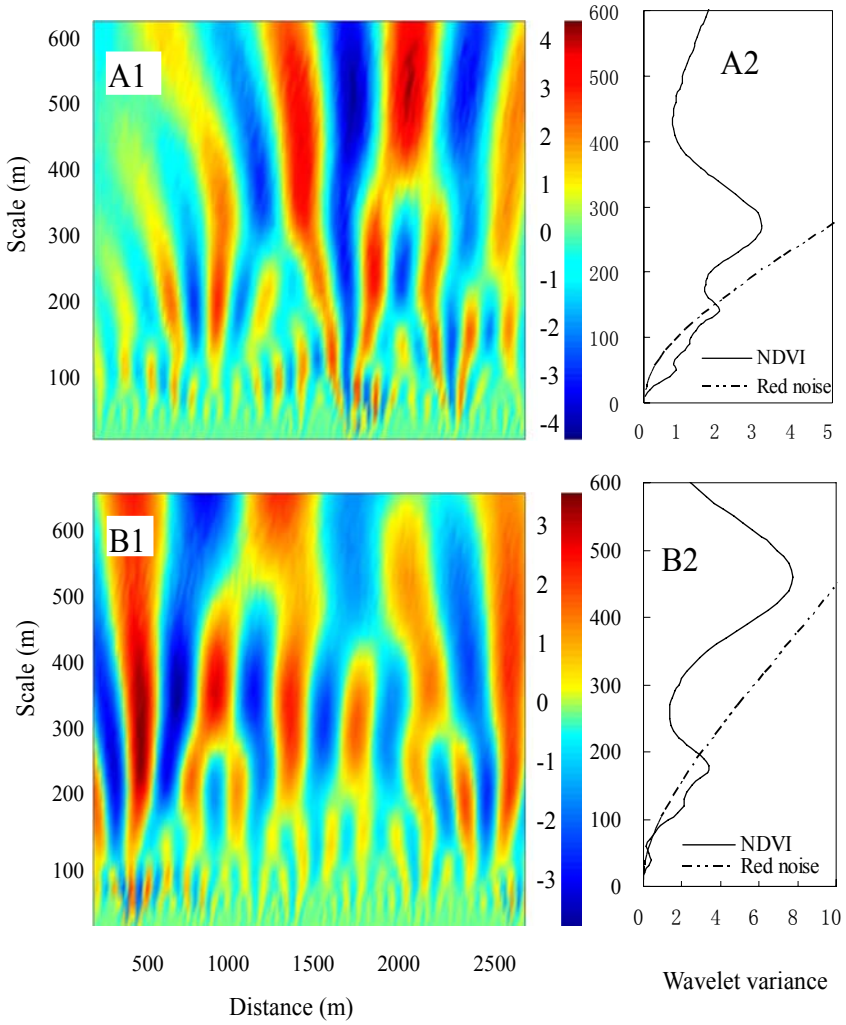


Figure 2.5 The local wavelet spectrum of the broadband NDVI in transect 1(A1) and transect 2 (B1). The wavelet variance of the broadband NDVI in transect 1 (A2) and transect 2 (B2). The solid line in A2 and B2 figures is wavelet variance. The dashed line is the power spectrum of red noise at a confidence level of 95%

## 2.5 Conclusions and Discussion

This study revealed the correlation between LAI and soil moisture, also LAI and topographic parameters (relative elevation, upslope length, and wetness index). The strongest correlation was found between LAI and soil moisture. This is expected because soil water affects the rates of evapotranspiration, photosynthesis, and net carbon assimilation. When water is a limiting factor in semiarid grasslands, the soil moisture is the most important variable controlling vegetation patterns (Flanagan and Johnson, 2005). Soil moisture also affects decomposition and mineralization rates (Rodriguez-Iturbe et al., 1999) and the uptake rate of nitrogen and phosphorus in semiarid environments, which in turn determine the heterogeneity and diversity of grassland vegetation (Loiseau et al. 2005).

LAI is strongly correlates to topographic parameters, which indicates that grassland production depends, to a large extent, on topography. This is also consistent the conclusion by Green and Erskine (2004) that topography explained 38 to 48% of the spatial variance in crop yield. As we know, the growth of vegetation is usually influenced by three key factors: soil water content (Rodiyati et al., 2005), solar radiation (Sellers et al., 1997), and soil organic community (Sebastian, 2004). Soil water content, which is sensitive to soil type and topography, depends largely on the amount of precipitation accumulation, redistribution and runoff (Sellers et al., 1997). Topographic variation has also an effect on the absorption and reflectance or emission of radiation by the surface, which directly affects photosynthesis of plants. Topography affects soil organic content distribution as well, which is the main environmental gradient affecting grasslands vegetation at the landscape scale (Swanson et al., 1988). In conclusion, topography affects soil water content, solar radiation and soil organic content in the mixed grassland, and contributes to the variation of LAI.

The wetness index explained more of the total variation in LAI than both relative elevation and upslope length. This reflects the fact that the wetness index is equal to the ratio of the upslope length to the local slope at a given point in the landscape (Eq. (1)) and, as such, reflects the steepness of the slope at that point. The longer the upslope length is above a point on a hillslope, the more the area contributes snow and snowmelt water to the point. Water is less likely to accumulate at these steeper slopes. Therefore, the wetness index reflects more strongly the water storage in a location than other indicators, thus resulting in higher correlation to the LAI. This result differs from that of Si and Farrell (2004), which showed a stronger correlation between grain yield and upslope length than that between grain yield and wetness index. The different results might result from the difference between natural and cultivated landscapes. In natural grassland landscape, water and organic community accumulation is affected only by topography, whereas in cultivated land, this accumulation is affected by cultivation as well as topography. Cultivation changes water flow pathway and also results in tillage translocation of soil. Permanent vegetation cover traps more snow and reduces snowmelt water runoff; therefore, water accumulation is lower in cultivated area. In addition, grasslands have more well-developed macropore networks than cultivated lands (Bodhinayake and Si, 2004). As a result, grasslands have enhanced water infiltration and reduced runoff. Therefore, water storage in natural grassland is not only dependent upon slope length, but also slope steepness. Consequently, in semi-arid regions, natural vegetation production at a point is sensitive to both the steepness of the slope and the upslope length. It indicates the importance of applying the appropriate topographical parameter to investigate grassland productivity.

NDVI is significantly correlated with LAI and topography parameters, demonstrating that the variation of LAI can be detected by remote sensing data and that the 20 m resolution imagery can reveal, to some extent, the effect of topography on grassland vegetation. The

wetness index explains more of the total variation in the NDVI than relative elevation and upslope length along the three transects. This result matches well with the conclusion from ground biophysical data analysis.

Wavelet analysis showed the spatial variation of soil moisture at scales of 20 m and 40 m, closely associated with the spatial scales of LAI (20 m and 40 m). The effect of soil moisture on the spatial scales of vegetation has also been demonstrated by many other studies (Lange et al., 1982; Vinnikov et al., 1996; Hu and Islam, 1997; Reynolds et al., 1997; Seghieri et al., 1997). Since there is a wide variety of soil types in GNP (Csillag et al., 2001), the two small scales of LAI may result from an integrated effect of other environment factors (soil texture, depth, and chemical and physical properties) on soil moisture. However, soil moisture may vary with time (Green and Erskine, 2004) and the effect of the dynamic nature of soil moisture on LAI is unknown, which is beyond the scope of this study. The small scales also suggest that the imagery resolutions larger than 20 m might not be able to identify all spatial variability resulting from soil moisture in our study area.

Wavelet analysis also showed that topographic factors are responsible for the majority of the spatial variation of LAI at a large scale of about 120 m. These results clearly indicated the effect of topography on vegetation variation in the mixed grassland ecosystem, and provide a guideline for future researchers to select optimum remote sensing imagery for this region. The advantage of topographical data is that they are easy to obtain and relatively time-invariant compared to the measurements of more dynamic soil properties. Therefore, following the sampling theorem (McGrew and Monroe 2000), 30 m (one fourth of a period, 120 m) would be an optimum pixel size to detect potentially important patterns associated with topography in our study area. For example, landscape patterns of LAI, biomass, photosynthetic flux and evapotranspiration of vegetation in the study region can probably be well described using this

fundamental pixel size. Even though 30 m resolution (Landsat imagery) would be an optimum pixel size to detect potentially important patterns, we chose SPOT imagery to perfom analysis in this and following study. The reason that we used SPOT imagery with 20 m resolution but not Landsat imagery with 30 m resolution is that we taking image's quality and availability into account.

Heterogeneity of the broadband NDVI along two 2560 m transects demonstrated that vegetation variation at the large scale 120 m can be detected by SPOT imagery with a 20 m resolution. This result largely confirmed the conclusion that the NDVI variation is also related to topography at landscape scale (Brosofske et al., 1999) and that the appropriate resolution imagery can examine the spatial characteristics associated with topography for landscape level ecosystem studies (Gamon et al., 1993). In addition, the NDVI in transect 1 has a significant spatial scale of 50 m and in transect 2 has a significant spatial scale of 40 m, which must be a result of spatial variation from soil moisture, because ground measurement analysis showed that soil moisture affects grassland variation at relatively small scales (20 m and 40 m). The difference between the 50 m scale and the 20 or 40 m scale may be caused by the change in soil moisture over the years.

Both 'global' features of the NDVI along the two extensive transects did not show spatial variation at the 20 m scale (associated with soil moisture), which is identified by the ground biophysical data. The result is predictable. According to sampling theorems (McGrew and Monroe, 2000), imagery with a 4 m resolution (one fourth of 20 m) would retain most distinct functional properties for grassland variation at the 20 m scale. The resolution of the SPOT image (20 m) used in this study is much coarser than the optimum. This result also indicates that some small features that create heterogeneity (such as soil moisture) might not be

identified at broader scales. In addition, considering soil moisture varies by year, and NDVI may not identify minor spatial variation, a 4 m pixel size may still miss some finer spatial variability at the scale <20m.

The 20-30 m resolution determined from both ground measurement and satellite data is similar to an 18 to 20 m pixel size for Northern California grassland (Gamon et al. 1993). In that study, the 18 to 20 m scale is supposed to capture grassland variation associated with larger patterns of slope, aspect and soil type. The 4 m resolution from this study is comparable to a 6 m pixel size for Southern California grassland (Rahman et al., 2003), which can retain most of the characteristic spatial variation of grassland ecosystem functions. In addition, in the same study area, Davidson and Csillag (2001) also determined that commercially available satellite data at resolutions of 10 to 50 m may offer the potential for estimating coverage of C4 species. Though the first two studies conducted in different grassland ecosystems, and the last study only determined the optimum scale for C4 species coverage, those matches provide confidence in our study’s results. Therefore, we can conclude that, in our study area, a 20-30 m coarse resolution can be used to analyze grassland biophysical spatial variation associated with topography, and a fine resolution (4 m) may capture spatial variation resulting from soil moisture.

In conclusion, the implications of this study are that: (1) in investigating grassland variation, one should consider the effect of both soil moisture and topography, not only at the fine scale but also at the coarse scale; (2) to estimate grassland productivity, applying the appropriate topographical parameter is important; (3) the wavelet approach is useful for revealing both localized and global features of soil moisture and topography that exert significant effects on grassland vegetation; (4) remote sensing data can reveal the variation of grassland biophysical properties and monitor the effect of topography on grassland vegetation by

performing wavelet approach, and (5) 20 to 30 m (one fourth of a period, 120 m) would be an optimum pixel size to detect potentially important patterns associated with topography in our study area.

## 2.6 References

Ahern, F.J., Teillet, P.M., and Goodenough, D.G. 1977. Transformation of atmospheric and solar illumination conditions on the CCRS Image Analysis System. Machine Processing of Remotely Sensed Data Symposium.

Armesto, J.J., Pickett, S.T.A., and Mcdonnell, M.J. 1991. Spatial heterogeneity during succession: a cyclic model of invasion and exclusion, In: Ecological heterogeneity, J. Kolasa and S.T.A. Pickett (Eds.) (New York: Springer-Verlag) pp. 256-269.

Beven, K.J., and Kirkby, M.J. 1979. A physically-based, variable contributed area model of basin hydrology. Hydrology Science Bullet. 24(1), 43-69.

Blomqvist, M.M., Olff, H., Blaauw, M.B., Bongers, T., and van der Putten, W. H. 2000. Interactions between above- and below-ground biota: importance for small-scale vegetation mosaics in a grassland ecosystem. Oikos, 90, 582-598.

Bodhinayake W., and Si, B.C. 2004. Near-saturated surface hydraulic properties under different land use in the St Denis national Wildlife Area, Sasaktchewan, Canada. Hydrological processes. 18, 2835-2850.

Bradshaw, G.A., and Spies, T.A. 1992. Characterizing canopy gap structure in forests using wavelet analysis. Journal of Ecolology. 80, 205-215.

Bradshaw, G.S., and McIntosh, B.A. 1994. Detecting climate-induced patterns using wavelet analysis. Environmental Pollution. 83, 135-142.

Brosofske, K.D., Chen, J., Crow, T.R., and Saunders, S.C. 1999. Vegetation responses to landscape structure at multiple scales across a northern Wisconsin pine barren landscape. Plant Ecology. 143 (2), 203-218.

Bruce, L.M., Morgan, C., and Larsen, S. 2001. Automated detection of subpixel hyperspectral targets with continuous and discrete wavelet transforms, IEEE Transactions on Geoscience and Remote Sensing. 39, 2217-2227.

Brunsell, N.A., and Gillies, R.R. 2003. Determination of scaling characteristics of AVHRR data with wavelets: application to SGP97. International Journal of Remote sensing. 24(14), 2945–2957.

Callaway, R. M., Kikvidze, Z., and Kikodze, D. 2000. Facilitation by unpalatable weeds may conserve plant diversity in overgrazed meadows in the Caucasus Mountains. Oikos, 89, 275-282.

Cohen, W.B., Maiersperger, T.K., Gower, S.T., and Turner, D.P. 2003. An improved strategy for regression of biophysical variables and Landsat ETM+ data, Remote Sensing of Environment. 84, 561-571.

Csillag, F., and Kabos, S. 2002. Wavelets, boundaries, and the spatial analysis of landscape pattern. Ecoscience. 9, 177-190.

Csillag, F., Kertész, M., Davidson, A., and Mitchell, S. 2001. On the measurement of diversity-productivity relationships in a northern mixed grass prairie (Grasslands National Park, Saskatchewan, Canada). Community Ecology. 2, 145-159.

Dale, M.R.T., and Mah, M. 1998. The use of wavelets for spatial pattern analysis in ecology.

Journal of Vegetation Science. 9, 805-814.

Davidson, A., and Csillag, F. 2001. The influence of Vegetation Index and Spatial Resolution on a Two-Date Remote Sensing-Derived Relation to C4 Species Coverage. Remote Sensing of Environment. 75, 138-151.

Deering, D.W., Rouse, J.W., Haas, J.R.H., and Schell, J.A. 1975. Measuring forage production of grazing units from Landsat MSS data. Proceedings, 10th International Symposium on Remote Sensing of Environment. 2, 1169-1178.

Dennis, P., Aspinall, R.J., and Gordon, L.J. 2002. Spatial distribution of upland beetles in relation to landform, vegetation and grazing management. Basic and Applied Ecology. 3, 183-193.

Flanagan, L.B., and Johnson, B.G. 2005. Interacting effects of temperature, soil moisture and plant biomass production on ecosystem respiration in a northern temperate grassland, Agricultural and Forest Meteorology. 130(3-4), 37-253.

Gamon, A., Field, C.B., Roberts, D.A., Ustin, S.L., and Valentini, R. 1993. Functional patterns in an annual grassland during an AVIRIS overflight. Remote Sensing of Environment. 44, 1-15.

Green, T.R., and Erskine, R.H. 2004. Measurement, scaling, and topographic analyses of spatial crop yield and soil water content. Hydrological Processes. 18, 1447-1465.

Griffiths, G.H., Lee, J., and Eversham, B.C. 2000. Landscape pattern and species richness; regional scale analysis from remote sensing, International Journal of Remote Sensing. 21, 2685-2704.

Grinsted, A., Moore, J.C., and Jevrejeva, S. 2004. Application of the cross wavelet transform and wavelet coherence to geophysical time series. Nonlinear Processes in Geophysics. 11, 561-566.

Hu, Z.L., and Islam, S.F. 1997. Effects spatial variability on the scaling of land surface parameterizations. Boundary-Layer Meteorology. 83, 441-461.

Huete, A.R., Didan, K., and Yin Y. 2002. MODIS Vegetation Workshorp, Missoula, Montana, July 15-18; Terrestrial Biophyisics and Remote Sensing (TBRS) MODIS Team, University of Arizona, Available online at: http://utam.geophys.utah.edu/ebooks/gg527/modis/ndvi.html.

Ji, L., and Peters, A.J. 2003. Assessing vegetation response to drought in the northern Great Plains using vegetation and drought indices. Remote Sensing of Environment. 87, 85-98.

Lange, O. L., Nobel, P.S., Osmond, C.B., and Ziegler H. (Eds.) 1982. Physiological Plant Ecology II—Water Relations and Carbon Assimilation, (New York: Springer-Verlag).

Lanzl, F., and Richter, R. 1991. A fast atmospheric correction algorithm for small swath angle satellite sensors, ICO topical meeting on atmospheric, volume and surface scattering and propagation. Florence, Italy. pp. 455-458.

Lark, R.M., and Webster, R. 1999. Analysis and elucidation of soil variation using wavelets. European Journal of Soil Science. 50, 185-206.

Liu, J., Chen, J. M., Cihlar, J., and Park, W. 1997. A process-based Boreal Ecosystems Productivity Simulator using remote sensing inputs. Remote Sensing of Environment. 62, 158-175.

Lobo, A, Moloney, K., Chic, O., and Chiariello, N. 1998. Analysis of fine-scale spatial pattern of

a grassland from remotely-sensed imagery and field collected data. Landscape Ecology. 13, 111-131.

Loiseau, P., Louault, F., Roux, X. L., and Bardy, M. 2005. Does extensification of rich grasslands alter the C and N cycles, directly or via species composition? Basic and Applied Ecology. 6(3), 275-287.

Ludwig, J.A., and Tongway, D.J. 1995. Spatial organization of landscapes and its function in semi-arid woodlands. Landscape Ecology. 10(1), 51-63.

Marceau, D.J., and Hay, G.J. 1999. Remote sensing contributions to the scale issue. Canadian Journal of Remote Sensing. 25, 358-366.

McGrew, J.C., and Monroe, C.B. 2000. An introduction to statistical problem solving in geography (2nd ed.) (Boston: McGraw-Hill) pp. 110.

Mehlum, F., Huntjr, G.L., Klusek, Z., and Decker, M. B. 1999. Scale-dependent correlations between the abundance of Bruunnich's guillemots and their prey. Journal of Animal Ecology. 60, 60-72.

Mi, X., Ren, H., Ouyang, Z., Wei, W., and Ma, K. 2005. The use of the Mexican Hat and the Morlet wavelets for detection of ecological patterns, Plant Ecology. 179, 1-19.

Miller, M.P., Singer, M.J., and Nielsen, D. R. 1988. Spatial variability of wheat yield and soil properties on complex hills. Soil Science Society of America Journal. 52, 1133-1141.

Mitchley, J. 1994. Sward Structure with Regard to Conservation. In: Grassland management and nature conservation, Haggar, R. J. and Peel, S. (Eds.) (England: British Grassland Society) pp.

43-53.

Nellis, M. D., and Briggs, J. M. 1989. The effect of spatial scale on Konza landscape classification using textural analysis. Landscape ecology. 2(2), 93-100.

Plotnick, R.E., Gardner, R.H., and O'Neill, R.V. 1993. Lacunarity indices as measures of landscape texture. Landscape Ecology. 8, 201-211.

Rahman, A.F., Gamon, J.A., Sims, D.A., and Schmidts, M., 2003. Optimum pixel size for hyperspectral studies of ecosystem function in southern California chaparral and grassland. Remote Sensing of Environment. 84(2), 192-207.

Reed, R.A., Peet, R.K., Palmer, M.W., and White, P.S. 1993. Scale dependence of vegetation environment correlations: a case study of a North Carolina piedmont woodland. Journal of Vegetation Science. 4, 329-340.

Redding, T.E., Hope, G.D., Fortin, M.J., Schmidt, M.G., and Bailey, W.G. 2003. Spatial patterns of soil temperature and moisture across subalpine forest-clearcut edges in the southern interior of British Columbia. Canadian Journal of Soil Science. 83, 121-130.

Reynolds, H.L., Hungate, B.A., Chapin, F.S., and D'Antonio, C.M. 1997, Soil heterogeneity and plant competition in an annual grassland. Ecology. 78, 2076-2090.

Richter, R. 1991, Model SENSAT: a tool for evaluating the system performance of optical sensors. SPIE Propagation Engineering. 1312, 286-297.

Rodiyati, A., Arisoesilaningsih, E., Isagi, Y., and Nakagoshi, N. 2005. Responses of Cyperus brevifolius (Rottb.) Hassk. and Cyperus kyllingia Endl. to varying soil water availability.

Environmental and Experimental Botany. 53(3):259-269.

Rodriguez-Iturbe, I., D'Odorico, P., Porporato, A., and Ridolfi, L. 1999. On the spatial and temporal links between vegetation, climate, and soil moisture. Water Resources Research. 35(12), 3709-3722.

Rouse, J.W., Haas, J.R.H., Schell, J.A., and Deering, D.W. 1974, Monitoring vegetation systems in the Great Plains with ERTS. In: Proc. ERTS-1 Symp., 3rd . Greenbelt, MD. 10–15 Dec. 1973. Vol. 1. NASA SP-351. NASA, Washington, DC. pp. 309-317.

Saunders, S.C., Chen, J., Drummer, T.D., Crow, T.R., Brosofske, K.D., and Gustafson E.J. 2002. The patch mosaic and ecological decomposition across spatial scales in a managed landscape of northern Wisconsin, USA. Basic and Applied Ecology. 3, 49-64.

Saunders, S.C., Chen, J., Drummer, D., Gustafson, E.J., and Brosofske, K.D. 2005. Identifying scales of pattern in ecological data: a comparison of lacunarity, spectral and wavelet analyses. Ecological Complexity. 2(1), 87-105.

Schmidtlein, S., and Sassin, J. 2004. Mapping of continuous floristic gradients in grasslands using hyperspectral imagery. Remote Sensing of Environment. 92, 126-138.

Sebastian, M.T. 2004, Role of topography and soils in grassland structuring at the landscape and community scales. Basic and Applied Ecology. 5(4), 331-346.

Seghieri, J., Galle, S., Rajot, J.L., and Ehrmann, M. 1997. Relationships between soil moisture and growth of herbaceous plants in a natural vegetation mosaic in Niger. Journal of Arid Environments. 36(1), 87-102.

Sellers, P.J., Heiser, M.D., Halla, F.G., Vexma, S. B., Desjardins, R. L., Scheppe, P. M., and Macpherson, J. I. 1997. The impact of using area-averaged land surface properties-topography, vegetation condition, soil wetness-in calculations of intermediate scale (approximately 10 km') surface-atmosphere heat and moisture fluxes. Journal of Hydrology. 190(3-4), 269-301.

Shiyomi, M., Okada, M., Takahashi, S., and Tang, Y. H. 1998. Spatial pattern changes in aboveground plant biomass in a grazing pasture. Ecological Research. 13, 313-322.

Si, B.C. 2003. Scale and location dependent soil hydraulic properties in nonlevel landscapes. Scaling methods in soil physics (Y. Pachepsky, D. Radcliffe, and H.M. Selim, Eds) (Boca Raton, FL: CRC Press,) pp. 163-178.

Si, B.C., and Farrell, R.E. 2004. Scale-dependent relationship between wheat yield and topographic indices: a wavelet approach. Soil Science Society of America Journal. 68(2), 577-587.

Shumway, R. H., and Stoffer, D.S. 2000. Time series analysis and its applications. Springer-Verlag. New York.

Söderström, B., Svensson, B., Vessby, K., and Glimskär, A. 2001. Plants, insects and birds in semi-natural pastures in relation to local habitat and landscape factors. Biodiversity and Conservation. 10, 1839-1863.

Swanson, F. J., Kratz, T.K., Caine, N., and Woodmansee, R.G. 1988. Landform effects on ecosystems pattern and processes, BioScience. 38(1), 92-98.

Turner, S.J., O'Neill, R.V., Conley, W., Conley, M.R., and Humphries, H.C., 1991, Pattern and

scale: statistics for landscape ecology. In: Quantitative Methods in Landscape Ecology M.G. Turner and R.H. Gardner (Eds.) (Berlin: Springer-Verlag) pp. 18–49.

Torrence,T., and Compo, G.P. 1998. A practical guide to wavelet analysis. Bulletin of the American Meteorological Society. 79(1), 61-78.

Vinnikov, K.Y.A., Robock, A., Speranskaya, N.A., and Schlosser, C.A. 1996. Scales of temporal and spatial variability of midlatitude soil moisture. Journal of Geophysical Research. 101( D3), 7163-7174.

Wendroth, O., Alomran, A.M., Kirda, C., Richardt, K., and Nielsen, D.R. 1992. State-space approach to spatial variability of crop yield. Soil Science Society of America Journal. 56(3), 801-807.

Zhang, C. 2006. Monitoring Biological Heterogeneity in a Northern Mixed Prairie Using Hierarchical Remote Sensing Methods. Ph.D. Thesis, University of Saskatchewan.

# CHAPTER 3 –SUITABLE VEGETATION INDICES FOR STUDYING THE MIXED GRASSLAND ECOSYSTEM

## 3.1 Abstract

Remote sensing data can be effectively exploited for the study of ecosystem patterns and processes. However, remote sensing of semi-arid mixed grassland faces a challenge: to well understand the performance of different vegetation indices (VIs) in estimating biophysical properties of grassland with low amount of green vegetation, high amount of dead material on the ground and variable soil/ground conditions. Using ground-based hyperspectral, and biophysical data, this study has compared the predictive capability of VIs for estimation of grassland leaf area index (LAI). Results indicated that the relationships between grassland LAI and VIs are significant. The performance of the RDVI (Renormalized Difference Vegetation Index), ATSAVI (Adjusted Transformed Soil-Adjusted Vegetation Index), and MCARI2 (Modified Chlorophyll Absorption Ratio Index 2) were slightly better than the other VIs in the groups of ratio-based, soil-line-related, and chlorophyll-corrected VIs, respectively. By incorporating CAI (Cellulose Absorption Index) as a litter factor in ATSAVI, a new VI was computed (L-ATSAVI) and it improved LAI estimation capability in our study area by about 10%. In order to further confirm if the 20-30 m pixel size discovered in Chapter 2 is optimum to study the mixed grassland ecosystem, the scale of ground-based hyperspectral data and LAI along the transect has been simulated using low-pass filtering procedure with a 30 m moving window. Statistical analysis indicated that scale-simulated L-ATSAVI can explain much more

grassland LAI ($r^2$ up to 89%) than original finer resolution. This conclusion can be further applied to select optimal pixel size of remote sensing image and to detect hierarchical characteristics in grassland landscape.

## 3.2 Introduction

Leaf area index (LAI) is an important parameter in the ecosystem models and LAI can be used to estimate biophysical processes (e.g. spatial structure, heterogeneity, net primary production) and to infer to biochemical processes (e.g., photosynthesis and transpiration) of terrestrial ecosystems (Bonan, 1993; Pierce & Running, 1988). Therefore, LAI is chosen as a grassland biophysical parameter to study the mixed grassland ecosystem in this study.

Over the years, the quantification and variability of plant biophysical properties (such as LAI) have been estimated indirectly by use of VI from remotely sensed data (Badhwar et al., 1986; Peterson et al., 1987; Turner et al., 1999). These indices can roughly be grouped into two classes: biophysical indices and biochemical indices. Biophysical indices are those traditional or improved traditional indices, designed to correlate to vegetation structure and condition, such as simple ratio-based indices (Rouse et al., 1974; Pearson and Miller, 1972), soil-line-related indices (Qi, et al., 1994), and chlorophyll-corrected indices (Haboudane et al., 2004). These indices normally show strong relationships with vegetation biophysical properties (e.g. LAI and biomass) and weak relationships with leaf biochemical constituents (e.g. cellulose, chlorophyll, nitrogen, pigment, and water) (Zarco-Tejada, 2000). Biochemical indices are mainly used to estimate vegetation biochemical properties such as cellulose content (Daughtry et al., 1996). Example of such an index is CAI (Cellulose Absorption Index).

Based on the designed purpose, the biophysical vegetation indices have the theoretical advantage over biochemical indices in quantifying vegetation LAI. This theoretical advantage has been demonstrated by Broge and Lablance (2001), which compared the predictive power and stability of all VIs in estimating LAI, and found that SAVI2 (Second Soil-Adjusted VI, the biophysical index) is the best predictor of LAI, while that the biochemical indices poorly estimate LAI. Therefore, the emphasis in this study is to choose or develop VIs which have biophysical and biochemical basis for estimating LAI.

Even though some VIs have shown a satisfactory correlation with LAI, researchers generally face a challenge in using VIs because of the large non-vegetation component found (Guo, 2002; Tucker, 1979). This challenge was specifically true in our study area, the semi-arid mixed grassland ecosystem. The challenge with using VIs in the semi-arid environment is to remove the contribution of litter, soil, and other canopy characteristics (e.g. chlorophyll content) from plant spectral response (Rundquist, 2002). Specifically, the effects of dead litter, which often dominates the total fraction of aboveground biomass (Asner et al., 1998; Guo, 2002) and varies with different microclimatic conditions (Van Leeuwen and Huete, 1996), presents a serious problem to the interpretation of vegetation indices (Duncan et al., 1993). The contribution of bare soil extent and soil brightness is a significant barrier to the determination of LAI, energy absorption, and net primary productivity (NPP), and has also been widely recognized (Graetz and Gentle, 1982; Huete, 1988; Asrar et al., 1992). The chlorophyll content, which affects canopy reflectance in a spectral region similar to that of LAI (i.e., from the green (550 nm) to the red edge (750 nm)), thus affects the accuracy of LAI estimation and is hard to uncouple (Haboudane et al, 2004). In our study area, standing dead, moss, lichen, litter, rock, and bare soil constituted 47.2% of the ground cover (Zhang et al., 2005), and dead material composed of 47.0% of the total biomass (Guo et al., 2005).

In view of the challenge, substantial efforts were made in improving the current indices and in developing new indices aimed to compensate for the soil background influences (Bannari et al., 1996; Baret et al., 1989; Huete, 1988; Qi et al., 1994; Rondeaux et al., 1996), for atmospheric effects (Karnieli et al., 2001), for other canopy components such as litter (Nagler et al., 2003) and chlorophyll (Haboudane, et al., 2002). However, the effect of both bare soil and litter on the LAI-vegetation index relationship remains an unsolved problem. Furthermore, it is difficult to infer from existing studies which VI has the advantages in estimating LAI over other indices for our study area, in which litter is a dominant constituent of the canopy components.

Based on the preceding background, the goal of this research is to evaluate the performance of various hyperspectral vegetation indices in characterizing grassland biophysical variables in the mixed grassland ecosystem. Specifically, the goal of this paper is to: 1) examine the sensitivity of commonly-used hyperspectral VIs to LAI; 2) investigate the performance of a new hyperspectral vegetation index that aims to reduce the effects of litter and bare soil simultaneously on canopy reflectance in our study area; 3) further demonstrate if the determined 20-30 m resolution is suitable for studying the mixed grassland ecosystem.

### 3.3. Study Area and Data Collection

The study was conducted in Grasslands National Park, Saskatchewan, Canada (GNP). The area is characterized as a semi-arid mixed grass prairie ecosystem. The study site is located in the West Block of Grasslands National Park which consisted of an upland grass ecosystem. Field data collection was performed in the summer of 2004 along five parallel transects (381 m in length) across the landscape separated by a lateral distance of 10 m between transects. LAI, relative elevation, and reflectance measurements were taken at quadrats with 3 m intervals along

the center transect (128 locations) and at quadrats with 6 m intervals along other four transects (64 locations per transect). LAI was measured using a LiCOR LAI-2000 Plant Canopy Analyzer (LiCor Inc., Lincoln Nebraska) and a laser theodolite (ATT Metrology Services, Inc., Redmond, Wash.) was used to measure relative elevation, which is the vertical distance from the surface to a reference point. All following analysis used data from the center transect since measurements between 5 transects are not significantly different from each other.

Canopy reflectance was measured using an Analysis Spectral Devices, Inc. (Boulder, Colo.) FR Pro Spectroradiometer. The measurement wavelength range was 350-2500 nm, and the spectral resolution was 3 nm at 700 nm and 10 nm at 1400 nm and 2100 nm. The 25° field of view probe was used pointing down at the canopy at approximately 1 meter above ground. Measurements were taken within two hours of solar noon on sunny days. Calibration was made using a white spectralon reflectance panel (Labsphere, Inc., North Sutton, N.H.) at approximately 10 minute intervals to minimize the atmospheric condition changes.

### 3.4. Methodology

During the past decade the wavelengths applied in vegetation studies have been concentrated to VIS and NIR spectral regions because of i) the relatively high radiation absorption of red light (comparing with less radiation absorption of green and blue light) by leaves due to the presence of chlorophyll, and ii) the high reflectance of NIR light due to scattering in the leaf internal structure (Curran, 1980). However, studies have shown these wavelength regions to be unreliable measures of green vegetation, because of other factors (atmospheric composition, irradiance conditions, sun angle, soil color, and amount of litter) also contributing to the spectral reflectance. To reduce these effects, some factors (atmospheric

composition, irradiance conditions, and sun angle) have been studied and correctly modeled in physical models; other factors (soil color and amount of litter) have been redressed by translating reflectance data into a VI (Moulin & Guérif, 1999), usually calculated from the red and NIR bands. Numerous VIs have been developed, and they generally attempt to enhance the spectral reflectance of green plant fractions while minimizing the spectral effects caused by other variations in other factors. A detailed discussion on VI theory can be found in Huete (1989).

Exhaustive comparative studies have been already carried out to assess the predictive power of the different optical indices and their sensitivity to various canopy parameters and external factors (e.g., Broge and Leblanc, 2001; Chen, 1996; Haboudane et al., 2004). Nevertheless, few studies have evaluated the sensitivity of different VIs to biophysical properties of the mixed grassland. In this section, we adopted several commonly-used hyperspectral vegetation indices that are developed for vegetation biophysical properties, to compare their sensitivity to grassland LAI. Our list of indices was not exhaustive, but covered the major formulations and presents some of the latest indices as well.

### 3.4.1 Biophysical VIs Selected for This Research

The selected biophysical VIs (Table 3.1 with explanations) can be grouped into three categories: ratio-based VIs (NDVI, RDVI, and MSR), soil-line-related VIs (PVI, SAVI, MSAVI, TSAVI, ATSAVI and SARVI), and chlorophyll-corrected VIs (TVI, MCARI, MCARI1, MTVI1, MCARI2, and MTVI2). Basically, ratio-based VIs have been developed, based on the ratio of reflectance in the red-NIR regions of the electromagnetic spectrum to increase contrast and remove effects from the soil background (Elvidge and Lyon 1985, and Huete et al. 1985). Soil-line-related VIs have been developed to minimize the soil background influence by

establishing a soil line to characterize the soil spectra (Baret et al., 1989; Baret et al., 1992; Huete, 1988; Qi, et al., 1994). The soil line defined by the coefficients a and b gives the slope and intercept as determined by the linear regression of the soil reflectance in the red-NIR spectral regions (Richardson and Wiegand, 1977). Chlorophyll-corrected VIs were proposed to be more responsive to green LAI variations by suppressing the ratio of NIR to Red to lower the sensitivity to chlorophyll effects (Haboudane et al., 2004).

Table 3.3 Biophysical VIs investigated in this study

| VI | Name | Equation | Advantages | Reference |
|---|---|---|---|---|
| NDVI | Normalized Difference Vegetation Index | $\frac{\rho_{800}-\rho_{670}}{\rho_{800}+\rho_{670}}$ | Responds to changes in the amount of green biomass | Rouse et al., 1974; Haboudane et al., 2004 |
| RDVI | Renormalized Difference Vegetation Index | $\frac{\rho_{800}-\rho_{670}}{\sqrt{\rho_{800}+\rho_{670}}}$ | Suitable for low and high LAI values | Reujean and Breon, 1995; Haboudane et al., 2004 |
| MSR | Modified Simple Ratio | $(\frac{\rho_{800}}{\rho_{670}}-1)\Big/\sqrt{\frac{\rho_{800}}{\rho_{670}}+1}$ | More linearly related to vegetation parameters than RDVI. | Chen, 1996; Haboudane et al., 2004 |
| PVI | Perpendicular Vegetation Index | $\frac{\rho_{800}-\rho_{670}-b}{\sqrt{1+a^2}}$ | Minimizes the soil background influence based on the Euclidean distance to the soil line. | Richardson and Wiegand, 1977 |
| SAVI | Soil Adjusted Vegetation Index | $(1+L)\frac{(\rho_{800}-\rho_{670})}{\rho_{800}+\rho_{670}+L}, L=0.5$ | Minimizes the soil background influence by combining a canopy background adjustment factor, L. | Huete, 1988; Haboudane et al., 2004 |
| MSAVI | Modified Soil Adjusted Vegetation Index | $\frac{1}{2}\left[2(\rho_{800}+1)-\sqrt{(2\rho_{800}+1)^2-8(\rho_{800}-\rho_{670})}\right]$ | Less affected by canopy variations as well as soil spectra properties. | Qi, et al., 1994 ; Haboudane et al., 2004 |
| TSAVI | Transformed Soil-Adjusted Vegetation Index | $\frac{a(\rho_{800}-a\rho_{670}-b)}{a\rho_{800}+\rho_{670}-ab}$ | Less affected by soil background and better for estimating homogeneous canopy. | Baret et al., 1989 |
| ATSAVI | Adjusted Transformed Soil-Adjusted Vegetation Index | $\frac{a(\rho_{800}-a\rho_{670}-b)}{a\rho_{800}+\rho_{670}-ab+X(1+a^2)}$, X=0.08 | | Baret and Guyot, 1991 |

| | | | | |
|---|---|---|---|---|
| SARVI | Soil and Atmospheric Resistant Vegetation Index | $(1+L)(\rho_{800}-\rho_{rb})/(\rho_{800}+\rho_{rb}+L)$ *Where* $\rho_{rb}=2\rho_{red}-\rho_{blue}, L=0.5$ | Minimizes both canopy background and atmospheric effects. | Kaufman and Tanre, 1992; Haboudane et al., 2004 |
| TVI | Triangular Vegetation Index | $0.5[120(\rho_{750}-\rho_{550})-200(\rho_{670}-\rho_{550})]$ | Characterizes the radiant energy absorbed by leaf pigments. | Broge and Leblanc, 2001 |
| MCARI | Modified Chlorophyll Absorption Ratio Index | $[(\rho_{700}-\rho_{670})-0.2(\rho_{700}-\rho_{550})](\rho_{700}/\rho_{670})$ | Responsive to chlorophyll variation. | Daughtry et al., 2000 |
| MCARI 1 | Modified Chlorophyll Absorption Ratio Index 1 | $1.2[2.5(\rho_{800}-\rho_{670})-1.3(\rho_{800}-\rho_{550})]$ | Less sensitive to chlorophyll effects, more responsive to green LAI variations. | Haboudane et al., 2004 |
| MTVI1 | Modified Triangular Vegetation Index 1 | $1.2[1.2(\rho_{800}-\rho_{550})-2.5(\rho_{670}-\rho_{550})]$ | More suitable for LAI estimations than TVI. | Haboudane et al., 2004 |
| MCARI 2 | Modified Chlorophyll Absorption Ratio Index 2 | $\frac{1.5[2.5(\rho_{800}-\rho_{670})-1.3(\rho_{800}-\rho_{550})]}{\sqrt{(2\rho_{800}+1)^2-(6\rho_{800}-5\sqrt{\rho_{670}})-0.5}}$ | Preserves sensitivity to LAI as well as resistance to chlorophyll influence. | Haboudane et al., 2004 |
| MTVI2 | Modified Triangular Vegetation Index 2 | $\frac{1.5[1.2(\rho_{800}-\rho_{550})-2.5(\rho_{670}-\rho_{550})]}{\sqrt{(2\rho_{800}+1)^2-(6\rho_{800}-5\sqrt{\rho_{670}})-0.5}}$ | | Haboudane et al., 2004 |

Note: The coefficients a (gain) and b (offset) in the equations for PVI, TSAVI, and ATSAVI are derived from the NIR vs. Red rock-soil baseline. In our study area, a is 1.22 and b is 0.03 (X. Guo, unpublished data). ρ, reflectance.

The detailed formulation and proposed advantages can be found from Table 3.1. When reflectance measured in bands is used in the formulation of a VI, the band centre wavelength is provided as a subscript (in nanometers). Many of the VIs' formulations encompass the red band (670 nm) and/or the NIR band (800 nm), but some also include the green band (550 nm). These spectral regions are used because they relate to abundance and activity of green vegetation, including LAI, percentage green cover, chlorophyll content, green biomass, and absorbed photosynthetically active radiation (Jensen, 2000).

### 3.4.2 New Vegetation Index for LAI Prediction

Among the vegetation indices mentioned above, ATSAVI index was developed to consider the actual gain (a) and intercept (b) values of the soil line and an adjustment factor X, which is set to minimize background effects (X = 0.08 in the original paper by Baret and Guyot, 1991). Therefore, this index has strong theoretical basis to be a good LAI indicator in certain areas with soil background variations. However, this index has limitations in removing the effect of litter; this has been demonstrated by Van Leeuwen and Huete (1996) who found that soil-line-related VIs are difficult to estimate LAI with increasing litter amount mixed with green vegetation. For this reason, we developed modified versions of ATSAVI that are suitable in LAI estimation in our study area. The central idea behind this modification was to render the index (ATSAVI) less sensitive to both soil background and litter effects and to be more responsive to green LAI variations.

We incorporated a litter adjustment factor to ATSAVI to minimize litter effects. The CAI was adopted as the litter adjustment factor because of its usefulness in discriminating plant litter from soil and green vegetation (Nagler et al., 2003). It has been demonstrated that the vegetation CAI will change depending on the proportion of litter when litter is a fraction of aboveground biomass. The litter-corrected ATSAVI (L-ATSAVI) is formulated as:

$$\text{L-ATSAVI} = \frac{a(\rho_{800} - a\rho_{670} - b)}{a\rho_{800} + \rho_{670} - ab + X(1 + a^2) + L \times CAI} \quad (1)$$

Where, ρ is the reflectance (with the subscript indicating the wavelength) and CAI= $0.5 \times (\rho_{2000} + \rho_{2200}) - \rho_{2100}$; therefore,

$$\text{L-ATSAVI} = \frac{a(\rho_{800} - a\rho_{670} - b)}{a\rho_{800} + \rho_{670} - ab + X(1+a^2) + L \times (0.5 \times (\rho_{2000} + \rho_{2200}) - \rho_{2100})} \quad (2)$$

In L-ATSAVI formulation (1) and (2), we multiplied CAI L times to enlarge the litter effects while considering that the negative correlation of both soil and green leaves to litter could counteract the positive relationship between CAI and litter (Nagler et al., 2003). L is a litter adjusting factor and depends on the proportion of litter, soil, and green aboveground biomass. We changed L value from 0 to 100 with 0.5 interval to examine the relationship between L-ATSAVI and LAI, and found L = 10 to be the optimal adjustment factor in reducing litter noise in this study. Further research is needed to explore the adjustment of the L factor in order to optimize the normalization of litter influence over a wide range of cover situations.

### 3.4.3 Statistical Analysis

VIs are often related to LAI through a linear or exponential regression model, depending on the presence of saturation effects. Wang et al. (2005) found that strong linear relationships are obtained between VIs and LAI when LAI is low, but the relationship is poor during periods of maximum LAI. Linear regression models were appropriate for our study area as it is a semi-arid grassland with sparse vegetation, thus no saturation occurs. The performances of VIs in LAI estimation were evaluated by comparing $r^2$, which is the proportion of variation in the dependent variable explained by the regression model based upon a significance level (99%). A t-test and a one-way analysis of variation (ANOVA) were applied to the means of $r^2$ values among different classes of vegetation indices in order to detect significant differences. In this paper, regression models were validated using the Jack-Knife cross-validation method. This approach is implemented by withholding one sample and building the regression model using the

data from the remaining samples. The process of removing one sample from the dataset was repeated until all samples had been withheld.

### 3.4.4 Scale-simulated Method

With the discovery of the dominant spatial variation of grassland LAI through the wavelet approaches, we determined that the optimal pixel size of remotely sensed data is 20-30 m for studying the mixed grassland ecosystem. In order to confirm whether the discovered 20-30 m resolution is appropriate, we simulated hyperspectral and LAI data along the transect at this scale with a moving window using "low-pass filtering procedure". This filtering procedure involves moving a 'window' of certain measurements (new scale /3 m interval) along the transect, and replacing the central measurement with the new value averaged from these measurements within each window. The calculation is repeated until the entire transect has been filtered and a "new" transect with "new scale" interval has been generated. The result is expected to reduce the high frequency noise of data and be more representative of grassland at the landscape level. Using simulated hyperspectral and LAI data, again we calculate L-ATSAVI. By comparing $r^2$ of scale-simulated L-ATSAVI and LAI with original r2, we can demonstrate whether or not the proposed spatial scale is appropriate for grassland LAI at the landscape level.

## 3.5 Results and Discussion

### 3.5.1 Grassland LAI Characteristics

Figure 3.1 illustrates the characteristics and distribution of LAI in a grassland environment. The measured LAI ranged from 0 to 2.5 and averaged 1.09 (Figure 3.1). The Kolmogorov-Smirnov Test indicated that the measured LAI distribution corresponds to the

normal distribution ($p>0.05$). Comparing the LAI with relative elevation (Figure 3.1), a similar trend can be observed: large LAI values in the depressions and small LAI values on the knoll. The Paired Samples Test showed that there is no significant difference between the means for LAI and relative elevation (Green and Salkind, 2003). This result indicates that spatial variation of grassland LAI within our study area exhibits localized features, which may be related to spatial variation of relative elevation. Considering the relationship between LAI and relative elevation is only from the limited dataset used in this study, the relationship between LAI and topography should be investigated further in future research.

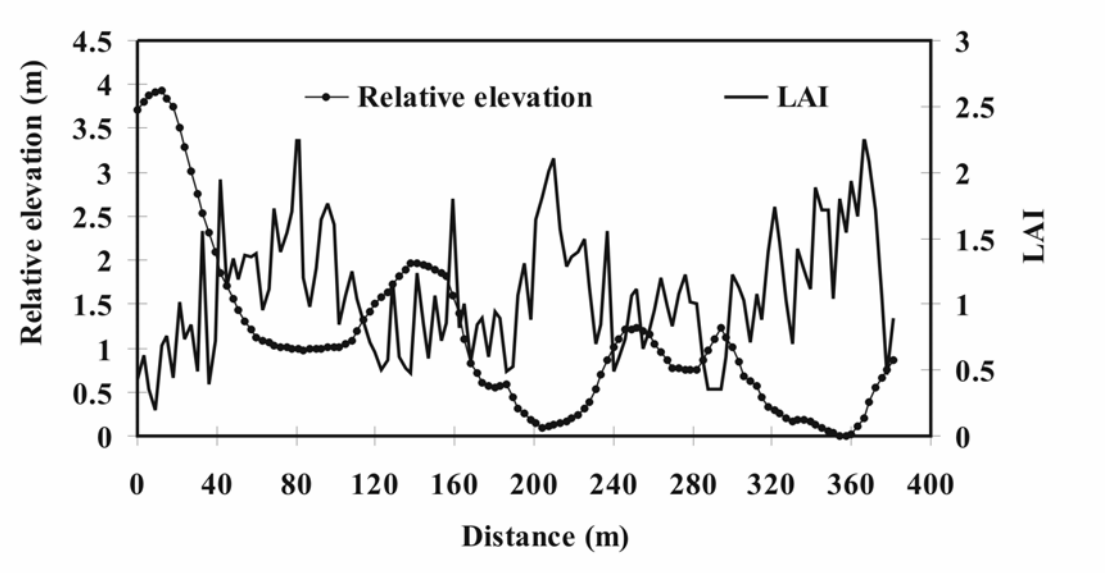


Figure 3.1 Grassland LAI and the measured relative elevation (the vertical distance from surface to a reference point)

### 3.5.2 Spectral Reflectance Characteristics

Different biophysical and biochemical properties of vegetation contribute to the spectra of vegetation (Gates et al., 1965; Knipling, 1970). Figure 3.2 shows the reflectance spectra of

mixed grassland for our study site. Spectral reflectance of the mixed grassland has general features similar to that of typical vegetation - red absorption region, near-infrared (NIR) reflectance region and water absorption regions. The absorption and reflectance regions, however, are not as strong as those of typical vegetation. For example, in the mixed grassland, the reflectance is much higher in the green reflection region and weaker in the NIR region, compared to the spectral curve of typical vegetation.

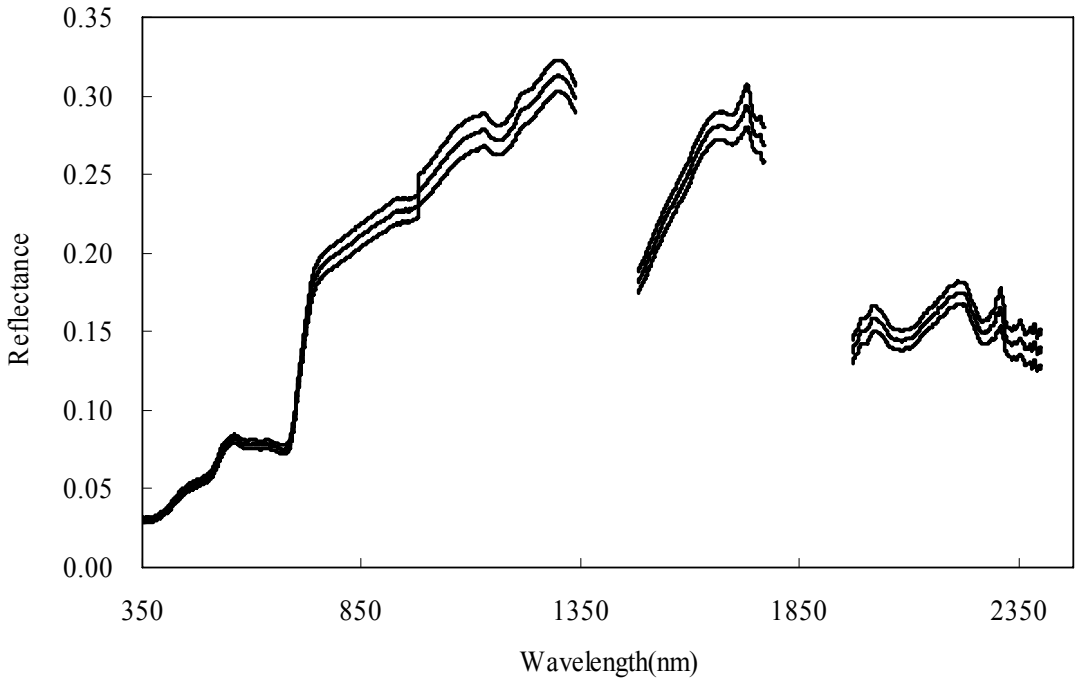


Figure 3.2 Hyperspectral response curve of mixed grassland within our study site with 95% upper and lower confident limits (UCL & LCL). Three primary water absorption (noise) regions (1361-1395 nm, 1811-1925 nm, 2475-2500 nm) for the field measurements were deleted

### 3.5.3 Relationships Between LAI and Biophysical VIs

To determine the optimal VIs in estimating grassland LAI, the $r^2$ values between VIs and LAI were computed and are shown in Figure 3.3. All of the $r^2$ values are significant ($P<0.01$), which indicates a high correlation between grassland LAI and the selected VIs. Among the three groups of biophysical VIs, the range of $r^2$ found with ratio-based VIs (0.42-0.44), and in soil-line-related VIs (0.40-0.44) were better than the $r^2$ range found with chlorophyll-corrected VIs (0.37-0.40). ANOVA results also confirmed that $r^2$ values of chlorophyll-corrected VIs were significantly different from that of ratio-based and soil-line-related VIs, which may be explained by the emphasis of these three groups and vegetation condition of our study area. Both ratio-based VIs and soil-line-related VIs were developed to reduce either soil brightness or background effects, which are major limiting factors in the semi-arid mixed grassland. Chlorophyll-corrected VIs focus on decreasing the chlorophyll effect. However, the effect from chlorophyll may not be as strong as the effect from soil and litter in grass spectra since the average LAI was found to be very low in the study area. It has been demonstrated that chlorophyll-corrected indices are the best green LAI indicators in agriculture area (Haboudane et al., 2004). However, the results from this paper were derived from a limited dataset, and the performance of chlorophyll-corrected VIs has to be further investigated in semi-arid regions.

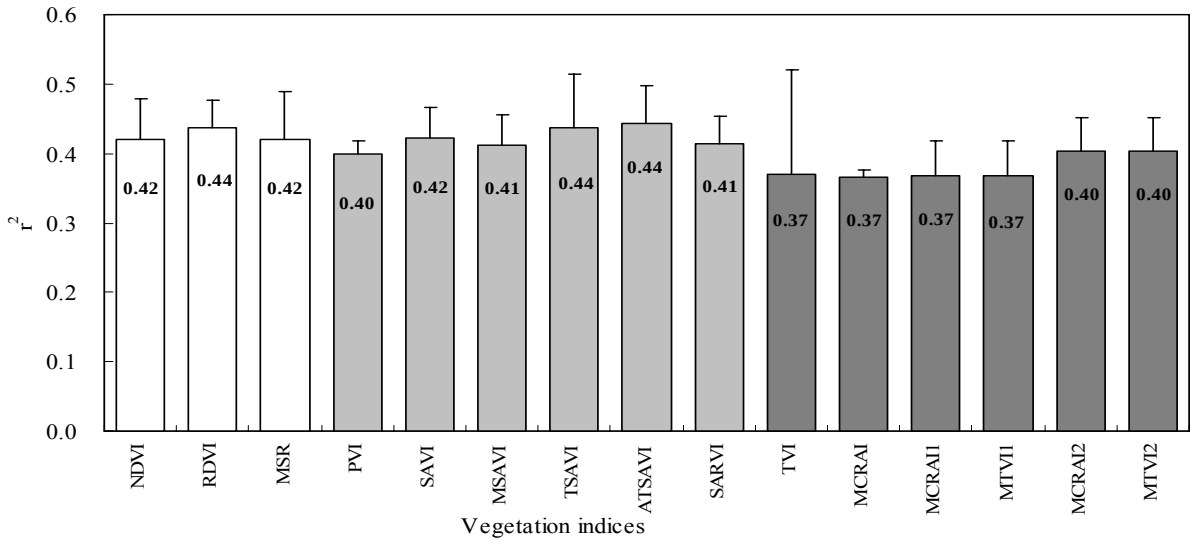


Figure 3.3 The $r^2$ values with error bar between LAI and VIs in the three groups. All evaluated VIs show a significant relationship with LAI at a 0.01 significance level (128 samples)

Within each group, $r^2$ values of RDVI (0.44), ATSAVI (0.44), and MCRAI2 (0.40) are slightly higher than for other VIs in their groups. The performance of RDVI, ATSAVI, and MCRAI2 over other VIs can be explained from their abilities in softening background effects. RDVI is a hybrid index between DVI and NDVI, and combines the advantages of DVI and NDVI for low and high vegetation coverage, respectively. ATSAVI incorporates the actual gain (a) and intercept (b) values of the soil line rather than assuming them to be 1 and 0 respectively; furthermore, it involves adjustment factor X, which is set to further minimize background effects. MCRAI2 is optimized with the constraint of preserving the sensitivity to LAI as well as the resistance to chlorophyll influence. Therefore, these indices have more robust theoretical basis over other VIs in their groups, to deal with low average LAI with high variation of vegetation coverage in the mixed grassland.

### 3.5.4 Relationship Between LAI and L-ATSAVI

The $r^2$ value of LAI and L-ATSAVI is 0.55 which is higher than that of LAI and other VIs (Figure 3.4). This result indicates that incorporating CAI into ATSAVI can improve the ability of LAI estimations in our study area at about 10%. This is expected because there is large amount of litter material in our study area, and CAI increases linearly as the amount of plant litter increased from 0% (bare soil) to 100% cover (Nagler et al., 2003). However, the efficiency of this index has to be further tested based on more data from different sites. Further comparison found that $r^2$ values between LAI and VIs in our study area are much lower than that from other study areas, such as agriculture field ($r^2$ ranging from 0.7-0.9) (Haboudane et al., 2004) and forest area ($r^2$ is approximatly 0.7) (Kovacs et al, 2004). This result suggests further research to develop more robust vegetation indices for semi-arid mixed grassland ecosystems.

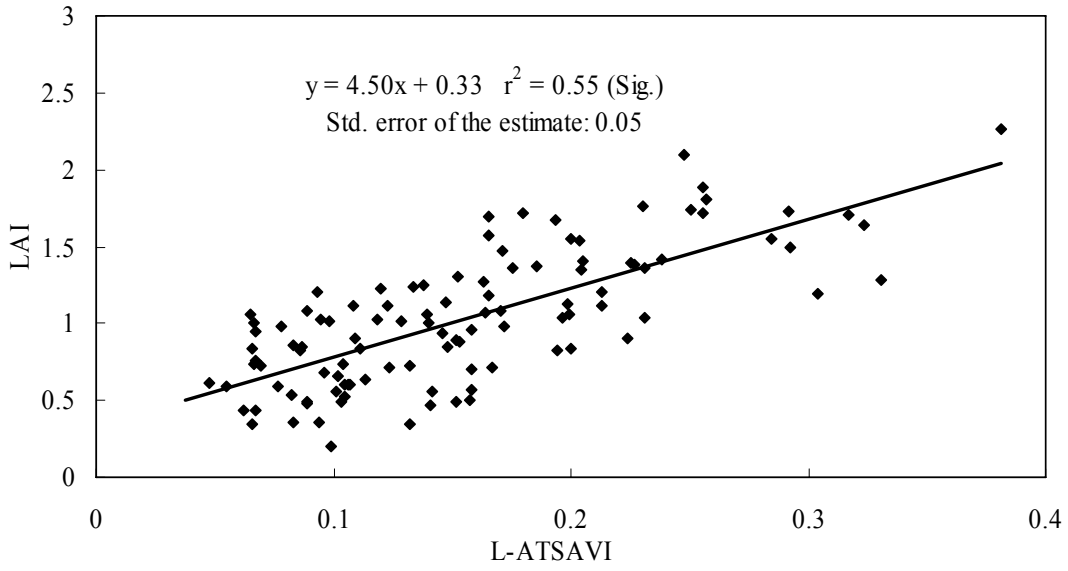


Figure 3.4 Regression equation and $r^2$ between ATSAVI1 and LAI

### 3.5.5 The Scale-simulated Results

With a moving window of 30 m, the scale of hyperspectral VI and LAI was simulated at the landscape level. All proposed indices were calculated again. The $r^2$ values between scale-simulated VIs and LAI were presented in Figure 3.5. The results indicated that scale-simulated VIs can explain much more grassland LAI. The Paired-Samples T Test also showed that there is a significant difference between scale-simulated $r^2$ and original $r^2$. The maximum $r^2$ was still found with the relationship between grassland LAI and L-ATSAVI, explaining 89% of grassland LAI and making a great improvement over the original L-ATSAVI, (which explains only 55% of grassland LAI). The scale-simulated results indicate that grassland LAI can be better explained by upscaling the resolution of remote sensing data to 30 m rather than utilizing a finer resolution of 3 m. This further confirms that the spatial scale of about 30 m can be used to analyze the grassland biophysical properties at the landscape level in our study area.

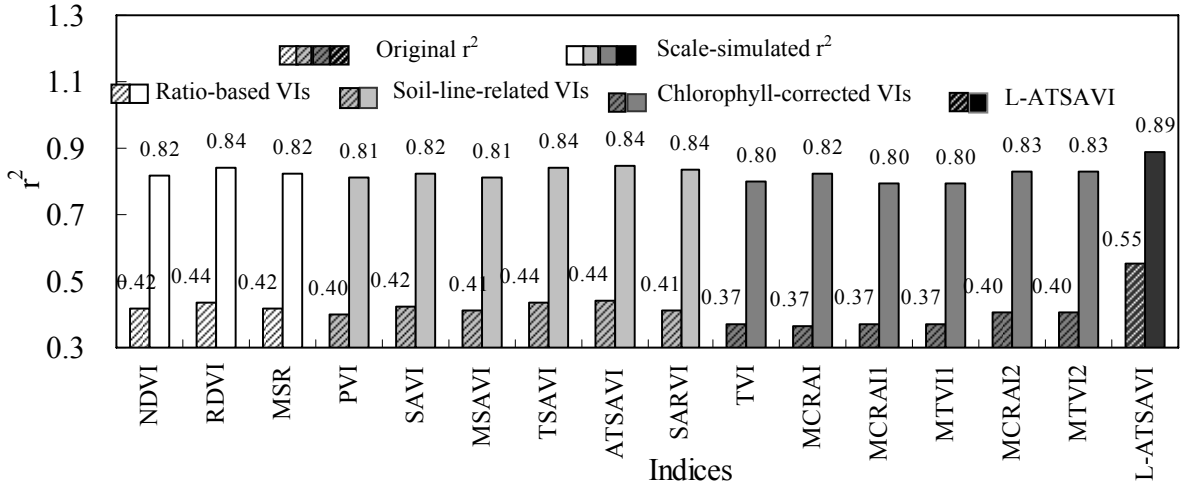


Figure 3.5 Comparison of scale-simulated $r^2$ with original $r^2$ between LAI and VIs

## 3.6 Conclusions

The relationships between grassland LAI and selected VIs were found to be significant. Among the biophysical indices, ratio-based VIs and soil-line-related VIs were better than chlorophyll-corrected VIs in LAI estimation. Of the three groups of VIs investigated in this study: ratio-based, soil-line-related, and chlorophyll-corrected, RDVI, ATSAVI, and MCRAI2 where the best of each category (respectively) for estimation of grassland LAI.

The litter-corrected ATSAVI (L-ATSAVI) appeared to be the best indicator in estimating LAI. L-ATSAVI could explain 55% of grassland LAI and improved LAI estimation capability in our study area by about 10% compared with other selected VIs. This result indicates that previous vegetation indices have limitations in removing the effect of litter and that incorporating CAI into ATSAVI can improve the ability of LAI estimations in the study area.

The scale-simulated results indicated that grassland LAI can be better explained by upscaling the resolution of remote sensing data to 30 m rather than using 3 m resolution. This further confirmed that a spatial scale of approximately 30 m can be used to analyze grassland biophysical properties at the landscape level.

Although the current study used a dataset collected along a transect with a large vegetation variability, the results of this study are confined to our study site, one mixed grassland ecosystem. Future research should test the feasibility of these vegetation indices through radiative transfer models or ground truth data from other vegetation types and different study sites, and also apply the improved vegetation index, L-ATSAVI, to remotely sensed imagery.

## 3.7 References

Asrar, G., Myneni, R.B., and Choudhury, B.J. 1992. Spatial heterogeneity in vegetation canopies and remote sensing of absorbed photosynthetically active radiation: A modeling study. Remote Sensing of Environment. 41, 85–103.

Asner, G.P., Wessman, C.A., Schimel, D.S., and Archer. S. 1998. Variability in leaf and litter optical properties: Implications for canopy BRDF model inversions using AVHRR, MODIS, and MISR. Remote Sensing of Environment. 63, 200–215.

Badhwar, G.D., MacDonald, R.B., and Mehta, N.C. 1986. Satellite-derived leaf area index and vegetation maps as input to global carbon cycle models: A hierarchical approach. International Journal of Remote Sensing. **7**, 265–281.

Bannari, A., Huete, A.R., Morin, D., and Zagolski, F. 1996. Effets de la couleur et de la brillance du sol sur les indices de végétation. International Journal of Remote Sensing. 17, 1885–1906.

Baret, F., and Guyot, G. 1991. Potentials and limits of vegetation indices for LAI and APAR assessment. Remote Sensing of Environment. 35, 161–173.

Baret, F., Guyot, G., and Major, D.J. 1989. TSAVI: a vegetation index which minimizes soil brightness effects on LAI and APAR estimation. In: IGARSS '89, Proceeding of the IEEE International Geoscience and Remote Sensing Symposium and 12th Canadian Symposium on Remote Sensing on Remote Sensing, 10–14 July 1989,Vancouver, B.C. IEEE, Piscataway, N.J. 3,

1355–1358.

Baret, F., Jacquemoud, S., Guyot, G., and Leprieur, C. 1992. Modeled analysis of the biophysical nature of spectral shifts and comparison with information content of broad bands. Remote Sensing of Environment. 41, 133–142.

Bonan, G. 1993. Importance of leaf area index and forest type when estimating photosynthesis in boreal forests. Remote Sensing of Environment. 43, 303–314.

Broge, N.H., and Leblanc, E. 2001. Comparing prediction power and stability of broadband and hyperspectral vegetation indices for estimation of green leaf area index and canopy chlorophyll density. Remote Sensing of Environment. 76, 156–172.

Chen, J. 1996. Evaluation of vegetation indices and modified simple ratio for boreal applications. Canadian Journal of Remote Sensing. 22, 229–242.

Curran, P. 1980. Multispectral Photographic Remote Sensing of Vegetation Amount and Productivity. In: Proceedings of the Fourteenth International Symposium on Remote Sensing of the Environment, Ann Arbor, MI, 623-637." to "Curran, P. 1980. Multispectral photographic remote sensing of vegetation amount. Progress in Physical Geography. 4, 315-341

Daughtry, C.S.T., McMurtrey III, J.E., Nagler, P.L., Kim, M.S. and Chappelle, E.W. 1996. Spectral reflectance of soils and crop residues. In: Near infrared spectroscopy: The future waves. Edited by A.M.C. Davies and P. Williams. NIR Publications, Chichester, UK. 505–511.

Daughtry, C.S.T., Walthall, C.L., Kim, M.S., Brown de Colstoun, E., and McMurtrey III, J. E. 2000. Estimating corn leaf chlorophyll concentration from leaf and canopy reflectance, Remote

Sensing of Environment. 74, 229–239.

Duncan, J., Stow, D., Franklin, J., and Hope, A. 1993. Assessing the relationship between spectral vegetation indices and shrub cover in the Jornada Basin, New Mexico. International Journal of Remote Sensing. 14, 3395–3416.

Elvidge, C.D., and Lyon, R.J.P. 1985. Influence of rock-soil spectral variation on the assessment of green biomass. Remote Sensing of Environment. 17, 37–53.

Gates, D.M., Keegan, H.J., Schleter, J.C., and Weidner, V.R. 1965. Spectral properties of plants. Applied Optics. 4, 11–20.

Gausmann, H.W., Allen, W.A., and Cardenas, R. 1969, Reflectance of Cotton Leaves and their Structure. Remote Sensing of Environment. 1, 110-22.

Gobron, N., Pinty, B., and Verstraete, M.M. 1997. Theoretical limits to the estimation of the leaf area index on the basis of visible and near-infrared remote sensing data. IEEE Transactions on Geoscience and Remote Sensing. 35, 1438–1445.

Graetz, R.D., and Gentle, M.R. 1982. The relationships between reflectance in the Landsat wavebands and the composition of an Australian semi-arid shrub rangeland. Photogrammetric Engineering & Remote Sensing. 11, 2253–2267.

Guo, X. 2002. Discrimination of Saskatchewan prairie ecoregions using multitemporal 10-day composite NDVI data. Prairie Perspectives. 5, 174–186.

Guo, X., Zhang, C., Wilmshurst, J., and Sissons, R. 2005. Monitoring grassland health with remote sensing approaches. Prairie Perspectives. 8, 11-22.

Haboudane, D., Miller, J.R., Tremblay, N., Zarco-Tejada, P.J., and Dextraze, L. 2002. Integrated narrow-band vegetation indices for prediction of crop chlorophyll content for application to precision agriculture. Remote Sensing of Environment. 81, 416–426.

Haboudane, D., Miller, J.R., Pattery, E., Zarco-Tejad, P.J., and Strachan, I.B. 2004. Hyperspectral vegetation indices and novel algorithms for predicting green LAI of crop canopies: Modeling and validation in the context of precision agriculture. Remote Sensing of Environment. 90, 337–352.

Huete, A.R. 1988. A soil adjusted vegetation index (SAVI). International Journal of remote Sensing. 9, 295–309.

Huete, A.R. 1989. Soil influences in remotely sensed vegetation-canopy spectra. In: Asrar, G., Editor, 1989. Theory and applications of optical remote sensing, Wiley, New York, 107–141.

Huete, A.R., Jackson, R.D., and Post, D.F.. 1985. Spectral response of a plant canopy with di. erent soil backgrounds. Remote Sensing of Environment. 17, 37- 53.

Jackson, R.D., and Pinter, Jr., P.J. 1986. Spectral response of architecturally different wheat canopies. Remote Sensing of the Environment. 20, 43–56.

Jensen, J. R., 2000. Remote Sensing of the Environment, Upper Saddle River: Prentice-Hall, 361.

Kaufman, Y. J., and Tanre, D. 1992. Atmospherically Resistant Vegetation Index (ARVI) for EOS-MODIS. IEEE Transactions on Geoscience and Remote Sensing, 30, pp 261–270.Karnieli, A., Kaufman, Y.J., Remer, L., and Wald, A. 2001. AFRI-aerosol free vegetation index. Remote Sensing of Environment. 77, 10–21.

Knipling, E.B. 1970. Physical and physiological basis for the reflectance of visible and

near-infrared radiation from vegetation. Remote Sensing of Environment. 1, 155–159.

Kovacs, J.M., Flores-Verdugo, F., Wang, J., and Aspden, L.P. 2004. Estimating leaf area index of a degraded mangrove forest using high spatial resolution satellite data. Aquatic Botany. 80, 13–22.

Levin, S.A. 1992. The problem of pattern and scale in ecology. Ecology. 73, 1943–1967.

Liang, T., and Chen, Q. 1999. Applications of GIS and Remote Sensing Technologies on Grassland Monitoring and Management in China. In Geoinformatics and Socioinformatics: Proceedings of the Geoinformatics ’99 Conference, 19-21 June 1999, Ann Arbor, Mich. Edited by B. Li. pp 1–13.

Lobo, A., Moloney, K., Chic, O., and Chiariello, N. 1998. Analysis of fine-scale spatial pattern of a grassland from remotely sensed imagery and field collected data. Landscape Ecology. 13, 111–131.

Ludwig, J.A., and Tongway, D.J. 1995. Spatial organization of landscapes and its function in semi-arid woodlands. Landscape Ecology. 10, 51–63.

Marceau, D.J., and Hay, G.J. 1999. Remote Sensing Contributions to the Scale Issue. Canadian Journal of Remote Sensing. 25, 357–366.

Myer, A.L., and Cameron, G.N. 2003. Consideration of grain and extent in landscape studies of terrestrial vertebrate ecology. Landscape Urban Plan. 65**,** 201–217.

Mayer, V.I., 1970, Soil, Water and Plant Relations. In: Remote Sensing with Special Reflectance to Agriculture and Forestry, Washington, DC: National Academy of Science, 253-297.

Moulin, S., and Guérif, M. 1999. Impacts of model parameter uncertainties on crop reflectance estimates: a regional case study on wheat. International Journal of Remote Sensing. 20, 213–218.

Nagler, P.L., Inoue, Y., Glenn, E.P., Russ, A.L., and Daughtry, C.S.T. 2003. Cellulose absorption index (CAI) to quantify mixed soil–plant litter scenes. Remote Sensing of Environment. 87, 310–325.

Pearson, R.L., Miller, L.D. 1972. Remote mapping of standing crop biomass for estimation of the productivity of the short-grass prairie, Pawnee National Grasslands, Colorado. In: Proceedings of the 8th International Symposium on Remote Sensing of Environment, 2-6 October 1972. ERIM International, 1357–1381 Ann Arbor, MI, USA.

Peterson, D.L., Spanner, M.A., Running, S.W., Teuber, K. 1987. Relationship of thematic mapper data to leaf area index of temperate coniferous forests. Remote Sensing of Environment. 22, 323–341.

Pierce, L.L. and Running, S.W. 1988. Rapid estimation of coniferous forest leaf area index using a portable integrating radiometer. Ecology. 69, 1762–1767.

Pinter Jr., P.J., Jackson, R.D., Ezra, C.E., and Gausman, H.W. 1985. Sun-angle and canopy-architecture effects on the spectral reflectance of six wheat cultivars. International Journal of Remote Sensing. 6, 1813–1825.

Pu, R., and Gong, P. 2004. Wavelet transform applied to EO-1 hyperspectral data for forest LAI and crown closure mapping. Remote Sensing of Environment. 91, 212–224.

Qi, J., Chehbouni, A., Huete, A.R., Kerr, Y.H., and Sorooshian, S. 1994. A modified soil adjusted

vegetation index. Remote Sensing of Environment. 48, 119–126.

Rahman, A.F., Gamon, J.A., Sims, D.A., and Schmidts, M. 2003. Optimum pixel size for hyperspectral studies of ecosystem function in southern California chaparral and grassland. Remote Sensing of Environment. 84, 192–207.

Reujean, J., and Breon, F. 1995. Estimating PAR absorbed by vegetation from bidirectional reflectance measurements. Remote Sensing of Environment. 51, 375–384.

Richardson, A.J., and Wiegand, C.L. 1977. Distinguishing vegetation from soil background information, Photogrammetric Engineering and Remote Sensing. 43, 1541–1552.

Rondeaux, G., Steven, M., and Baret, F. 1996. Optimization of soil-adjusted vegetation indices. Remote Sensing of Environment. 55, 95–107.

Rouse, J.W., Haas, R.H., Schell, J.A., Deering, D.W., Harlan, J.C. 1974. Monitoring the vernal advancement of retrogradation of natural vegetation. NASA/GSFC, Type III, Final Report, Greenbelt, MD, USA, 1–371.

Rundquist, B.C. 2002. The influence of canopy green vegetation fraction on spectral measurements over native tallgrass prairie. Remote Sensing of Environment. 81, 129–135.

Tucker, C.J. 1979. Red and photographic infrared linear combinations for monitoring vegetation. Remote sensing of environment. 8, 127–150.

Turner, D., Cohen, W., Kennedy, R., Fassnacht, K., and Briggs. J. 1999. Relationships between leaf area index and Landsat TM spectral vegetation indices across three temperate zone sites. Remote Sensing of Environment. 70, 2–68.

Turner, M.G. 1989. Landscape Ecology: the effect of pattern on process. Annual Review of Environment and Resources. 20, 171–197.

Van Leeuwen, W.J.D., and Huete, A.R. 1996. Effects of standing litter on the biophysical interpretation of plant canopies with spectral indices. Remote Sensing of Environment. 55, 123–134.

Wang, Q., Samuel, A., Tenhunen, J., and Granier A. 2005. On the relationship of NDVI with leaf area index in a deciduous forest site. Remote Sensing of Environment. 94, 244-255

Wu, J., Shen, W., Sun, W., and Tueller, P.T. 2002. Empirical patterns of the effects of changing scale on landscape metrics. Landscpae Ecology. 17, 761–782.

Zarco-Tejada, P.J. 2000. Hyperspectral remote sensing of closed forest canopies: Estimation of chlorophyll fluorescence and pigment content. PhD thesis, Graduate programme in Earth and Space Science, York University, Toronto, Ontario, Canada. 210.

Zhang, C., Guo, X., Wilmshurst, J., and Sissons, R. 2005. The evaluation of broadband vegetation indices on monitoring Northern mixed grassland. Prairie Perspectives. 8, 27-37.

# CHAPTER 4 – REMOTE SENSING MAPS OF GRASSLAND BIOPHYSICAL PARAMETERS

## 4.1 Abstract

Leaf area index (LAI), as an easily obtained variable, has been demonstrated to be a good indicator for estimating vegetation biophysical properties, and is simultaneously well correlated with remote sensing vegetation indices. The goal of the study is to develop an efficient method to retrieve spatially distributed vegetation biophysical properties based on ground LAI measurements and satellite data to aid ecosystem models. The field data (i.e. green biomass, dead biomass, and canopy height) were collected in Grassland National Park (GNP), Saskatchewan, Canada. Two vegetation indices, ATSAVI and RDVI, were derived from a SPOT 4 HRV image to estimate LAI and to prepare LAI and biophysical maps for modeling within GNP. The results of the linear regressions demonstrated strong relationships between LAI and both selected vegetation indices. However, a detailed assessment of the accuracy of the regression models indicated that ATSAVI was better for estimating and mapping LAI than the RDVI for the mixed grassland ecosystem. The accuracy of the LAI map, derived from ATSAVI was calculated to be 66.7% and this map represented the spatial distribution of the vegetation acceptably. The significant relationships between measured LAI and the biophisical data solved the difficulty for mapping biophysical information due to insufficient sampling coverage for GNP. Our results demonstrated that in native prairie ecosystems, reflectance can be used to measure spatially distributed vegetation biophysical properties and thus to aid ecosystem models.

## 4.2 Introduction

Effectively managing grassland ecosystems for economic and ecological returns requires that land managers have a good understanding of management effects at large spatial scales. This has always been a challenge, owing to the inordinate effort required to measure biological community responses in a very dynamic and heterogeneous ecosystem that covers vast areas. In response to this challenge, ecosystem models have been developed that provide consistent outputs of the condition of grasslands that can be completed rapidly.

The need for information on the biophysical conditions (i.e. biomass of green and senescent vegetation, canopy height, shrub stem densities, and frequency of bare soil) of grasslands at the landscape scale is great when modeling grassland productivity. Remote sensing has long been touted as the answer to the question of how to provide efficient, quantitative assessments of the biophysical characteristics in grassland ecosystems (Cihlar et al., 1991; Clarke, 2003; Gamon et al., 1993; Todd et al., 1998; Tueller, 1991). While remote sensing tools have been successful at measuring vegetation characteristics in crops, where structure and composition are by and large uniform, there has been less success in native rangeland where heterogeneity is the rule (Asrar et al., 1986). However, advances in the resolution of reflectance imagery, a growing body of research to support ground applications of remotely sensed data and the increasing affordability of satellite imagery has improved the utility of reflectance based data in recent years (Asner et al., 1998; Rahman et al., 2003; Tanser and Palmer, 1999).

In theory, reflectance technology should provide suitable measures for grassland ecosystems. Reflectance images either integrate light wavelengths into a limited number of broad "bands" that correspond to colors or regions of non-visible light or, in the case of hyperspectral imagery, sense and record the reflected wavelengths individually resulting in hundreds of

readings per pixel in every image. There is a well established literature on how then to combine bands or wavelengths into "vegetation indices" that, based on the physical properties of the vegetation being measured and the landscape in which they are being measured, reveal the abundance of green tissue in the image (Baret et al., 1989; Broge & Leblanc, 2000; Haboudane et al., 2004; Huete, 1988; Qi et al., 1994; Richardson & Wiegand, 1977; Rouse et al., 1974). The best known of these is the Normalized Difference Vegetation Index (NDVI) that combines the red and near infrared bands, and integrated over time, to measure vegetation productivity (Rouse et al., 1974). Many more vegetation indices have been developed that are modifications of NDVI or work on a similar principle. However, the heterogeneous, three-dimensional structure of vegetation, the variable accumulation of litter correlated with landform and community type, seasonal variation in canopy moisture as well as the presence or absence of bare ground in grassland ecosystems, have proven to be insurmountable challenges to most vegetation indices making them ineffective in native prairie (Asner et al., 2000).

As part of a program to manage a prairie ecosystem for ecological integrity at Grasslands National Park of Canada (GNP), located in southeastern Saskatchewan, Canada we have been measuring the biophysical structure and composition of the grassland community in relation to reflectance measures both collected on the ground using a hand-held unit as well as from satellite images. The objective of this study is to demonstrate that in native prairie ecosystems, reflectance can be used to measure the structure and the composition of grasslands, and to further indicate that the utility of the imagery can be extended to ecosystem modeling and other management activities such as fire management, species-at-risk and grazing utilization measures. Specifically, this study sought to use leaf area index (LAI) as an intermedial variable to indirectly establish the relationships between remote sensing vegetation indices and vegetation

biophysical properties (e.g. biomass and canopy height). The theoretic background of this study is that LAI, as an easily obtained variable, has been demonstrated to be a good indicator for estimating vegetation biophysical properties (Zhang, 2006), and simultaneously well correlated with remote sensing vegetation indices. The goal of the study is to develop an efficient method to retrieve vegetation biophysical properties to aid ecosystem modeling.

## 4.3 Materials and Methods

### 4.3.1 Study Area Description and Site Distribution

Grasslands National Park (Figure 4.1, GNP, N 49° 12’, W 107° 24’) lies within the mixed-grass prairie of the Northern Great Plains. The climate in the study area is semi-arid; average temperatures range from -12.4° C in January to 18.3° C in July, and average precipitation is approximately 350 mm per year (Environment Canada, 2000). All study sites were located in the West block of GNP, which was historically used for grazing with some limited cultivation for crops and hay. The soils in this area are brown Chernozemic clay loam soils (Saskatchewan Soil Survey, 1992). GNP consists of upland, sloped land, and valley grasslands, and the dominant native grasses are June grass (Koeleria macrantha), needle-and-thread grass (Hesperostipa comata), blue grama (Bouteloua gracilis), and western wheat grass (Pascopyrum smithii). In addition, exotic grasses, forbs, and shrubs are widely distributed throughout the study area. This park and surrounding pasture areas are ideal for biophysical assessment studies of vegetation communities because of the variety in management practices in the area.

During June of 2005, the 60 randomly selected sampling sites were visited for leaf area index (LAI), biomass, and canopy height data. These sites included rangelands, conserved native prairie, and invaded grasslands, distributed over the upland, sloped, and valley area (Figure 4.1).

At each of these sites, field sampling was conducted along two 100 m transects that ran perpendicular in the north-south and west-east directions, intersecting in the centre to form a cross. The georeferenced coordinates for each of the cross center were determined, within a 6 m accuracy using a handheld Geographic Positioning System (GPS). The transect locations were permanently marked on the ground and these coordinates were later digitized into the Park's GIS data layers.

### 4.3.2 Field Measures and Sample Processing

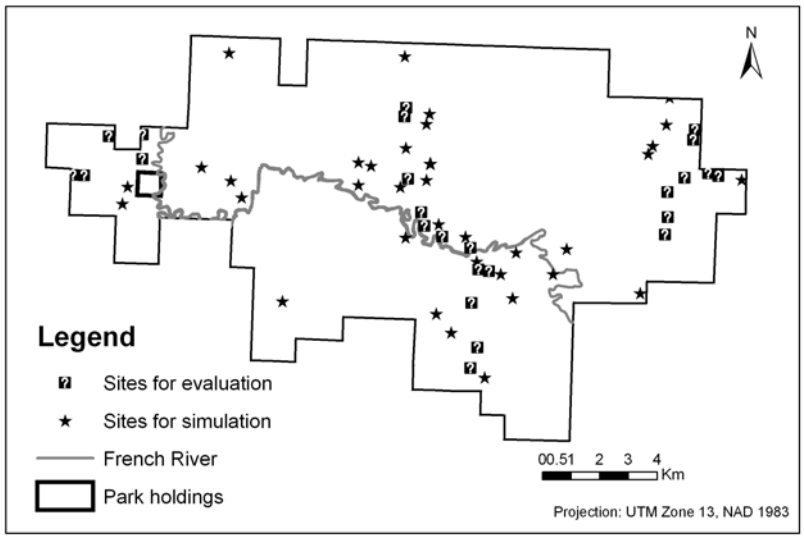


Figure 4.1 Map of the study area: Grassland National Park, Southern Saskatchewan, Canada, located at the international boundary of Canada and the United States. The star marks in the map indicate the study sites for model simulation, and the question marks indicate the study sites for model evaluation

Along each of the 100 m transects, canopy height was collected at 10 m intervals, and biomass was collected at 20 m intervals using a 20 cm x 50 cm daubenmire frame. Clipped fresh biomass was sorted into four groups: grass, forb, shrub, and dead materials. The four groups of

biomass samples were then dried in an oven for 48 hours at 60oC separately in order to compare the map product of green biomass with that of dead biomass.

LAI (the projected area of all vegetation parts normalized by the subtending ground area) was measured using a LiCor LAI-2000 Plant Canopy Analyzer (LI-COR Inc., Lincoln, Nebraska, USA) at 10 m interval along each transect. The LAI-2000 was shaded when measurements were being taken to reduce the effect of glare from direct sunshine. At each site, LAI is the average of 20 automatically calculated LAI values; each was the comparison result of one above canopy reading followed by 9 below canopy readings completed within two minutes to avoid atmospheric variation. The LAI discussed in this paper indicates canopy area index or plant area index. The measured data were then amalgamated into mean values for each site. This was completed in order to reduce variance, to obtain a measurement for each site that represents the average conditions.

### 4.3.3 SPOT Image Acquisition and Processing

A single SPOT 4 HRV image (Path 37, Row 26) for the study area was acquired on June 22, 2005 (approximately mid-point during the ground truth data collection). The satellite image was geometrically and radiometrically correctioned using PCI Geomatica 9.1. An accuracy of 0.3 RMS or better (representing approximately 6 meters or less error on the earth’s surface) was ensured in the geometric correction process. Topography distortions were corrected using a Digital Elevation Model (DEM), obtained from the GNP’s GIS database. Atmospheric and radiometric corrections were conducted using the ATCOR 2 module within PCI Geomatica V.9.1 software. After the corrections were completed, the digital number (DN) values were converted to reflectance values.

To better detect vegetation signals, RDVI (Renormalized Difference Vegetation Index, Reujean and Breon, 1995) and ATSAVI (Adjusted Transformed Soil-Adjusted Vegetation Index, Baret et al., 1992) were derived from the NIR and Red bands to estimate LAI:

$$RDVI = \frac{\rho_{NIR} - \rho_{Red}}{\sqrt{\rho_{NIR} + \rho_{Red}}} \quad (1)$$

$$ATSAVI = \frac{a(\rho_{NIR} - a\rho_{Red} - b)}{a\rho_{NIR} + \rho_{Red} - ab + X(1+a^2)} \text{ , X=0.08} \quad (2)$$

RDVI index is a hybrid index between DVI (Difference Vegetation Index) and NDVI, and is understood to combine the advantages of DVI for low vegetation coverage and NDVI for high vegetation coverage (Haboudane et al., 2004). ATSAVI index was developed to consider the actual gain (a) and intercept (b) values of the soil line and an adjustment factor X, which is set to minimize background effects (X = 0.08 in the original paper by Baret & Guyot, 1991). Therefore, these two indices have strong theoretical basis to estimate LAI in locations with soil background variations. In addition, these two indices have been demonstrated to be good LAI indicators when using ground hyperspectral data in the same study region (He et al., 2006). This study has incorporated both RDVI and ATSAVI to estimate grassland biophysical parameters. In order for the remote sensing data to better correspond with the LAI values obtained for each site, we extracted and averaged the pixel data within the sites.

### 4.3.4 Analyses Linking VI to LAI

From the 60 sites sampled, 36 were used to build the linear regression models between VI and LAI, and 24 sites were used to evaluate the models (Figure 4.1). The models were

validated using the Jack-knife Cross validation procedure. This approach is implemented by withholding one sample and building the regression model using the data from the remaining samples. The process of removing one sample from the dataset was repeated until all samples had been withheld. The relative error (RE), root mean squared error (RMSE) and map accuracy (MA) have been calculated to evaluate the models accuracy for mapping LAI and biophysical data (Pu & Gong, 2004). The relative error, RMSE and MA can be computed as:

$$\mathrm{RE} = \frac{x_i - \hat{x}_i}{x_i} \quad (3)$$

$$RMSE = \sqrt{\frac{1}{n}\sum_{i=1}^{n}(x_i - \hat{x}_i)^2} \quad (4)$$

$$MA = (1 - \frac{RMSE}{\frac{1}{n}\sum_{i=1}^{n} x_i}) \times 100.00 \quad (5)$$

Where n is the site number, i is each site sequence, $x_i$ is measured values and $\hat{x}_i$ is simulated values calculated from the regression model. After the accuracy assessment, the LAI map was developed based on the more accurate regression model.

### 4.3.5 Analyses Linking LAI to Biophysical Data

In order to model biophysical (biomass and canopy height) values, the predicted LAI was chosen as the intermediary parameter to estimate the biomass and canopy height for whole park area according to the regression equations between biophysical data (biomass and canopy height) and LAI from the 36 sites. We did not estimate biophysical data for the study area directly based on the regression models between biophysical and remote sensing data, in order to develop an efficient method to estimate biophysical data from an easily-obtained variable (LAI).

The biophysical data from the remaining 24 sites were used to evaluate the estimates of the biomass and canopy height derived from the LAI map. The RMSE, RE, and MA have also been calculated to evaluate the map accuracy.

## 4.4 Results

### 4.4.1 Statistics of LAI Data

Leaf area index varied considerably across our study area (C.V. = 0.47) and had a large range (0.44-3.85) demonstrating that the spatial variation of the grassland vegetation cover was sufficient among study sites to allow us to track changes with biophysical landscape features (Table 4.1). Within GNP, high LAI values (3.85) are generally found in areas with invading grasses, forbs and shrubs and, lower LAI values (0.44) occur in the badlands or lowland areas of high salinity. The mean LAI value of 1.25 indicates that the northern mixed grass prairie has relatively low vegetation cover, only marginally greater than 1 m2 of leaf area per m2 of land area.

Table 4.4 LAI descriptive statistics

| Sites Category | Number of Sites | Mean LAI | Range LAI | Max. LAI | Min. LAI | Std. Deviation |
|---|---|---|---|---|---|---|
| Upland | 13 | 1.34 | 1.25 | 1.98 | 0.73 | 0.40 |
| Sloped land | 24 | 1.10 | 1.58 | 2.06 | 0.48 | 0.51 |
| Valley | 22 | 1.38 | 3.41 | 3.85 | 0.44 | 0.74 |
| Total | 60 | 1.25 | 3.41 | 3.85 | 0.44 | 0.59 |

### 4.4.2 Regression Models Between VI and LAI

36 sites were chosen for creating the regression models in this analysis (Figure 4.2). Two points with very high RDVI values (Figure 4.2) are not outliers, but rather represent sites with very dense vegetation including invasive grasses and shrubs. Regression results demonstrated that strong relationships exist between LAI and the selected vegetation indices, with ATSAVI having only a marginally higher $r^2$ (0.64) than RDVI (0.63) in estimating LAI.

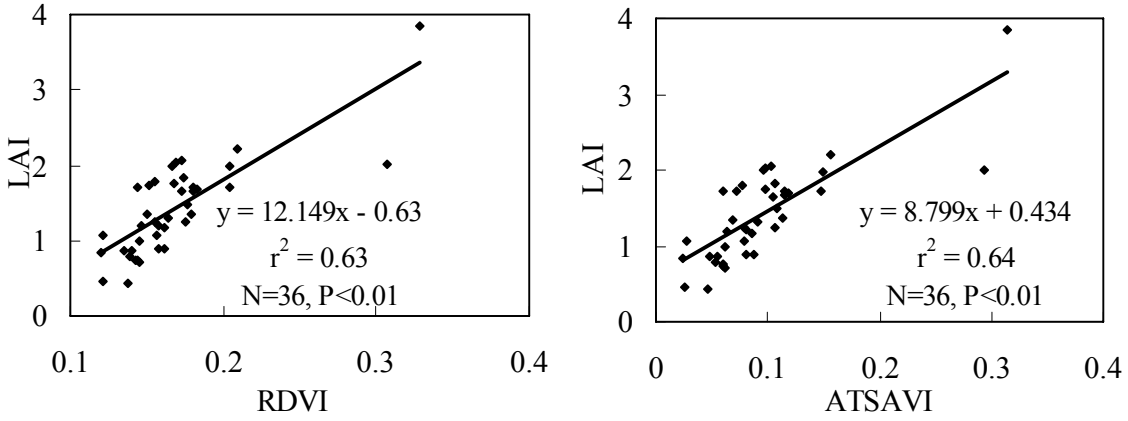


Figure 4.2 Regressions of LAI and selected vegetation indices (RDVI and ATSAVI). N is the number of observations

### 4.4.3 Model Accuracy Assessment and LAI Map

Based on the linear regression models performed between the selected VI and LAI, we used the remaining 24 remotely sensed measurements to estimate LAI. Figure 4.3 shows the significant relationship ($P<0.01$) identified between measured LAI and estimated LAI (using both VIs). For both VIs, the coefficient of X (0.997 for RDVI, 0.908 for ATSAVI) indicates that both regression models give satisfactory estimates of LAI, although LAI was slightly underestimated. The $r^2$ values indicate that ATSAVI (0.489) was only marginally better than RDVI (0.486) in estimating LAI. ATSAVI also had lower average RE, RMSE, and higher map accuracy than

RDVI in estimating LAI for the 20 sites (Table 4.2). This result further indicates that ATSAVI has a slight advantage in estimating LAI over the RDVI.

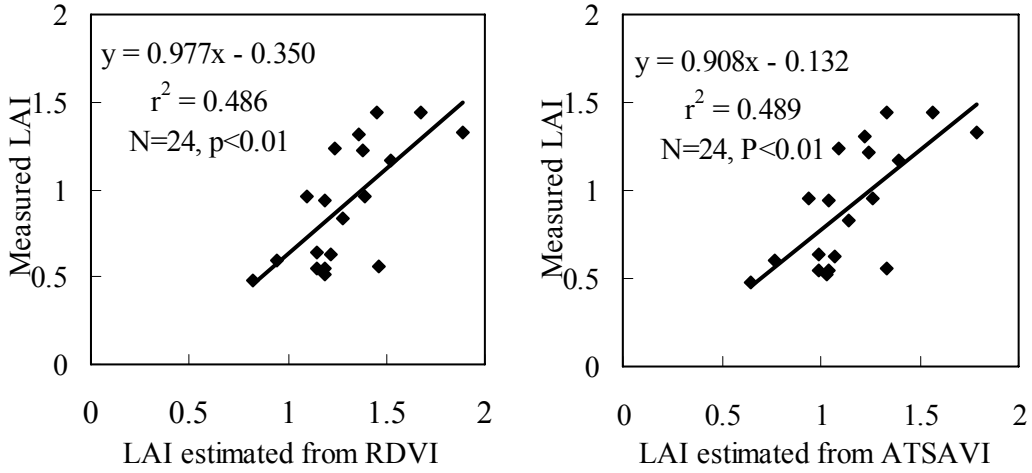


Figure 4.3 The relationships between measured LAI and estimated LAI

Table 4.5 Accuracy assessment of the regression models in LAI estimation

| | Average error | RMSE | Map accuracy |
|---|---|---|---|
| RDVI | 0.858 | 0.411 | 53.9% |
| ATSAVI | 0.771 | 0.297 | 66.7% |

Based on the accuracy assessment results, we produced an LAI map for the West Block of GNP using the ATSAVI map. In the final map product (Figure 4.4), white color within park holdings represents low LAI values or decreased vegetation cover. Light grey color represents LAI values ranging from 1 to 2, which account for the majority of the park area. The dark grey represents higher LAI values (2.0-3.5) or increased vegetation cover. In general, areas with the highest LAI values are located along the riparian zone of the Frenchman River, and the lowest LAI values are located towards the north-west portion of GNP. The results are reasonable, as the darker areas on the map are associated with areas of higher available moisture for vegetation

growth along the river. The lighter areas on the map are associated with badland topography located towards the upper left area.

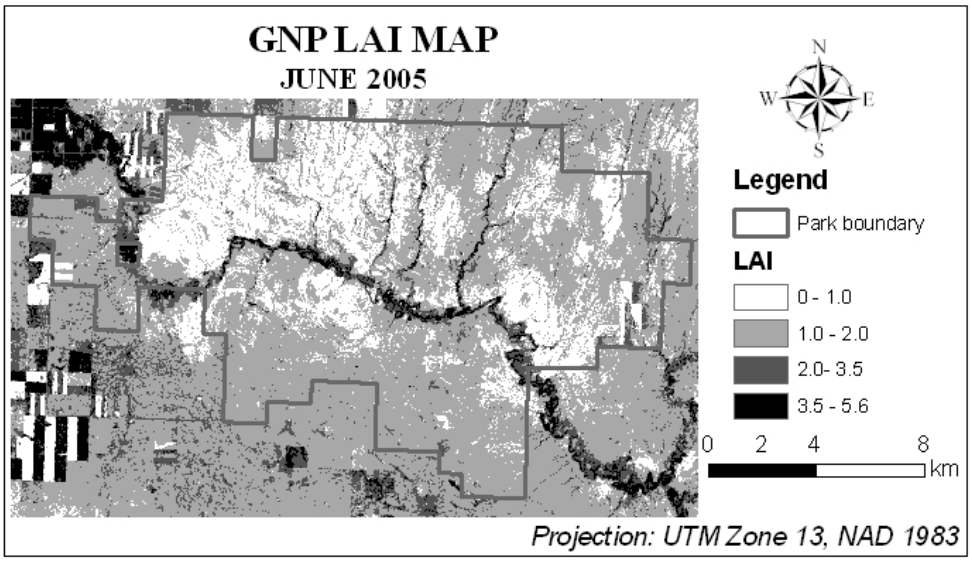


Figure 4.4 LAI map derived from a SPOT image using the regression model between ATSAVI and LAI

### 4.4.4 Relationships Between Measured LAI and Biophysical Data

The linear relationship between measured LAI and biophysical data (i.e. green biomass, dead biomass, and canopy height) were significant ($P<0.01$, Figure 4.5). The 36 sites used to develop the relationships included information from a variety of grass communities. The $r^2$ value for the relationship between the green biomass and measured LAI was 0.38, much lower than those for dead biomass and measure LAI (0.68). Canopy height strongly correlated to the measured LAI ($r^2=0.58$, $P<0.01$). These significant relationships indicate that it is possible to estimate biophysical information using LAI data.

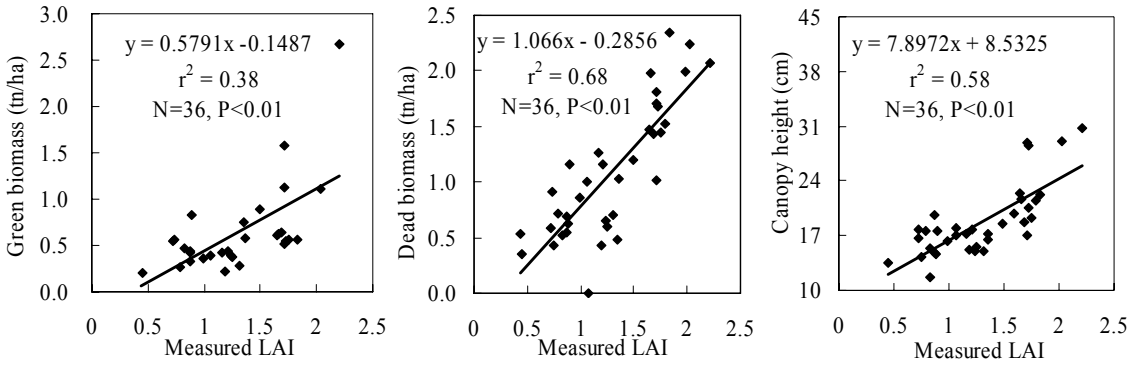


Figure 4.5 Regressions between measured various biophysical data and LAI, N is number of observations

### 4.4.5 Biophysical Maps and Validation

Biophysical maps were developed from the LAI map using the regression models between biophysical data and measured LAI (Figure 4.6). Figure 4.6 A-C demonstrate the green biomass map, dead biomass map, and canopy height map, respectively. A careful examination of these maps showed that, in general, the three maps accurately represent the biophysical information as explained for the LAI map. The white area representing low biophysical quantities is typically found in badland areas, while the darker color representing higher biophysical information appears along the river or in cropland. Table 4.3 presents some simple statistics to interpret the mapped biophysical information against measured data from the remaining 24 sites. Comparing statistical results in the table, it is apparent that the canopy height map results in the highest map accuracy, followed by green biomass, while the least accurate is dead biomass. The map accuracy for green and dead biomass maps does not seem logical when considering their correlations with LAI. In Figure 4.5, we found the weakest relationship is between LAI and green

biomass, therefore we might infer that the lowest accuracy should be observed in green biomass map.

Table 4.6 Accuracy assessment of the biophysical maps

| | Green biomass map | Dead biomass map | Canopy height map |
|---|---|---|---|
| Average error | -0.03 | -0.32 | -1.57 |
| RMSE | 0.20 | 0.54 | 3.17 |
| Map accuracy | 55.7% | 51.2% | 83.1% |

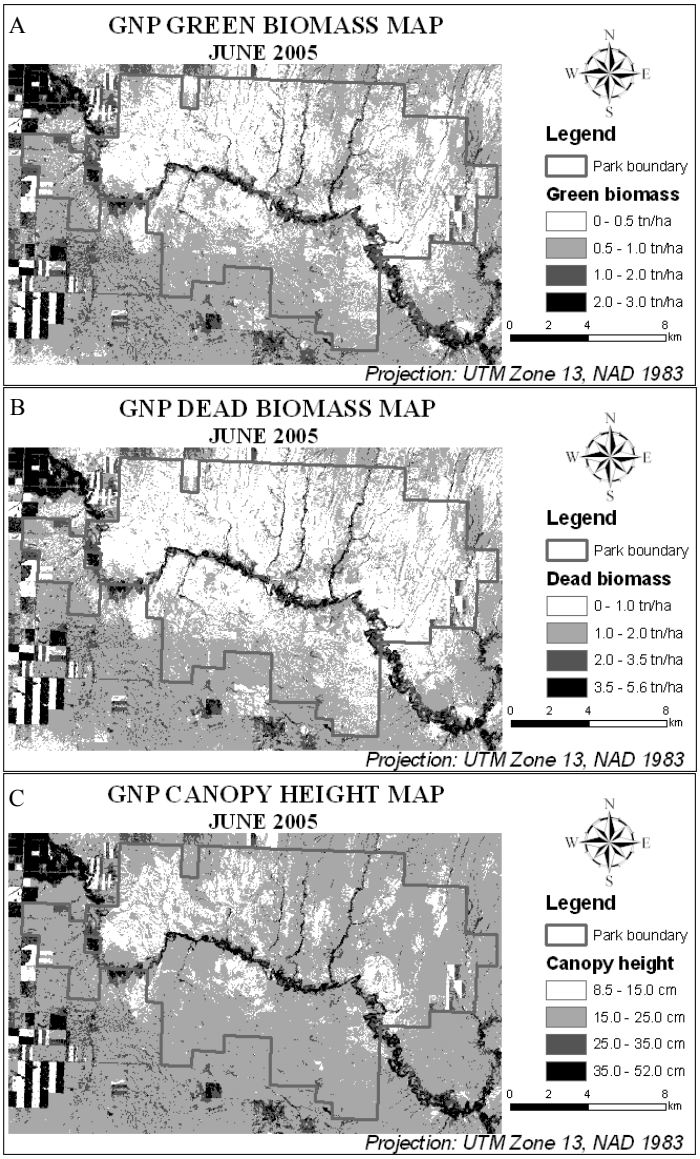

Figure 4.6 Green biomass map (A), dead biomass map (B), and canopy height map (C) obtained from LAI map using the regression models between biophysical data and LAI

To explore this unexpected result, the absolute values of relative error for green biomass and dead biomass were further calculated to interpret the error variation. From Figure 4.7 A, we can see that the error of green biomass shows a conic trend, which indicates that the estimated green biomass values greater than 1.0 ton/ha or less than 0.28 ton/ha will introduce more error. This result demonstrates that the proposed method for estimating green biomass would be more appropriate to estimate medium density grassland than to estimate either sparse vegetation or dense vegetation cover. Figure 4.7 B shows an exponential trend: the estimating error of dead biomass is lower in areas with small amounts of litter, and increases with denser litter. In GNP, medium density grassland occupies the majority of area with a large amount of dead materials. This might explain why, when creating the green biomass map, less map error was produced. Conversely, the large amount of dead material in the study area resulted in the least accuracy for the dead biomass map.

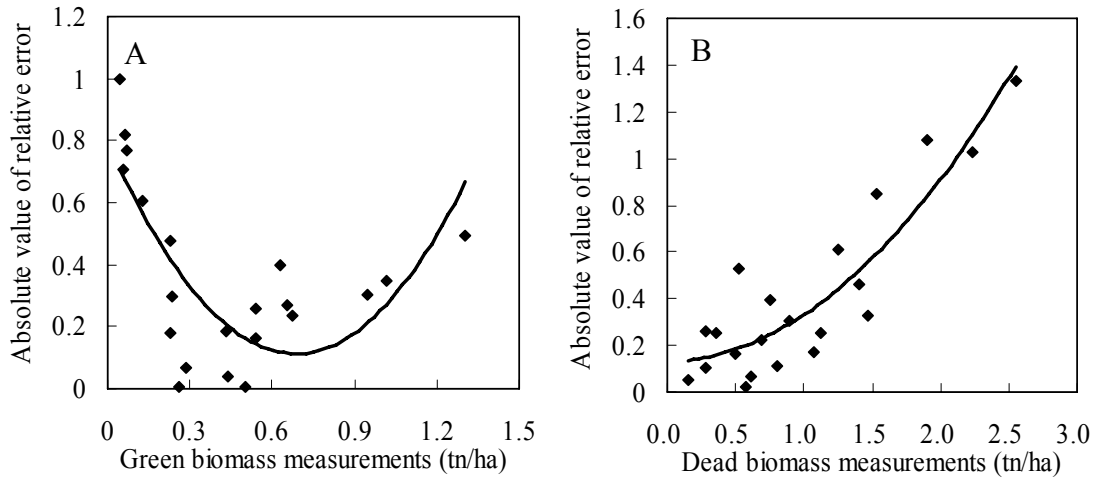


Figure 4.7 The absolute values of relative error for green biomass and dead biomass

## 4.5 Discussion

We tested two indices, ATSAVI and RDVI, to estimate LAI and to prepare LAI and biophysical maps for the GNP. The results of the linear regressions demonstrated strong relationships between LAI and both selected vegetation indices. However, a detailed assessment of the accuracy of the regression models indicated that ATSAVI was better for estimating and mapping LAI than the RDVI for a northern mixed grassland ecosystem. The accuracy of the LAI map, derived from ATSAVI was calculated to be 66.7% and this map represented the spatial distribution of the vegetation for the study area.

The significant relationship between ATSAVI and LAI found in this study we attribute to the intrinsic properties of ATSAVI; predominantly its explicit consideration of exposed soil (Baret 1992). In most grassland ecosystems the cover of a live canopy will be discontinuous, either interupted by exposed soil in heavily exploited or dry grasslands or by dead vegetation litter in conservation grasslands. Hence, converting reflectance to any characteristic of the biophysical environment in grasslands will profit from explicit consideration of the unvegetated cover. This result also adds support to previous studies conducted in the same area in which LAI variation at very small spatial scales was also found to be dependent upon the frequency of bare ground and microtopography (He et al., 2006).

While others have found as strong or stronger relationships between reflectance vegetation incides (NDVI) and biophysical characteristics of grasslands as the current study ( Kawamura et al., 2005; Paruelo et al., 1997; Wylie et al., 2002), generally these studies have been conducted at the larger, regional spatial scale. Studies at finer scales (those within grassland communities) have resulted in less consistent success (e.g. Beck et al., 1990; Cihlar et al., 1991; Davidson & Csillag, 2003; Goodin & Henebry, 1998; Posse & Cingolani, 2004) particularly

within the semi-arid climatic zone (see Frank & Karn, 2003). The use of soil adjusted vegetation indices, such as ATSAVI in relatively sparse, native grasslands has been successful in other studies (Lawrence & Ripple, 1998; Muldavin et al., 2001).

The irony of improving the resolution of remotely sensed images is that this tends to erode the strength of the relationship between reflectance and biophysical features. At very large spatial scales, subtle variation within ecosystems is masked by well-described landscape patterns that correlate well with even general reflectance measures such as the NDVI. However, as we zoom in, variation within ecosystems and communities becomes more important, and thus, data collected at fine scales against which to correlate reflectance values also becomes more important. Hence, as practitioners work towards incorporating fine scale remote imagery into their management practices, we are faced with either collecting more and finer scale training site data or, alternatively accepting poorer correlations with biophysical parameters. Indeed, despite the advantage of ATSAVI, the use of spectral vegetation indices such as ATSAVI as a surrogate for vegetation biophysical properties is still limited by scene specific characteristics. Perhaps the largest sources of error in the ATSAVI-based estimates were related to problems associated with assigning point-based ground data to area-integrated measurements from satellites (Fridel et al., 1994). Furthermore, uncertainty may be present in both the coordinates of the ground stations, and also in the geometric rectification of the image.

Unmanaged, conservation and native grasslands will always pose a challenge for remote sensing. The observed between the vegetation indices we used and LAI were considerably weaker than that observed in previous studies. For example, Haboudane et al. (2004), working on crops observed $r^2$ values ranging from 0.7 to 0.9 for linear models of LAI versus a variety of spectral vegetation indices. Map accuracy at 66.7% in this study is acceptable, but still low when compared to results from a similar study by Pu and Gong (2004) where forest LAI was mapped

with as accuracy of 74.2% when using the best method to extract features. The relatively low $r^2$ values and map accuracy observed in the current are likely due to effects such as the registration and scale problems identified above. Validation of our estimates of green and dead biomass from the GNP vegetation maps indicated that in both cases our estimates are subject to heterogeneity of variance in which, as the mean biomass increases, so does the variation in that biomass. This is to be expected in a heterogeneous vegetation community such as ours (Ehleringer & Field, 1993; Tian et al., 2003). This can be resolved by transforming our biophysical parameters prior to statistical analysis. Additionally, with live biomass, our estimates increased as biomass decreased. This could be due to increasing bare soil coverage in low green biomass sites that, despite the ATSAVI's explicit treatment, still introduces error into the reflectance values (Baret & Guyot, 1991). Given that we have used a "book" value for the soil line in our study, we could reduce or eliminate this error by deriving a site specific soil line for GNP (Broge & Leblanc, 2000 ). Nevertheless, because we can expect the variance in biophysical parameters, such as biomass and productivity, to increase as the mean of these variables increases in natural systems, correlations with reflectance will weaken in more heterogeneous vegetation communities. As we have previoiusly discussed, improvements in reflectance models in grassland ecossytems will come with improving our measures of ground based biophysical features.

The significant relationships between measured LAI and the biophisical data (i.e. green biomass, dead biomass, and canopy height) solves the difficulty for mapping biophysical information due to insufficient sampling coverage for GNP. Many of the biophysical measurements made in GNP are taken not only to monitor changes in the vegetation community itself, but also to understand the dependencies of the associated faunal community on the vegetation and physical landscape. Research has shown that many fauna are selective for vegetation structure as opposed to composition within ecosystems. LAI is an effective indicator

of grassland structure, incorporating elements of height and density but is more readily measured than either of these two parameters in a complex sward. Therefor grassland LAI should be a useful tool for spatial modeling including as a currency for measuring gradients for analysis of community structure (McGill et al., 2006). Indeed, GNP is moving forward to incorporate these maps in aid of productivity modeling, spatial fire fuels modeling, habitat modeling for species at risk and biomass monitoring after reintroducing a herd of plains bison. However, the analysis for the relative error demonstrated that the proposed maps should be treated carefully in areas of higher or lower vegetation cover. To avoid this type of problem in future experiments, more samples from areas with higher or lower vegetation cover should be measured to ensure that observations are representative of the study area. Furthermore, some error propagation might exist when using additional univariate steps for predicting biophysical parameters, even if LAI measure represents a powerful intermediate variable between satellite data and field biophysical data. In this study, we did not consider the residual by further regressing estimated LAI vs. biophysical parameters, but unfortunately it exists. Studies in the future should take the issue into account.

## 4.6 References

Asner, G.P., Elmore, A.J., Flint Hughes, R., Warner, A.S., and Vitousek, P.M. 2005. Ecosystem structure along bioclimatic gradients in Hawai'i from imaging spectroscopy. Remote Sensing of Environment. 96, 497-508.

Asner, G.P., Wessman, C.A., and Schimel, D.S. 1998. Heterogeneity of savanna canopy structure and function from imaging spectrometry and inverse modeling. Ecological Applications. 8, 926-941.

Asner, G.P., Wessman, C.A., Bateson, C.A., and Privette, J.L. 2000. Impact of tissue, canopy and landscape factors on reflectance variability of arid ecosystems. Remote Sensing of Environment. 74, 69-84.

Asrar, G., Weiser, R. L., Johnson, D. E., Kanemasu, E. T., and Killeen, J. M. 1986. Distinguishing among tallgrass prairie cover types from measurements of multispectral reflectance. Remote Sensing Environment. 19, 159-169.

Baret, F., and Guyot, G. 1991. Potentials and limits of vegetation indices for LAI and APAR assessment. Remote Sensing of Environment. 35, 161-173.

Baret, F., Guyot, G., and Major, D.J. 1989. TSAVI: a vegetation index which minimizes soil brightness effects on LAI and APAR estimation. In: Proceedings of IGARSS '89. 12th Canadian symposium on remote sensing, Vancouver, Canada, July 10–14, 1989, vol. 3, pp. 1355–1358.

Baret, F., Jacquemoud, S., Guyot, G., and Leprieur, C. 1992. Modeled analysis of the biophysical nature of spectral shifts and comparison with information content of broad bands. Remote Sensing of Environment. 41, 133–142.

Beck, L.R., Hutchinson, C.F., and Zauderer, J. 1990. A comparison of greenness measures in two semi-arid grasslands. Climatic Change. 17, 287-303.

Broge, N.H., and Leblanc, E. 2000. Comparing prediction power and stability of broadband and hyperspectral vegetation indices for estimation of green leaf area index and canopy chlorophyll density. Remote Sensing of Environment. 76, 156-172.

Cihlar, J., St. Laurent, L., and Dyer, J.A. 1991. Relation between the normalized difference vegetation index and ecological variables. Remote Sensing of Environment. 35, 279-298.

Clarke, P. J. 2003. Composition of grazed and cleared temperate grassy woodlands in eastern Australia: patterns in space and inferences in time. Journal of Vegetation Science. 14, 5-14.

Davidson, A., and Csillag, F. 2003. A comparison of three approaches for predicting C4 species cover of northern mixed grass prairie. Remote Sensing of Environment. 86, 70-82.

Ehleringer, J.R., and Field, C.B. 1993. Scaling physiological processes leaf to globe. Boston: Academic.

Frank, A.B., and Karn, J.F. 2003. Vegetation indices, CO2 flux, and biomass for Northern Plains Grasslands. Journal of Range Management. 56, 382-387.

Environment Canada. 2000. National Climate Data and Information Archive. Available on line at: http://www.climate.weatheroffice.ec.gc.ca/Welcome_e.html (Accessed: 20 April, 2006).

Gamon, J.A., Field, C.B., Roberts, D.A., Ustin, S.L. and Valentini, R. 1993. Functional patterns in an annual grassland during an AVIRIS overflight. Remote Sensing of Environment. 44, 1-15.

Goodin, D.G., and Henebry, G.M. 1998. Seasonality of finely-resolved spatial structure of NDVI and its component reflectances in tallgrass prairie. International of Journal of Remote Sensing. 19, 3213 - 3220

Haboudane, D., Miller, J.R., Pattery, E., Zarco-Tejad, P.J., and Strachan, I.B. 2004. Hyperspectral vegetation indices and novel algorithms for predicting green LAI of crop canopies: Modeling and validation in the context of precision agriculture. Remote Sensing of Environment. 90, 337-352.

He, Y., Guo, X., and Wilmshurst, J. 2006. Studying mixed grassland ecosystems I: suitable hyperspectral vegetation indices. Canadian Journal of Remote Sensing. 32, 98-107.

Huete, A.R. 1988. A soil adjusted vegetation index (SAVI). International Journal of remote Sensing. 9, 295-309.

Kawamura, K., Akiyama, T., Yokota, H.-o., Tsutsumi, M., Yasuda, T., Watanabe, O., and Wang, S. 2005. Comparing MODIS vegetation indices with AVHRR NDVI for monitoring the forage quantity and quality in Inner Mongolia grassland, China. Grassland Science. 51, 33-40.

Lawrence R. L., and Ripple, W. J. 1998. Comparisons among vegetation indices and bandwise regression in a highly disturbed, heterogeneous landscape: Mount St. Helens, Washington. Remote Sensing of Environment. 64, 91-102.

McGill, B.J., Enquist, B.J., Weiher, E., and Westoby, M. 2006. Rebuilding community ecology from functional traits. Trends in Ecology & Evolution. 21, 178-185.

Muldavin, E.H., Neville, P., and Harper, G. 2001. Indices of grassland biodiversity in the Chihuahuan Desert ecoregion derived from remote sensing. Conservation Biology. 15, 844-855.

Paruelo, J.M., Epstein, H.E., Lauenroth, W.K., and Burke, I.C. 1997. ANPP estimates from NDVI for the Central Grassland Region of the United States. Ecology. 78, 953-958.

Posse, G., and Cingolani, A.M. 2004. A test of the use of NDVI data to predict secondary productivity. Applied Vegetation Science. 7, 201-208.

Pu, R., and Gong, P. 2004. Wavelet transform applied to EO-1 hyperspectral data for forest LAI and crown closure mapping. Remote Sensing of Environment. 91, 212-224.

Qi, J., Chehbouni, A., Huete, A.R., Kerr, Y.H., and Sorooshian, S. 1994. A modified soil adjusted vegetation index. Remote Sensing of Environment. 48, 119-126.

Rahman, A. F., Gamon, J. A., Sims, D. A., and Schmidts, M. 2003. Optimum pixel size for hyperspectral studies of ecosystem function in southern California chaparral and grassland. Remote Sensing of Environment. 84, 192-207.

Reujean, J., and Breon, F. 1995. Estimating PAR absorbed by vegetation from bidirectional reflectance measurements. Remote Sensing of Environment. 51, 375-384.

Richardson, A.J., and Wiegand, C.L. 1977. Distinguishing vegetation from soil background information. Photogrammetric Engineering and Remote Sensing. 43, 1541-1552.

Rouse, J.W., Haas, R.H., Schell, J.A., Deering, D.W., and Harlan, J.C. 1974. Monitoring the vernal advancement of retrogradation of natural vegetation. NASA/GSFC, Type III, Final Report, Greenbelt, MD, USA, pp. 1–371.

Saskatchewan Soil Survey, 1992. Grasslands National Park Soil Survey. Unpublished report. University of Saskatchewan, Saskatoon, Saskatchewan, Canada.

Tanser F.C., Palmer A.R. 1999. The application of a remotely-sensed diversity index to monitor degradation patterns in a semi-arid, heterogeneous, South African landscape. Journal of Arid Environments. 43, 477-484.

Tian, Y., Wang, Y., Zhang, Y., Knyazikhin, Y., Bogaert, J., and Myneni, R. B. 2003. Radiative transfer based scaling of LAI/FPAR retrievals from reflectance data of different resolutions. Remote Sensing of Environment. 84, 143-159.

Todd, S.W., Hoffer, R.M., Milchunas, D.G. 1998. Biomass estimation on grazed and ungrazed rangelands using spectral indices. International Journal of Remote Sensing. 19, 427-438.

Tueller, P.T. 1991. Remote sensing applications for monitoring rangeland vegetation. Journal of Grassland Society Southern Africa. 8, 160-166.

Wylie, B.K., Meyer, D.J., Tieszen, L.L., and Mannel, S. 2002. Satellite mapping of surface biophysical parameters at the biome scale over the North American grasslands: A case study. Remote Sensing of Environment. 79, 266-278.

Zhang, C. 2006. Monitoring Biological Heterogeneity in a Northern Mixed Prairie Using Hierarchical Remote Sensing Methods. Ph.D. thesis, University of Saskatchewan.

# CHAPTER 5 – LAND COVER MAP AND VEGETATION PHENOLOGY PARAMETERS OF THE MIXED GRASSLAND ECOSYSTEM

## 5.1 Abstract

Ecosystem models require diverse parameters and inputs. When simulating vegetation productivity at the landscape level, two major inputs have to be considered: vegetation classification maps and vegetation phenology parameters. By deriving the two major inputs, this study investigates how remote sensing techniques can be applied to ecosystem models. Data collected for this study were from both field and satellite level. Field data measurements include biophysical parameters (leaf area index (LAI), cover, and biomass) and remote sensing data (ground hyperspectral reflectance), collected in the summer of 2005. At the satellite level, two SPOT 4 and one SPOT 5, one Landsat 5, and 22-year 10-day AVHRR NDVI images were aquired for the study area. Methods for this study were based on the three objectives, extracting different spectral signatures of different land cover types and grassland communities, comparing different classification algorithms, and determining vegetation phenology using 22-year AVHRR NDVI images. Through extracting spectral signals from different land cover types, we found that it is easier to differentiate land cover types, such as vegetation covered area and non-vegetation covered area, however, the accuracy is lower when distinguishing different grassland communities. The SPOT 4 20 m data sets have high enough spectral, spatial, and temporal resolution to be able to classify 7 major land cover types with an overall accuracy of 89%, and to classify 8 finer classes with an overall accuracy of 85%. Among classification algorithms, the

object oriented method showed better results. The temporal characteristics of the mixed grassland were identified by 10-day AVHRR NDVI data and vegetation phenology parameters were obtained for the study area.

## 5.2 Introduction

The mixed grassland ecosystem is an appropriate location to investigate the ability of satellite data for modeling productivity in the landscape level because this area is among the most biologically diverse grasslands in the world with different utilization practices, diverse topographic pattern, and complex vegetation types over large geographic areas. Two major inputs are critical when modeling grassland productivity spatially: 1) an accurate classification map, which is the foundation for modeling heterogeneous grassland in the landscape level; and 2) ideal vegetation phenology parameters to start or end ecosystem models simulating for each year. These two inputs require either high spatial or temporal resolution satellite imagery. High spatial resolution images (e.g. Landsat and SPOT) with low temporal resolution cost high, but are possible to provide models with the first input. High temporal resolution images (e.g., AVHRR, VEGETATION, and MODIS) with low spatial resolution cost less, but can be used to calculate the vegetation phenology.

Extracting spectral properties of different land cover types and different grassland communities is the basis for classifying the mixed grassland ecosystem. In recent years, discriminant analysis, a multivariate approach to pattern recognition and interpretation, has been used extensively in land cover investigations. One objective of the discriminant analysis is to predict the group to which an observation belongs, based on its measurement values. Alternatively, the objective may be to exhibit optimal ‘separation’ of groups, based on certain

linear transformations of the measurement variables. This latter approach is called descriptive discriminant analysis, and the associated linear functions are known as canonical variates (Williams, 1983). For the purpose of extracting spectral properties, the second objective of discriminant analysis is to maximize the ratio of between-class variance to the within-class variance in any particular data set, thereby guaranteeing maximal separability. Extensive discussions of discriminant analysis may be found in Huberty (1994), Johnson and Wichern (1992), and Mclachlan (1992).

Classification is the main pursuit in remote sensing research and application. A lot of studies on grassland landcover classification using remotely sensed data have been conducted in the past years. The traditional classification methods, such as K-means Classifier, Maximum Likelihood Classifier (MLC), Minimum distance, and Clustering, are still applied in different studies and can get a certain accuracy, especially the conventional MLC approach (Franklin et al., 2000; Qiu et al., 2004). In practice, however, these traditional classification methods are all pixel-based. Typically, the pixel-based classifiers have considerable difficulties dealing with the rich information content of Very High Resolution (VHR) or moderate resolution imagery such as Landsat TM or SPOT 4 & 5; they produce a characteristic, inconsistent salt-and-pepper classification, and they are far from being capable of extracting objects of interest.

Due to the nature of classical classification methods mentioned above, the application of new type supervised classifier has recently been introduced to classification studies. This new classifier employs an object oriented method, which uses the ‘image object’ or ‘local pixel group’ as a basis (deKok, et al., 2000). Thus, the image object can take the spatial context of the pixel population into account. The image object can be considered as the 4th attribute of a pixel, answering the question of ‘to which (spatial) pixel population does this pixel belong’ (deKok et

al., 2000). Consequently, the registration of the neighborhood results in a construction of a database. This database registration is advanced and therefore should be able to efficiently classify the mixed grassland ecosystem with heterogeneous landscape in this study.

However, to the best of our knowledge, no studies have been conducted to compare the difference between traditional pixel-based classification methods and the object oriented analysis for classifying the mixed grassland ecosystem. Besides a lack of investigating the classification methods for grassland communities mapping, examining vegetation phenology over large area extension is another challenge. There has been a long history of applying satellite remote sensing in studying vegetation phenology parameters (Weiss et al., 2004). Among all the applications, AVHRR NDVI Maximum Value Composite (MVC) with certain composite periods (e.g., 7, 10, 14, or 16 days), has been commonly applied in monitoring temporal changes (e.g. onset and end of growing season in the year) for its high temporal resolution and long history of records. Various methods have been developed to measure the start date of spring green-up and the end date of vegetation growth. Specifically, reported methods include NDVI thresholds (Lloyd, 1990), backward and forward moving windows from the annual cycle (Reed et al., 1994), and fitting linear segments to NDVI time series. More recently, Zhang et al. (2003) developed a method to estimate phenological events based on the curvature-change rate. To date, few studies have been conducted to detect annual change of vegetation in the mixed grassland ecosystem (Zhang, 2006).

Regarding the above mentioned background, the main objective of this study is to investigate how remote sensing techniques can be applied to ecosystem modeling efficiently. More specifically, three objectives of this study are to: 1) evaluate spectral differentiations of land cover types and grassland communities, 2) compare different classification methods on grassland classification, and 3) determine the phenology parameters for the mixed grassland ecosystem.

## 5.3 Study Area

The study area is located in the West Block of Grasslands National Park (GNP) and surrounding lands, in southwest Saskatchewan, Canada (N 49° 12', W 107° 24'). This area falls within the Great Plains, which are characterized by semiarid climate, flat landscape and large areas dominated by grass species (Coupland, 1993). Grasslands National Park is located within the mixed grass prairie, one type of biome found within the Great Plains. This biome is a transitional zone between tall grass and short grass prairie (Bragg, 1995). The climate in the study area is semi-arid; winters are long, cold and dry while the summers are short, hot and comparatively wet. Average temperatures range from -12.4° C in January to 18.3° C in July, and average precipitation is approximately 350 mm per year. The soil in the study area is brown Chernozemic clay loam soil (Saskatchewan Soil Survey, 1992).

Vegetation production in GNP is typically restricted by moisture. The moisture levels in GNP's valley grasslands are highest, making it easier for shrubs and trees to get started and grow. In contrast, most of the upland areas of the park are simply too dry for woody species to ever dominate. The dominant native grass species found in the GNP's upland are June grass (*Koeleria gracilis*), needle-and-thread grass (*Stipa comata*), blue grama (*Bouteloua gracilis*), and western wheat grass (*Agropyron smithii*). There also have been some invasive or introduced grasses, such as smooth brome, crested wheat grass, and Russian wild rye. They are of concern because they were used as hay/pasture species and continue to dominate the areas where they were seeded.

Although the dominant type of land cover in the park is grassland, there are still large areas of ploughed soil. Of the park land acquired to date, 1.2% (522.2 ha) continues to be cultivated for the production of cereal crops. Agriculture is one of the most important economic

activities in this area as well as the main stressor for the conservation of this ecological region. In an area of approximately 16,800 sq. km around the park, approximately 63% of the land is uncultivated. Much of the uncultivated land is clustered around the proposed park boundaries. Large areas around the park have been plowed in the past years. The conversion of prairie to cropland reduces the amount of habitat, and may fragment what is left, for many prairie species.

## 5.4 Methods

### 5.4.1 Field Data Collection

Field data collection was conducted in the summer of 2005 on native prairies (upland, sloped land, and valley grassland) for both grazed and ungrazed management regimes. Field data were collected in two categories, biophysical parameters and spectral measurements. Two 100 meter transects were set in each plot perpendicularly at north-south and west-east directions. A 20 x 50 cm quadrat was placed at each 10 meter interval along each transect. Percent cover of grass, forbs, shrub, standing dead, litter, moss, lichen, and bare ground was collected at each quadrat. LAI was measured using a LiCor LAI-2000 Plant Canopy Analyzer at each quadrat. Biomass was clipped in each quadrat at 20 m interval along each transect. Biomass samples were weighted immediately after clipping as wet biomass and sorted based on categories of green grass, forbs, shrub and dead later on, and then they were left in an oven for over 48 hours at 60° C. The difference between wet biomass and the dry biomass was the plant moisture content. Canopy reflectance was measured using an ASD FR Pro Spectroradiometer (Analytical Spectral Devices, Inc., USA). The measurement wavelength range was 350-2500 nm, and the spectral resolution was 3 nm at 700 nm and 10 nm at 1400 nm and 2100 nm. The 25° field of view probe was used pointing down at the canopy at approximately 1 meter above ground. Measurements were taken

within two hours of solar noon on sunny days. Calibration was made using a white spectralon reflectance panel (Labsphere, USA) at approximately 10 minute intervals to minimize the atmospheric condition changes.

### 5.4.2 Satellite Imagery Acquisition and Preprocessing

To achieve objective 1 and objective 2, two SPOT 4 HRVIR images (one in June and one in July) with 20 m resolution and one Landsat TM image (July) with 30 m resolution were purchased for the study area. The SPOT 4 image includes four bands of green, red, near infrared (NIR), and short wave infrared (SWIR). The Landsat image includes seven bands of blue, green, red, NIR, Middle infrared 1 (MIR1), Thermal, and MIR2. Both the SPOT and Landsat TM images were geometrically and radiometrically corrected using PCI Geomatica V. 9.1 software. First, the geometric correction was done with an accuracy of better than 0.3 RMS, representing approximately 6 m for SPOT (9 m for Landsat) or less error on the earth's surface. Distortions caused by variations in topography were further corrected using a Digital Elevation Model (DEM), which was obtained from GNP's GIS database. Atmospheric and radiometric corrections were conducted, based on Chavez's improved dark object image subtraction (1988). After correction, the digital number (DN) values were converted to reflectance values.

The NDVI and the adjusted transformed soil-adjusted vegetation index (ATSAVI, Baret et al., 1992) were calculated for three images and the data range was stretched. The formulas are as follows:

$$NDVI = \left( \frac{NIR - RED}{NIR + RED} \right) \times 256$$

$$\text{ATSAVI} = \frac{a(\rho_{NIR} - a\rho_{\text{Red}} - b)}{a\rho_{NIR} + a\rho_{\text{Red}} - ab + X(1+a^2)} \times 256$$ ($X$=0.08, a is 1.22 and $b$ is 0.03 for the study area)

To achieve objective 3, AVHRR NDVI 10-day composites from 1985 to 2004 were obtained for the GNP area, as a subset of the Canada-wide 1 km AVHRR 10-day composite. The NDVI layers were computed from the bidirectional reflectance distribution function (BRDF)-corrected surface reflectance for channels 1 and 2. After contaminated pixels were replaced by temporal interpolation of seasonal data, a 5-point smoothing filter was applied to the seasonal NDVI curve. Only images related to growing season, from April to October, were utilized in this study because NDVI time series of the non-growing season are not helpful for phenological separation (Ramsey et al., 1995; Senay and Elliott, 2000; Weiss et al., 2004). The NDVI image subset was reprojected to a UTM projection to overlay with the geographical layers, e.g., the river and roads. After inspecting the position of the Frenchman river and the neighboring cropland, we decided that the geographical layer of the GNP has a shift less than 1 pixel (<1000 m), therefore, the park boundary is directly used to clip the NDVI images.

### 5.4.3 Objective 1: Extracting Spectral Properties of Different Land Cover Types and Different Grassland Communities

Mixed grassland classification systems have, for the most part, been oriented towards management goals, and the information used to assign management priorities. It is recognized by most of the research community that there is a great need to develop a standardized international mixed grassland classification scheme that would allow researchers to communicate and exchange data more readily. However due to the richness and diversity of terms used to describe,

and environmental condition in which they are situated, agreement and consistency can be a difficult task. One reason for the inconsistencies between mixed grassland classifications is that mixed grassland, can be grouped differently, depending on the needs of the user. For example, the perceptions of a wildlife or biologist, an agronomist, a hydrologist can be vastly different when considering the same mixed grassland.

In this study, classification scheme was decided simply based on the knowledge of the ecology and characteristics of the study area which would be useful for managers looking at plant productivity distribution within mixed grassland. The two levels of classes (seven major land cover types and eight sub-land cover types) were adopted in this research. The seven classes, including grassland, crop, fallow, shrub, forbs and dense grass, badland, and water, represent the dominate types of land cover in GNP and surroundings (Figure 5.1). The eight finer classes considered to separate two dominant grass types (native grass-sparse and invade grass-dense, Figure 5.1).

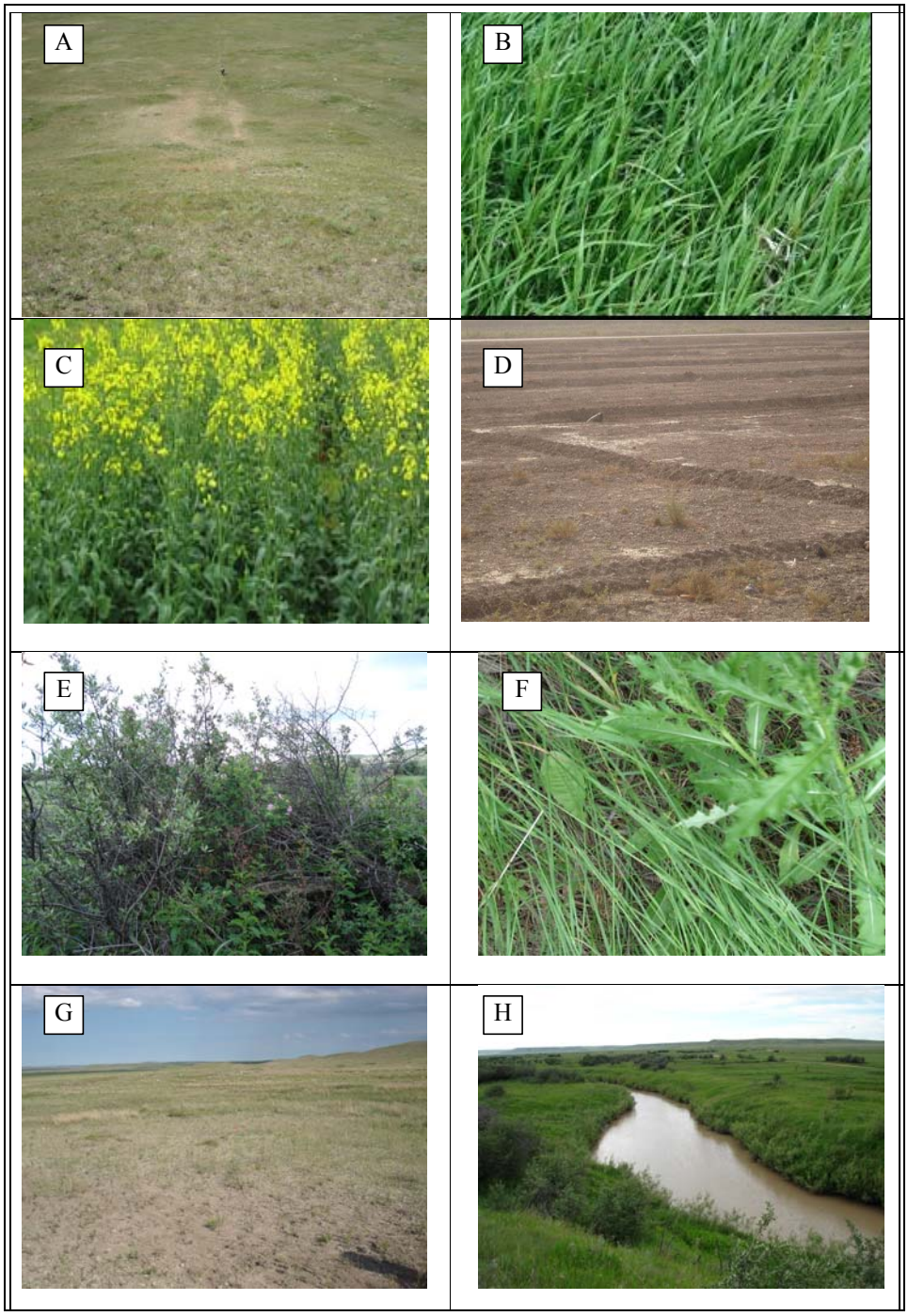


Figure 5.1 Pictures of eight classes in GNP and surrounding area (A: Native grass, B: Invasive grass, C: Crop, D: Fallow, E: Shrub, F: Forbs and dense grass, G: Badland, H: Water).

In order to analyze the separability of seven major classes, discriminant analysis (SPSS 12.0 software) was used to classify the typical spectra extracted from the training sites in June and July SPOT 4 images. The spectral data were extracted from the images for different land cover types based on GPS readings. In our study area, vegetation is seasonally spectrally distinct and can therefore be discriminated by data from both June and July imagery. According to Congalton and Green (1998), at least 50 samples for each class should be used to evaluate classification accuracy. The accuracy of our discriminant function classification was tested using in-sample accuracy assessment and a Jack-Knife cross validation approach. The Jack-knife Cross Validation approach was implemented by withholding a spectral value and building the discriminant functions using the remaining data. The process of removing one value from the dataset was repeated until all data points had been withheld.

### 5.4.4 Objective 2: Comparing Different Imagery Acquisition Dates, Different Band Combinations and Vegetation Indices, Different Classification Algorithms, and Different Resolution Imagery

For this objective, we classified the image to the seven major classes and eight sub-classes as mentioned in 4.4.3. To take maximum advantage of the spectral information of pixels in each of the spectral bands used, field samples were used to create spectral signatures defining a single class and for statistical analyses and land cover mapping.

To investigate the classification methods, two traditional methods (K-means unsupervised classification, maximum likelihood (MLC) supervised classification) and the object oriented supervised classification were adopted in this study. The two traditional classifications were performed for the SPOT image with PCI 9.1 software. The object oriented classification was conducted with eCognition 4.0 software for both SPOT images and the Landsat image. Many

different input combinations, including the combinations of SPOT bands and vegetation index (NDVI and ATSAVI), were tested on each single image and compared for both classification and post-classification accuracy. The difference between SPOT and Landsat imagery was also compared based on the classification results. The 70% of samples (437 samples for image of June, 330 for image of July, respectively) were randomly selected as training sites for classification and the training data for all classifications were consistent.

In order to determine the accuracy of all classifications, remaining 30% of random samples were used in post-classification analysis. This was completed by comparing classified pixels with actual reference classes via computation of the Kappa coefficient of agreement from a classification error matrix. Three types of accuracies are stated for remote sensing classification maps: overall accuracy, producer’s accuracy, and user’s accuracy. The overall accuracy of a classification can be found by dividing the total correct pixels by the total number of pixels in the error matrix. Producer’s accuracy is the number of correctly classified pixels divided by the total number of reference pixels (column total); this shows the probability of a reference pixel being classified correctly. User’s accuracy is the total number of correctly classified pixels divided by the total number of pixels classified as that class (row total); this defines the probability that a pixel classified represents that on the ground.

### 5.4.5 Objective 3: Examining Vegetation Phenology Parameters

To examine the time-series of NDVI and find the onset and end of the growing season, we combined temperature, NDVI values, and the change in slopes of the NDVI curve, as described in Zhang’s study (2006). Using 22 year 10-day composite NDVI imagery, the NDVI values were averaged for each 10 days from April through to October and therefore the annual

NDVI curve will represent a general vegetation growing cycle in the mixed grassland ecosystem. The onset date of green-up was decided by the first largest NDVI increase when air temperature is above 5 $^{o}$C (Frank and Hofmann, 1989). The largest NDVI drop from above 0.14 to below 0.14 is selected as the end of the growing season. This value was selected by considering phenological characteristics of the mixed grassland ecosystem and corresponding changes of the dataset.

## 5.5 Results and Discussion

### 5.5.1 Discriminating Land Cover Types and Grassland Communities Using SPOT Imagery

The performance of June and July SPOT 4 images for separating seven major classes is shown on scatter plots (Figure 5.2) and also an accuracy assessment (Figure 5.3). It is clear that both images could discriminate the seven classes with high accuracy, and the July image is slightly better for discriminating than the June image. A multi-temporal classification approach (combining the June and July imagery) slightly improved spectral discrimination among the seven major classes.

However, different images have different advantages for separating classes. The function 1(X-axis) from the June image (Figure 5.2 A) can be used to separate the classes into two groups: vegetation and non-vegetation. The function 2 (Y-axis) can be used to classify the vegetation density, which varied from low density to high density (grass, shrubs, and crops) along the Y-axis with some overlapping between classes. The overlapping is due to similar reflectance features in the two images, especially in the near infrared channel. From the July image (Figure 5.2 B), function 1 (also X axis) is less advantageous for separating the classes to two groups, but there is less between class overlapping in the July image compared to that found

in the June image. In summary, the June image showed more differences between vegetation and non-vegetation groups, while the July image showed more difference within three pairs of classes (grass, shrub, and crop). The results indicated that the June image could be used to separate vegetation communities, while the July image could be used to separate major land cover types.

The overlapping shown in Figure 5.2 indicates that it may be difficult to classify the overlapped land cover types, as expected by traditional classifiers when using reflectance information only. Considering their different texture, shape and slope, such as crops and fallow usually have well-organized pattern, regular shape, and located at the flat terrain, while shrubs and badlands are natural pattern with irregular shape, we might be able to use these characteristics to separate them.

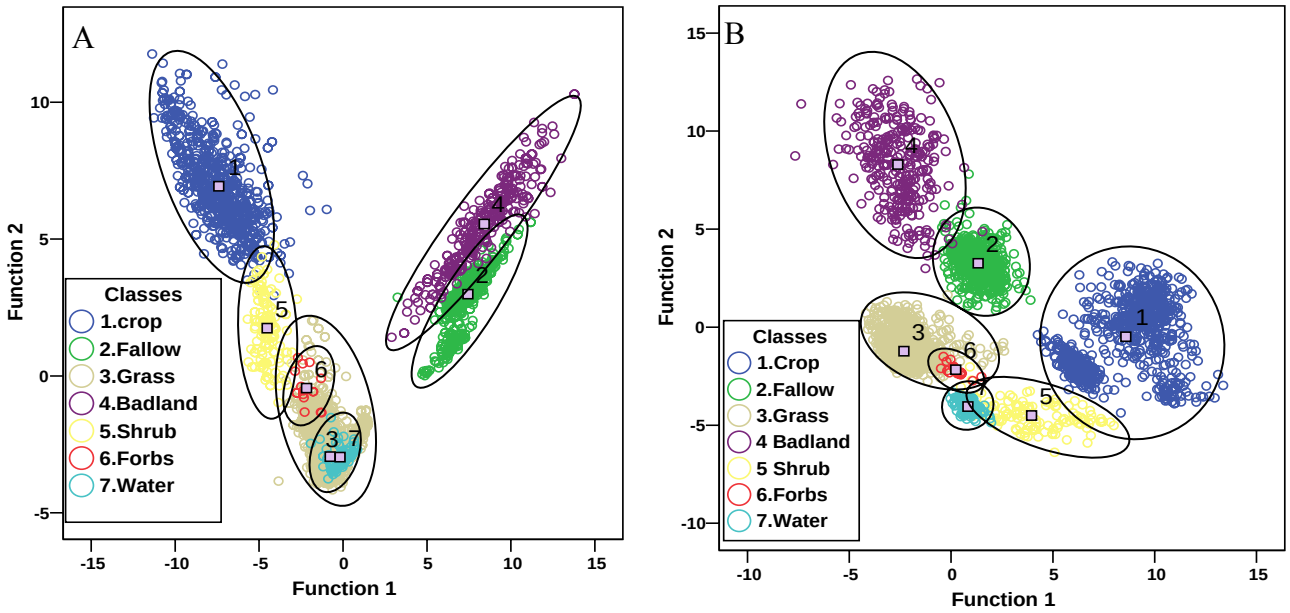


Figure 5.2 Discriminant functions of seven major land cover types in the mixed grassland prairie by using June (A) and July (B) SPOT 4 imagery

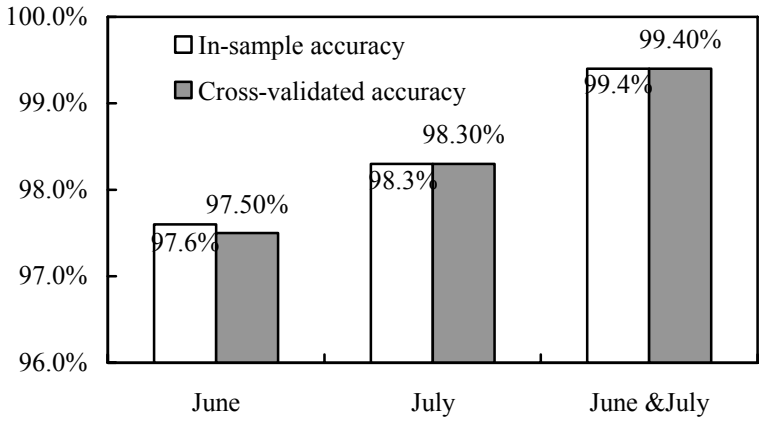


Figure 5.3 Discriminant classification accuracy for seven major land cover types

### 5.5.2 Optimizing Grassland Classification Approach in a Mixed Grass Prairie

#### 5.5.2.1 Comparing Different SPOT Band Combinations, Imagery Acquisition Dates and Vegetation Indices from MLC Supervised Classification

We used MLC supervised classifier to classify the six land cover types and did not include the forbs and dense grass class. This is because 1) MLC has been demonstrated to be an efficient classifier as mentioned in the introduction section; and 2) we just wanted to focus on the comparison of band combinations, imagery acquisition dates, and vegetation indices, but not the comparison of different classifiers. Forbs and dense grass class was excluded in this section because the classification accuracy was very low when it was included (it was classified as either grass or shrub when using MLC method). Considering the similar spectra between shrubs and crops, and badlands and fallow, we first masked the cropland (crops and fallow) and classified the rest of classes, and then masked other classes in order to separate crops and fallow.

Based on the post-classification analysis (Table 5.1), most band combinations can obtain good classification results using MLC based on the two images. The best one is the combination

of all bands (Green, Red, NIR, and MIR) where the overall accuracy was 87.2% for the June image and 88.5% for the July image). The fact that the July image achieved slightly higher accuracy than the June image is consistent with the results from the discriminant analysis.

Comparing the accuracy for individual classes, we found that different band combinations have their own advantages for classifying different classes. For example, bands 1, 3, and 4 are better for classifying grassland and badlands; bands 1, 2, 3, and 4, along with ATSAVI are better to classify crops; bands 1, 2, 3, and 4, along with NDVI is better to classify fallow; bands 2, 3, and 4 are better to classify shrub; bands 1, 2, 3, and 4, with slope data is better to classify water. These results indicate that different combinations have the potential to better classify different land cover types.

Table 5.7 Classification accuracy from SPOT June image with classifiers of MLC (accuracy assessment was based on 437 samples)

| Band Combination | Grass | | | Crop | | | Fallow | | | Shrub | | | Badland | | | Water | | | Overall Accuracy /kappa |
|---|---|---|---|---|---|---|---|---|---|---|---|---|---|---|---|---|---|---|---|
| | P | U | K | P | U | K | P | U | K | P | U | K | P | U | K | P | U | K | |
| 1234 | 90.0 | 96.3 | 0.91 | 78.4 | 89.2 | 0.87 | 87.1 | 84.4 | 0.83 | 89.5 | 36.2 | 0.33 | 83.9 | 83.9 | 0.83 | 87.0 | 100.0 | 1.0 | 87.2/0.80 |
| 123 | 90.3 | 95.1 | 0.88 | 77.0 | 87.7 | 0.85 | 87.1 | 87.1 | 0.86 | 84.2 | 32.7 | 0.30 | 74.2 | 88.5 | 0.88 | 87.0 | 100.0 | 1.0 | 86.3/0.78 |
| 124 | 89.6 | 96.3 | 0.91 | 77.0 | 87.7 | 0.85 | 80.6 | 86.2 | 0.85 | 89.4 | 34.7 | 0.32 | 77.4 | 77.4 | 0.76 | 95.7 | 100.0 | 1.0 | 86.3/0.78 |
| 134 | 89.2 | 96.7 | 0.92 | 70.3 | 89.7 | 0.88 | 90.3 | 80.0 | 0.78 | 89.5 | 31.5 | 0.28 | 83.9 | 92.9 | 0.92 | 100.0 | 100.0 | 1.0 | 86.3/0.78 |
| 234 | 89.6 | 90.3 | 0.76 | 45.9 | 70.8 | 0.65 | 90.3 | 82.4 | 0.81 | 89.5 | 39.5 | 0.37 | 90.3 | 80.0 | 0.78 | 87.0 | 100.0 | 1.0 | 82.2/0.71 |
| 1234-NDVI | 88.4 | 94.2 | 0.86 | 66.2 | 89.1 | 0.87 | 87.1 | 87.1 | 0.86 | 94.7 | 30.5 | 0.27 | 80.6 | 83.3 | 0.82 | 82.6 | 100.0 | 1.0 | 84.0/0.75 |
| 1234-ATSAVI | 89.9 | 96.3 | 0.91 | 71.6 | 92.9 | 0.92 | 87.1 | 81.8 | 0.80 | 94.7 | 33.9 | 0.31 | 87.1 | 87.1 | 0.86 | 91.3 | 100 | 1.0 | 86.7/0.79 |
| 1234-Slope | 86.5 | 94.9 | 0.88 | 77.0 | 86.4 | 0.84 | 87.1 | 81.8 | 0.80 | 84.2 | 32.7 | 0.30 | 83.9 | 86.7 | 0.86 | 100.0 | 100.0 | 1.0 | 83.4/0.77 |
| NDVI | 87.3 | 82.2 | 0.56 | 13.5 | 32.3 | 0.18 | 90.9 | 81.5 | 0.80 | 31.6 | 16.7 | 0.13 | 64.5 | 42.6 | 0.38 | 30.4 | 33.3 | 0.3 | 66.6/0.44 |
| ATSAVI | 77.6 | 82.0 | 0.56 | 1.4 | 100 | 1.0 | 80.6 | 83.3 | 0.82 | 68.4 | 25.5 | 0.22 | 77.4 | 33.3 | 0.28 | 13.0 | 7.9 | 0.0 | 61.1/0.39 |
| MD-1234 | 91.5 | 87.1 | 0.68 | 39.2 | 90.6 | 0.89 | 77.4 | 66.7 | 0.64 | 89.5 | 33.3 | 0.30 | 38.7 | 52.2 | 0.49 | 100 | 100 | 1.0 | 78.3/0.64 |
| 1234+DT | 93.4 | 92.1 | 0.80 | 78.4 | 87.9 | 0.85 | 87.1 | 84.4 | 0.83 | 78.9 | 56.0 | 0.54 | 83.9 | 83.9 | 0.83 | 87.0 | 100 | 1.0 | 88.6/0.81 |

Note: 1-NIR, 2-Red, 3- Green, 4- MIR; P-producer's accuracy; U-user's accuracy; K-kappa

The MLC classification map from the combination of all bands resulted in the highest overall classification accuracy, shown in Figure 5.3 A. For grasslands, most combinations can achieve a higher accuracy (approximately 90%) using MLC supervised classifier. However, some

pixels are misclassified. The classes with similar spectral data such as low biomass cropland and grasslands are confused with one another. Shrubs are over classified due to their spectral similarity to crops and some types of grasslands. Since shrubs are generally distributed along rivers or streams because of the higher available moisture, a modification was done to classify shrubs by incorporating a DEM GIS dataset and some "decision rules". The decision rules are: 1) within 500 m from the river, and 2) elevation is lower than average. Significant improvement was found after this modification (Figure 5.3): some pixels originally classified as shrubs have been correctly identified as cropland or grassland. The overall classification accuracy/Kappa is increased from 88.6% to 91%. However, comparing the mapped shrubs in Figure 5.3 with our field observations, the impression is that shrubby groundcover is over classified. Some of mapped shrubs should be either forbs or dense grass.

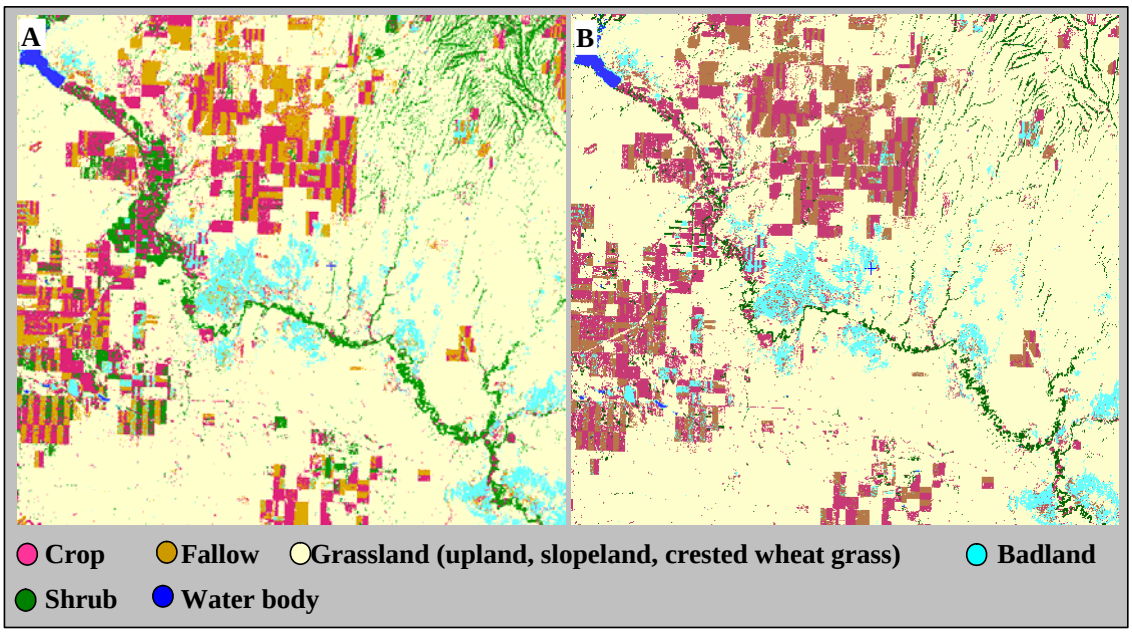


Figure 5.4 Classification maps using MLC (Green, Red, NIR, and SWIR bands combination, June SPOT image) (A) and after modification (B)

#### 5.5.2.2 Comparing Different Classification Algorithms

We also compared traditional classification methods and the object oriented classification. We selected the June image for this purpose as the June image showed possibility for separating land cover types into two major groups. As well, the discriminant analysis did not show a significant difference in using different imagery (Figure 5.2) in section 5.5.1.1. The traditional classification results (Figure 5.4) showed that grass, shrubs, forbs and grass, badlands, and cropland can be well separated. However, when we performed the traditional classification algorithms, we masked cropland together since it was difficult to separate fallow from badlands and crops from shrubs, due to their similar spectral characteristics. Table 5.2 is the result of the accuracy assessment from post-classification analysis. Based on the overall accuracy, the unsupervised and supervised traditional classifications did not differ considerably. This could be due to the similarity of the classifiers used: basing on pixel spectral information only. The traditional MLC supervised classification (69.8%) is slightly better than traditional K-Means unsupervised classification (66.7%). Furthermore, the different accuracy of MLC methods shown in the Table 5.2 (69.8%) and Table 5.1 (88.6%) indicate that the forbs and grass class significantly decreased the classification accuracy. The decreased accuracy informed us that forbs and dense grass is the most challenging to be classified by traditional classifiers.

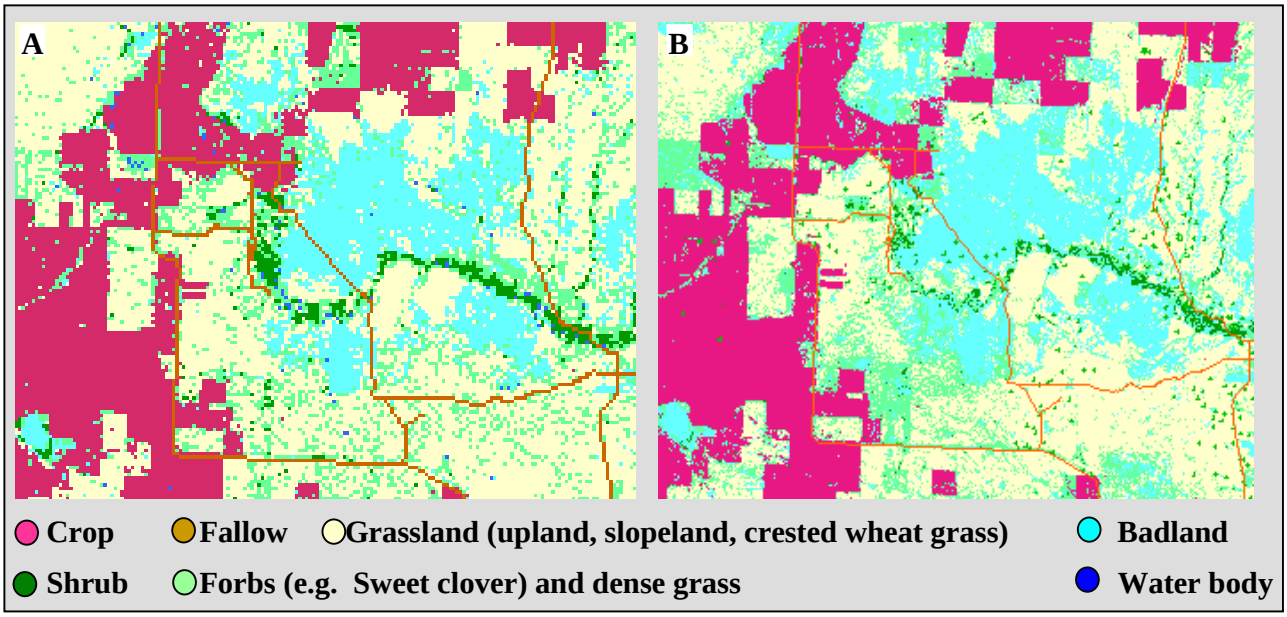


Figure 5.5 Results of traditional classification: A is from K-Means unsupervised classification (Based on green, red, NIR, and SWIR bands in June 22 SPOT image) and B is from MLC supervised classification (Based on green, red, NIR, and SWIR bands in June 22 SPOT image

For the object oriented classification, the classification can be divided into two steps. In the first step, a separation of four classes (water, grasslands, shrubs and crops, badlands and fallow) was achieved. In this step, a segmentation of four spectral channels (Green, Red, NIR and MIR bands) with a relatively high scale parameter of 20, and form and compactness parameter of 0.2 was made, so that the large objects were classified using the spectral values of the four bands and area parameters. The classified objects of each class were fused with a knowledge-based classification and the resulting objects were used as the highest object level. In the next step, a second segmentation was based the elevation channel (which was clipped and resampled from DEM map from the GIS database) with a scale parameter of 20 and form and compactness parameter of 0.8, producing objects suitable for the separation of shrubs and crops, badlands and

fallow. All objects within the primary polygons identified were classified into individual classes, using the nearest neighbor classifier in combination with training areas. Within the nearest neighbor classifier, we chose several features to separate crops from shrubs, and fallow from badlands. These features are 1) the mean value of the elevation channel, 2) the shapes of objects, and 3) the distance of objects from one another (e.g. crop is near fallow, while badlands are near shrubs). The classified objects of each class were also fused to establish the second level of the class hierarchy. The third step was to separate grasslands, which is introduced in the next section.

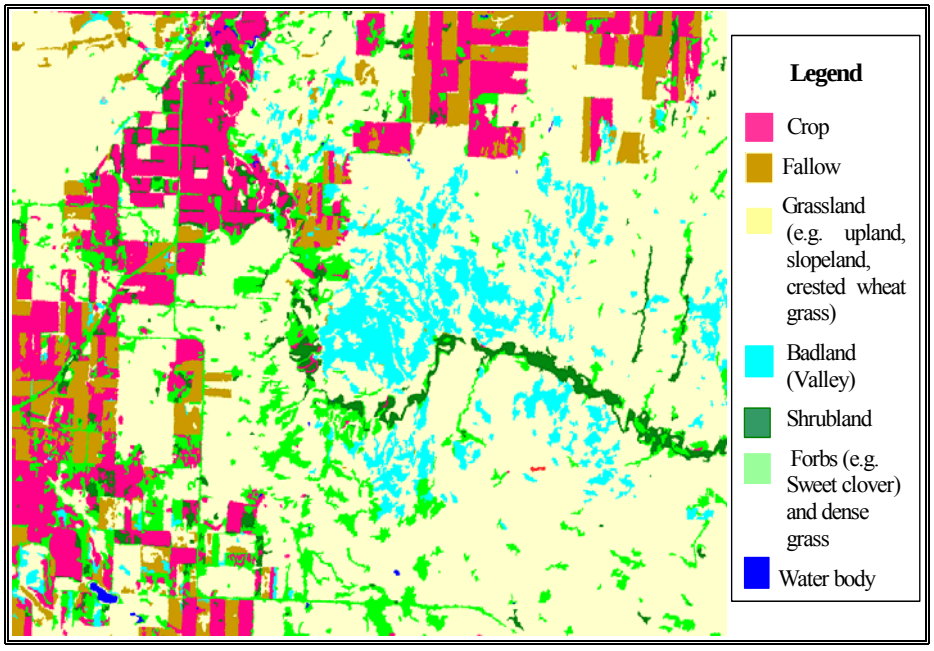


Figure 5.6 Results of object oriented supervised classification (Based on June 22 SPOT image bands green, red, NIR, and SWIR; eCognition software)

The result of the object oriented classification (Figure 5.5) was preferred in this study because it clearly separated the classes of shrubs and crops, and badlands and crops, whereas the traditional maps (Figure 5.4 & Figure 5.5) showed confusing results between these classes. The accuracy assessment also demonstrated that the object oriented classification resulted in a much

higher overall accuracy (89.1%), an increase of almost 20% in comparison with traditional supervised classifications, and an increase of 25% in comparison with traditional unsupervised classification (Table 5.2). However, the accuracy of individual classes from the object-oriented classifier indicated that it is difficult to separate forbs and dense grass class using this classifier. The area of each land use type was calculated from the results of object oriented classification (Figure 5.6).

Table 5.8 The results of classification accuracy assessment from different classifiers

| | **K-Mean Unsupervised Classifier** | | | **Maximum Likelihood Supervised Classifier** | | | **Object Oriented Supervised Classifier** | | |
|---|---|---|---|---|---|---|---|---|---|
| Accuracy | Producer's | User's | Kappa | Producer's | User's | Kappa | Producer's | User's | Kappa |
| Croplands | 92% | 65.7% | 63.7% | 92% | 65.7% | 63.7% | 92.6% | 91.9% | 91.3% |
| Fallow | | | | | | | 100% | 92.5% | 100% |
| Water | 43.8% | 100% | 100% | 40.8% | 100 % | 100% | 100% | 100% | 100% |
| Forbs & dense grass | 19.3% | 30.2% | 14.4% | 40% | 63% | 60.9% | 14.9% | 100% | 13.6% |
| Shrubs | 81.3% | 68.4% | 67.3% | 81.3% | 75% | 74.1% | 100% | 71.7% | 100% |
| Grassland | 84.3% | 70.5% | 39.8% | 84.3% | 70.5% | 39.8% | 97.2% | 90.0% | 96.1% |
| Badlands (Salina valley) | 45.0% | 59.0% | 50.2% | 50.9% | 59.0% | 50.2% | 100% | 94.4% | 100% |
| Overall accuracy | 64.66% | | 43.7% | 69.8% | | 55.6% | 89.1% | | 86.1% |

In conclusion, the object oriented classifier, although resulted in lower accuracy with forbs and dense grass type, showed much higher overall accuracy than that of the traditional classifiers. The higher accuracy might result from the object oriented classifier itself because it takes the spatial context of the pixel population into account. A lternatively, the higher accuracy might result from the additional inputs that object-oriented classification allowed. The object-oriented classification enables the export of raster GIS layers established with attribute tables that can be filled with any kind of object information like elevation, area or texture.

### 5.5.2.3 Finer Classification for Grasslands Based on Best Algorithm and Band Combinations

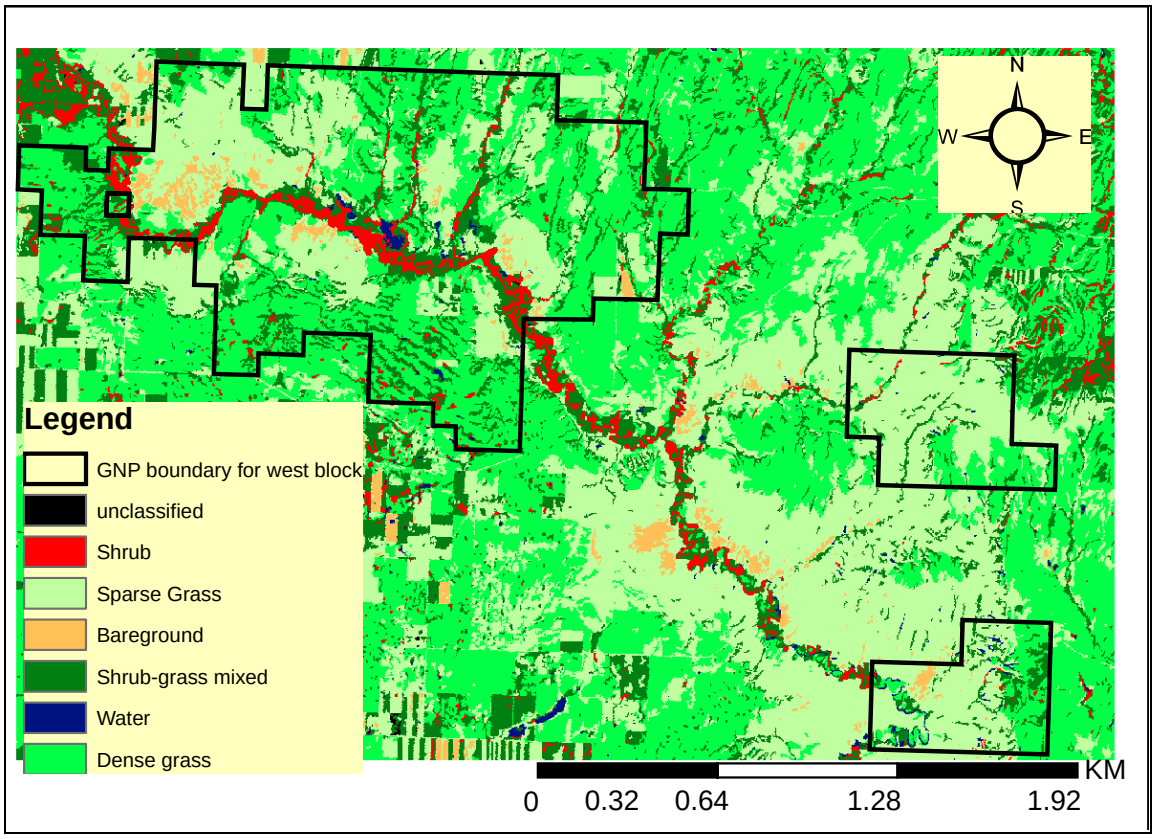


Figure 5.7 The map of object oriented supervised classification for finer Classes (Based on June 22 SPOT image bands green, red, NIR, and MIR; eCognition software)

This section used the object oriented classifier to classify four finer vegetation communities. The satellite data we used is the June SPOT image in order to obtain the comparable results to the previous section. This classification followed the two steps of the object-oriented classification to get the hierarchal classes. Then the third segmentation was made, using all four SPOT channels and one elevation channel in combination with a low scale parameter of 5. The form criteria and the compactness were set to 0.8. This time four classes were separated as the following: shrubs, shrubs-grass mixed, dense grass, and sparse grass. The

final classification map with sub-classes is shown in Figure 5.6. Using ground truth data, the overall accuracy of the map was found to be 87.5%.

### 5.2.5 Comparing the Ability of SPOT 4 and Landsat TM for Classifying the Mixed Grass Prairie Land Cover and Land Use Types

In order to compare the ability of SPOT 4 and Landsat TM for classifying grasslands, we also used the object oriented approach to classify the Landsat image, acquired on July 14, 2005 (dated between the two SPOT image acquisitions). First, we clipped the Landsat TM image using the boundary of the SPOT images in order to obtain consistent results. The same DEM data was resampled to 30 m and added as a new channel for the clipped Landsat image. The three classification steps mentioned for SPOT image were also applied to the Landsat image. The accuracy assessment showed that Landsat image yielded a lower overall Kappa accuracy (69%) in comparison to the SPOT (85%) (Figure 5.7). Similarly, most of the individual classes had lower accuracy when derived from the Landsat image than those from SPOT image, with the exception of forbs and dense grass. The Kappa accuracy for forbs and dense grass is 38% from Landsat TM, while it is only 14% from SPOT image. This may be because the training sites for forbs in this analysis are mostly the sweet clover. June and July of 2005 is flowering season of the sweet clover, which could be more easily identified by Landsat image with more MIR bands than the SPOT image. More training sites for forbs and dense grass may contribute to the higher accuracy.

The higher classification accuracy yielded from SPOT indicates that higher spatial resolution would be preferred for grasslands classification in our study area. Although Landsat TM imagery has more bands available, and therefore has the potential to detect more spectral

information of ground objects, the mixed grassland is comprised of diverse species and requires imagery with higher spatial resolution to identify the vegetation heterogeneity.

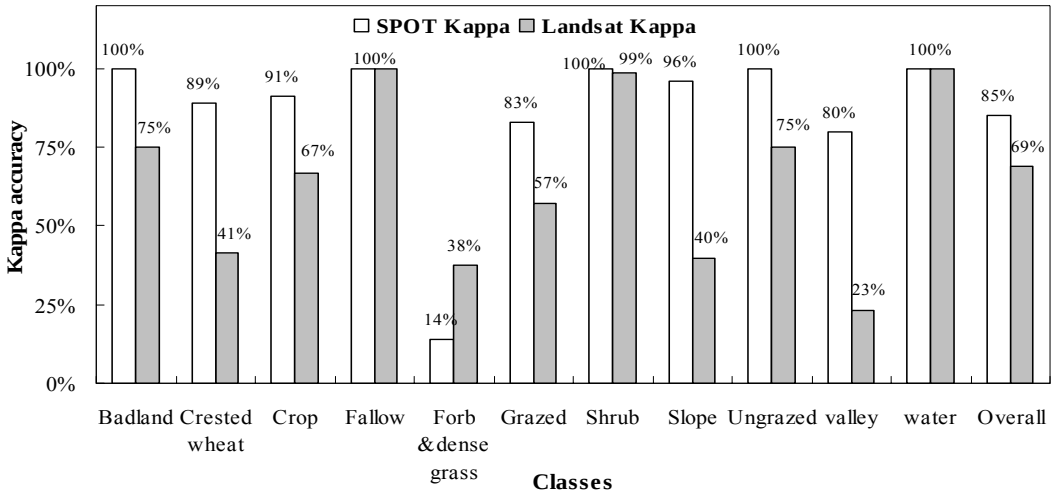


Figure 5.8 Results from the classification assessment for 11 Classes from both SPOT and Landsat images

Comprehensive comparison has perfomed in order to obtain best classification map. The results indicated that using object-oriented method to classify SPOT image, will provide the best classification map for the study region. However, people should aware that although the object-oreinted method, combined with additional data and rules, will provide more accurate maps, the limitations of this classification method is much more time consuming.

### 5.5.3 Seasonal NDVI Variation

Change in NDVI throughout the growing season (Figure 5.8) corresponded well with our field observations. NDVI started to increase in early May when NDVI was approximately 0.15, and over the next month and a half rapidly increased to 0.29. This corresponds with the

rapid green up period after precipitation occurs early growing season. The first high slope from May 1st to May 11th is corresponding to the green up of forb and shrub species and some grass species like crested wheatgrass. The second steep slope from June 11th to June 21st indicated the green-up of native grass species (e.g., needle and thread, western wheatgrass, and June grass). The peak NDVI value during the growing season was in early July, corresponding with the full growing season in the northern mixed grasslands. The process of senescence can be seen clearly from the decreasing NDVI values from mid-July through late September. Then NDVI stablizes around 0.14 for approximately 20 days and then drops again, indicating the end of the growing season. Similarly, the NDVI values are approximately 0.14 in late April when there are only dead materials, and bare soil. Therefore, it is reasonable to select 0.14 as the threshold value for the growing season. This threshold is different from the result in Zhang (2006)’s study for the same study area, in which he concluded that 0.25 is the threshold value for the growing season. The inconsistent results may result from different imagery and time span used in the two studies.

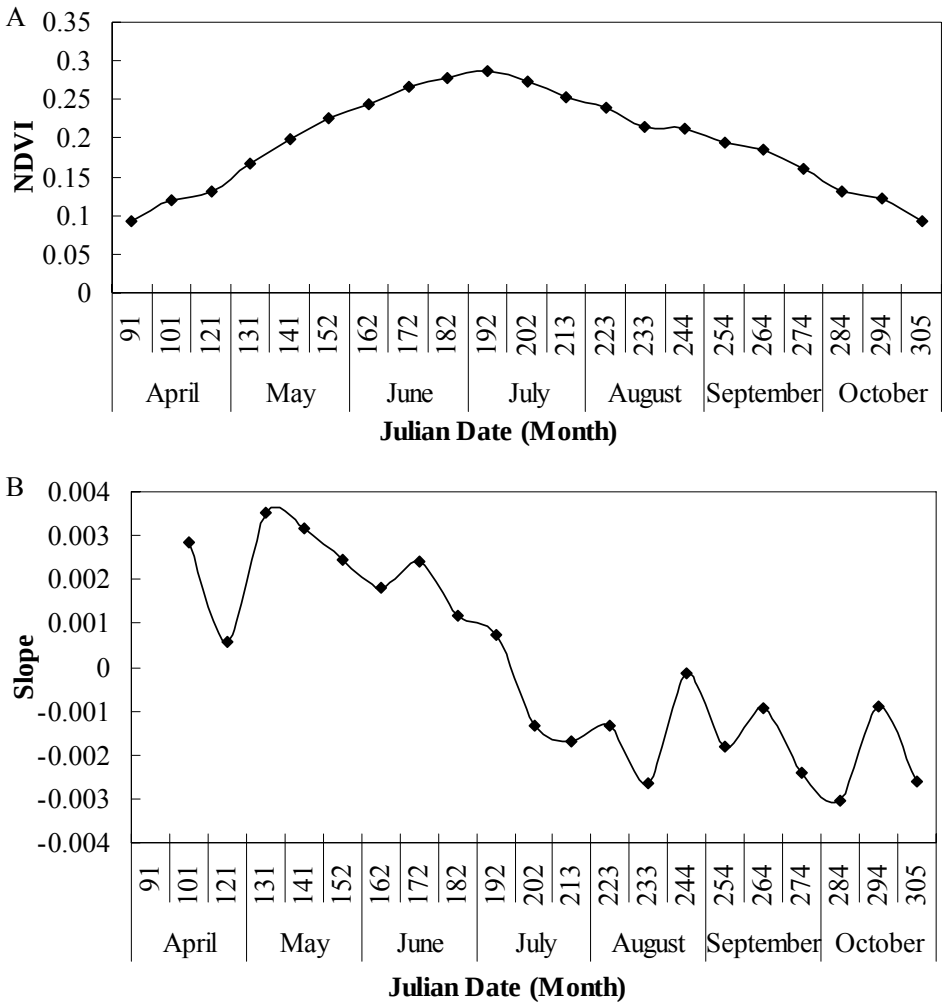


Figure 5.9 Seasonal variation of average NDVI (A) and the rate of NDVI change (Slope) (B) over the growing season from 1985 to 2006. Values in x axis represent the time of year

## 5.6 Conclusions

Through extracting spectral signals from different land cover types, we concluded that a hierarchical classification method is necessary as different level of classification use different spectral properties. It was easier to differentiate major land cover types, such as crop land, shrub land, and grassland. However, it was more difficult to distinguish different grassland

communities, such as native prairie and crested wheat grassland. The forbs are the most difficult ground cover classify.

This research indicated that SPOT 4 20 m data sets have a high enough spectral, spatial, and temporal resolution to be able to classify seven major land cover areas with an overall accuracy of 87%, and to classify eight finer classes with an overall accuracy of 85%. This study also showed that multi-temporal remotely sensed data are critical in grassland classification. However, a successful classification is not only based on a better classification algorithm, but also depends on the careful selection of training sites and the image acquisition date. Among classification algorithms, the object-oriented classification showed the best results. Vegetation indices did not improve the classification results. It is clear that the higher spatial resolution images (SPOT4) offers an advantage over Landsat TM in classifying finer classes.

In the mixed grass prairie, early May is the green up of forb and shrub species and some grass species like crested wheatgrass. The second green up period from June 11$^{st}$ to June 21$^{th}$ indicates the green-up of native grass species. The peak growing season appears in late June, and the end of growth season is in early October.

## 5.7 References

Baret, F., Jacquemoud, S., Guyot, G., and Leprieur, C. 1992. Modeled analysis of the biophysical nature of spectral shifts and comparison with information content of broad bands. Remote Sensing of Environment. 41, 133-142.

Bragg, T.B. 1995. Climate, soils and fire: the physical environment of North American grasslands. In: The Changing Prairie, (K. Keeler and A. Joerns, eds.) Oxford University Press, New York. IN Madden 1996.

Chavez, P. S. 1988. An Improved Dark-Object Subtraction Technique for Atmospheric Scattering Correction of Multispectral Data. Remote Sensing of Environment. 24, 459-479.

Congalton, R.G., Green, K. 1998. Assessing the Accuracy of Remotely Sensed Data: Principles and Practices. Lewis Publishers, New York, NY, pp. 180.

Coupland RT (ed), 1993. Ecosystems of the world 8A, 8B: natural grasslands. Elsevier, Amsterdam.

deKok, R., Buck, A., Schneider, Th., Ammer, U. 2000. Analysis of image objects from VHR imagery for forest GIS updating in the bavarian Alps; Procc. ISPRS Amsterdam, Working Group III/5.

eCognition User Guide 3. 2003. Definiens Imaging, pp.3.2-108

Frank, A.B., and Hofmann, L. 1989. Relationships among grazing management, growing degree

days, and morphological development for native grasses on the Northern Great Plains. Journal of Range Management. 42, 199-202.

Franklin, S. E.et al. 2001. An integrated decision tree approach (IDTA) mapping landcover using satellite remote sensing in support of Grizzly Bear Habitat analysis in the Alberta Yellowhead Ecosystem. Canadian Journal of Remote Sensing. 27, 6.

Horler, D.N.H., and Ahern, F.J. 1986. Forestry information content of thematic mapper data. International Journal of Remote Sensing. **7**, 405-428.

Huberty, C.J. 1994. Applied Discriminant Analysis. Wiley, New York, 466 pp.

Johnson, R.A., and Wichern, D.W. 1992. Applied Multivariate Statistical Analysis, 3rd ed. Prentice-Hall, Englewood Cliffs, NJ, 642 pp.

Lloyd, D. 1990. A phenological classification of terrestrial vegetation cover using shortwave vegetation index imagery. International Journal of Remote Sensing. 11, 2269-2279.

McLachlan, G.J. 1992. Discriminant Analysis and Statistical Pattern Recognition, Wiley, New York, 526 pp.

Qiu, F. et al. 2004. Opening the black box of neural networks for remote sensing image classification. International Journal of Remote Sensing. 25, 1749.

Ramsey, R.D., Falconer, A., and Jensen, J.R. 1995. The relationship between NOAA-AVHRR NDVI and ecoregions in Utah. Remote Sensing of Environment. 53, 188–198.

Reed, B.C. et al. 1994. Measuring phenological variability from satellite imagery. Journal of

Vegetation Science. 5, 703-714.

Saskatchewan Soil Survey. 1992. Grasslands National Park Soil Survey. Unpublished report. University of Saskatchewan, Saskatoon, Saskatchewan, Canada.

Senay, G.B., and Elliot, R.L. 2000. Combining AVHRR-NDVI and land use data to describe temporal and spatial dynamics of vegetation. Forest Ecology and Management. 128, 83-91.

Weiss, J.L., Gutzler, D.S., Coonrod, J.E.A. and Dahm, C.N. 2004. Long-term vegetation monitoring with NDVI in a diverse semi-arid setting, central New Mexico, USA. Journal of Arid Environments. 58, 249-272.

Williams, BK. 1983. Some observations on the use of discriminant analysis in ecology. Ecology. 64, 1283-1291.

Zhang, X. et al. 2003. Monitoring vegetation phenology using MODIS. Remote Sensing of Environment. 84, 471-475.

Zhang, C. 2006. Monitoring Biological Heterogeneity in a Northern Mixed Prairie Using Hierarchical Remote Sensing Methods. Ph.D. thesis, University of Saskatchewan.

# CHAPTER 6 – COMPARISON OF ECOSYSTEM MODELS AND DEVELOPMENT OF A NEW MODEL FRAME FOR THE MIXED GRASSLAND ECOSYSTEM

## 6.1 Abstract

Modeling vegetation productivity at the landscape scale requires understanding how ecosystem processes are governed at this scale. Current popular ecosystem models are mostly site-specific due to the shortage of spatially distributed parameters and inputs. Using ground measurements and climate data (site-specific data) from a mixed grassland ecosystem, this study evaluated the performance of two commonly used ecosystem process models (CENTURY and Biome-BGC) and examined the models' response to environmental change. The models had substantially higher correlations with ground truth measurements and climate data. However, both models also generated productivity values in some years which are significantly different from the observations, indicating a limitation of the models. Integrating remote sensing products (spatially-distributed data developed from the previous chapters) into the site-based BIOME-BGC model, the remote sensing-based ecosystem model frame was proposed. As well, the model-generated spatial patterns of above-ground productivity for the mixed grassland ecosystem were evaluated using ground truth data measured in 2005. The map accuracy of 71% indicated that the spatially-distributed ecosystem process model holds the potential to simulate and predict vegetation productivity in the landscape scale. However, knowledge of the effects of disturbance (human and natural) and spatial data describing disturbance regimes are needed for spatial modeling. Improved consideration of disturbance is a critical step for spatial ecosystem models.

## 6.2 Introduction

Over the past 30 years a considerable number of ecosystem process models have been developed to investigate many different aspects of ecosystems, including changing vegetation distributions and the land carbon sink (Adams et al., 2004). At the core of most of these models is a net primary productivity (NPP) sub-model but most NPP sub-models are site-specific. The site-specific NPP model can be used to simulate or predict global vegetation productivity among ecosystems. However, model applications have been hampered due to the shortage of a spatially-distributed set of required model parameters and initial conditions (e.g., Boote et al., 1996; Franks and Beven, 1999).

Early efforts to link ecosystem spatial responses to environmental gradients included only variables related to temperature and precipitation (e.g., Holdridge, 1967; Lieth, 1972). Current ecosystem process models use additional information on climate (radiation, humidity, and other sources) and soil properties, and include vegetation type-specific parameters (Burke et al., 1991; Burke and Lauenroth, 1993; McGuire et al., 1993; Running and Hunt, 1993; Schimel et al., 1994; VEMAP, 1995). These models simulate the components of spatial variability in ecosystem processes governed by climate, soil, and vegetation type. As a result, they require maps of these variables as input (Kittel et al., 1995).

Because of the difficulties in obtaining spatially distributed parameters required by the ecosystem models, the integration of remote sensing data and models has been a topic throughout the last couple of decades (Allen, 1990; Genovese, 1997; Meyer-Roux and King, 1992). Remote sensing offers the best opportunity to minimize the problems of site-specific models for several reasons. First, remote sensing offers the potential to derive key characteristics of the biospheres spatially, thus provides the probability to extend models beyond sites and certain ecosystems to

regional scales. Second, remote sensing data permits, in theory, the entire ecosystem to be classified at once. Finally, models incorporating remote sensing data are updatable. Like the vegetation communities themselves, the model is simulating change with time under the influence of disturbances. Ground surveys to measure this change are impossible given limited resources. However, assuming that measures developed from satellite images are sufficiently sensitive to detect change, monitoring change in vegetation cover and structure repeatedly within a decade should be possible from both a labor and cost perspective. This is is extremely important to aid in spatial modeling, as it will provide reliable predictive power in management decision making.

There has been a long and successful record remote sensing data use in ecosystem modeling (Moulin et al., 1998), and in recent years studies have been focused on the assimilation of remote sensing data in those models (White et al., 1998; Nouvellon et al., 2001). While the first applications of satellite data in spatially distributed models were restricted to a descriptive analysis of land use, more complex methodologies are now available which develop algorithms or models to correlate ecological quantities with remote sensing signals at local, regional, and global scales (Asrar et al., 1984; Fung et al., 1987) based on good empirical correlations and strong theoretical basis (Goward et al., 1985; Sellers, 1985; Fung et al., 1987; Schimel et al., 1991; Potter et al., 1993). Over time, the distributed models have benefited from remote sensing data either through the periodic update of the model state variables, or through re-initialization of the model, or by calibrating some of the model parameters. Examples of ecological variables that can be obtained from remote sensing data are: 1) biophysical parameters (the leaf area index and the minimum canopy resistance to evaporation), which can be assessed by vegetation indices (Sellers et al., 1992) to aid biological processes that control fluxes of mass; 2) surface temperature, which can be achieved from various satellite sensors to improve simulation of

energy balance components (Gillies et al., 1997), and 3) surface soil moisture content, which can be derived from microwave data (Schmugge, 1998) to improve the process modeling of bare soil (Bruckler and Witono, 1989) and sparsely vegetated surfaces (Houser et al., 1998) when assimilated in ecosystem models.

The feasibility of using remote sensing data in ecosystem models has been demonstrated in several land cover types, such as bare soil (Bruckler and Witono, 1989), grasslands (Cayrol et al., 2000; Nouvellon et al., 2001), forests (Liu et al., 1997; White et al., 1998; Ranson et al., 2001), and croplands (Bouman, 1992; Clevers and van Leeuwen, 1996; Guerif and Duke, 2000; Maas, 1988; Weiss et al., 2001). However, few studies have applied similar research in the mixed grassland prairie, and the spatial variation of distributed model outputs is rarely validated. Furthermore, in most satellite based studies, low resolution (1 km) remote sensing data were applied because of their high temporal availability (daily). For the application of such data in heterogeneous terrain such as mixed grasslands, the scaling characteristics of the remote sensing data (Moran et al., 1997) and the effect of sub-grid variations on the modeling of land surface processes (Sellers et al., 1997; Hasager and Jensen, 1999) needs to be considered.

Therefore, the objectives of this paper are twofold: 1) to compare the current popular ecosystem models (CENTURY and BIOME-BGC) in simulating productivity for the mixed grass ecosystem, and 2) to develop a new model frame (remote sensing-based spatial model) for studying the mixed grass prairie. A variety of remote sensing products are available for analysis. Coarse resolution images at 1km spatial scales (AVHRR) are available from archived databases held by Parks Canada. While the resolution may be too coarse to effectively match some of the smallest polygons mapped in our landscape, the rapid acquisition rate of this imagery (daily, composited at 10 day intervals) offers the ability to measure vegetation change within and among seasons. Other imagery (Landsat and SPOT 4&5) is of finer spatial resolution, but is not

necessarily available at short temporal scales. However it would be useful to determine whether the spatial mosaic depicted in the model reflects reality. In addition, soils maps (at moderate resolution) and a digital elevation model (DEM) are available to assist in classification.

## 6.3 Data and Methods

### 6.3.1 Study Area

The study was conducted in Grassland National Park (GNP), located in southern Saskatchewan (N 49° 12’, W 107° 24’) (Figure 6.1). Grasslands National Park is further located within the mixed grass prairie, one type of biome found within the Great Plains. This biome is a transitional zone between tall grass and short grass prairie (Bragg, 1995). The dominant native grass species found in the study site are needle-and-thread grass (Hesperostipa comata (Trin. & Rupr.) Barkworth), blue grama (Bouteloua gracilis (Willd. ex Kunth) Lag. ex Griffiths), and western wheat grass (Pascopyrum smithii (Rydb.) A. Löve). Other prominent invasive or introduced species at the study site includes smooth brome (Bromus inermis Leyss) and crested wheat grass (Agropyron cristatum(L.) Gaertn). There is also 5.2 to 15.5% of forbs and shrubs over the mean basal covered in the mixed grassland (Coupland, 1950).

Grasslands National Park has an area of 906 $km^2$, and the topography is typified as gently rolling terrain with elevation ranging from 710 to 1042 m above sea level. The annual precipitation is 325 mm with approximately half accumulated during the growing season. The mean monthly temperature ranges from -12.4° C in January to 18.3° C in July.

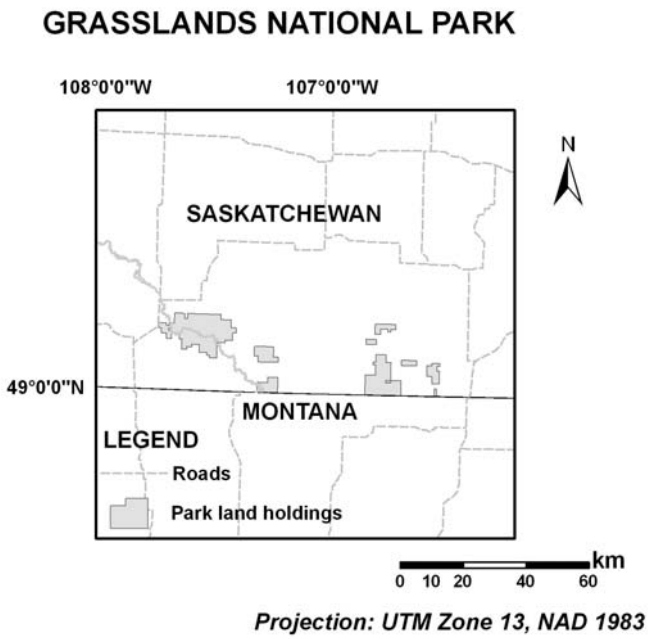


Figure 6.1 The study area: Grasslands National Park and surrounding pastures, southern Saskatchewan, Canada, located at the international boundary of Canada and the United States. The Park is composed of two blocks: East and West

### 6.3.2 Data

Measurements of productivity were made in GNP in 2003, 2004, and 2005. These results provided detailed information for this ecosystem and assisted in model parameterization and validation. A climate station (Val Marie weather station, 49° 22' N, 107° 51' W) immediately adjacent to the park provided meteorological data, including precipitation and temperature.

AVHRR NDVI 10-day MVC from 1985 to 2006 were obtained for the Park area, which has a spatial resolution of 1 km. The MVC is necessary, especially for the northern mixed prairie, because of the low availability of optical remote sensing imagery due to cloud cover during

growing seasons. Only images related to the growing season from April to October were utilized in this study because NDVI time series for the non-growing season are not helpful for phenological separation. The NDVI images were reprojected to a UTM projection to overlay with geographical layers, e.g. the Park boundary, the river, and roads for the park area.

### 6.3.3 Models Description

The two biogeochemistry models considered in this chapter (Biome-BGC and CENTURY) simulate the cycles of carbon, nitrogen, and water in terrestrial ecosystems (McGuire et al., 1993; Running and Hunt, 1993). An overview of model characteristics is shown in Table 1.1, and more detailed information is available in VEMAP (1995). The models employ general framework for all vegetation types, but have some parameters or functions that vary by vegetation type. Examples of such vegetation type-specific relationships include the fractional allocation to type of plant tissue (e.g., no wood specified in grasslands) and carbon-to-nitrogen ratios. The models simulate evapotranspiration (ET), photosynthesis and/or net primary production, decomposition, and soil nitrogen turnover as influenced by climate variables and soil properties. The models represent the structure of ecosystems with different degrees of aggregation, but both can produce estimates of net primary productivity (NPP), net nitrogen mineralization, evapotranspiration, and carbon storage for living (vegetation carbon), nonliving (soil carbon including carbon in detritus), and total ecosystem (living plus nonliving) compartments. The detailed description for each model follows.

CENTURY is a lumped-parameter ecosystem model with a monthly time step and aggregated plant and soil organic dynamics, simulating carbon and nitrogen cycling aboveground and within the top 20 cm of the soil. It concentrates on the biogeochemistry of carbon, nitrogen, phosphorus, and sulphur. It has been used successfully to simulate carbon dynamics, especially in

soil organic matter (SOM), across a variety of land use and climate types, and is particularly good in grass and crop ecosystems.

The main driving data for the model are:

- monthly average maximum and minimum air temperature,
- monthly precipitation,
- lignin content of plant material,
- plant N, S, and P content,
- soil texture,
- atmospheric and soil N inputs, and
- initial soil N, S, and P levels.

For the purposes of this study, the main CENTURY submodel is plant production. Plant production is modeled assuming that monthly maximum productivity is controlled by moisture and temperature, with reductions if insufficient nutrients are available. The pools and flows of the grass/crop model are presented in Figure 6.2.

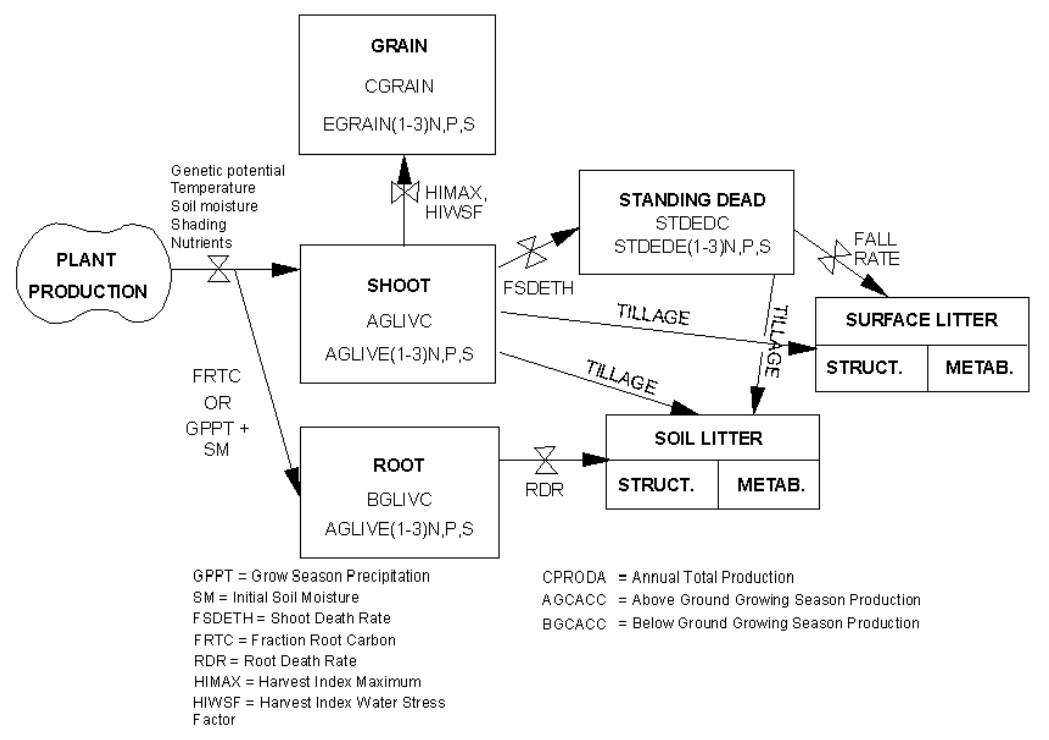


Figure 6.2 Grass submodel in CENTURY (Metherell et al., 1993)

BIOME – BGC simulates daily fluxes and states of carbon, water, and nitrogen for coarsely defined biomes at areas ranging from 1 $m^2$ to the entire globe (Figure 6.3). Plant physiological processes respond to diurnal environmental variation (Geiger and Servaites, 1994). BIOME – BGC uses a daily time step in order to take advantage of widely available daily temperature and precipitation data from which daylight averages of short wave radiation, vapor pressure deficits, and temperatures are estimated (Thornton et al., 1997; Thornton and Running, 1999). Nonlinear diurnal photosynthetic responses to radiation levels will not be captured by the use of daylight average radiation, but models initially designed to operate at daily timescales may still be used to accurately represent short-term variation in carbon fluxes (Kimball et al., 1997b).

In BIOME – BGC, 34 parameters within several main categories are used to distinguish separate biomes: 1) turnover and mortality parameters are used to describe the portion of the plant pools that are either replaced each year or removed through fire or plant death; 2) the allocation of photosynthetically accumulated carbon to leaf, stem, and root pools is controlled by a series of allometric parameters; 3) carbon to nitrogen ratios define nutrient requirements for new growth, plant respiration rates, photosynthetic capacity, and litter quality; 4) the percentage of lignin, cellulose, and labile material in fine roots, leaves, and dead wood control litter recalcitrance and influences decomposition rates; 5) three morphological parameters control the distribution of LAI at the leaf and canopy level; 6) several ecophysiological parameters are used to control rates of and limitations to leaf conductance; 7) single parameters are used to control water interception, canopy radiation absorption, and the rate of carbon assimilation. Conceptually, the parameter groups describe biomes by rejecting excessive detail and unobtainable parameters while maintaining broadly significant vegetation descriptions.

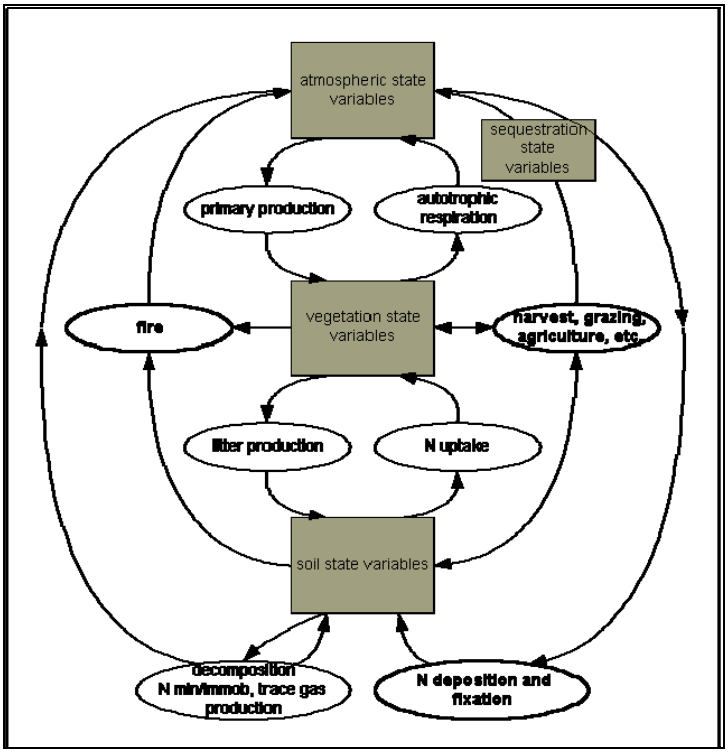


Figure 6.3 Biome-BGC: C and N dynamics with disturbance components (cited from: http://www.ntsg.umt.edu/models/bgc/index.php?option=com_content&task=view&id=16&Itemid=27, accessed on 11/20/2007)

### 6.3.4 Methods

Our study approach for model comparison consists of three major steps: (1) generate a common data set of meteorological variables; (2) define a common set of site input parameters values; (3) compare model results with the data from the field sites, against temperature and precipitation values to account for climate discrepancies, and with spatially remote sensing data sets (the AVHRR NDVI data).

After comparison, we will choose one site-specific process model to integrate it with remote sensing products. One of the important remote sensing products was leaf area index (LAI)

map since LAI is recognized as a critical vegetation parameter regulating the exchange of trace gases and energy between land surface and the atmosphere. Reliable remote sensing LAI data are a prerequisite for regional application of a process model (Liu et al., 1997). We developed a LAI map from a 20 m resolution SPOT 4 image over the entire study area to aid spatial modeling. Based on the LAI map, the other biophysical maps (green biomass, dead material, and canopy height) were also developed as model inputs. The model setting for onset and end of greenness is another key parameter controlling the length of growing season and determining the potential productivity. This parameter was derived from high temporal resolution imagery (AVHRR NDVI) in Chapter 5. A land cover map (20 m resolution) is also important because the functionalities of various vegetation communities are very different and changes in cover type affect productivity statistics for a region (Liu et al., 1997). The land cover map was also developed for the selected area in Chapter 5. A soil map was used as well, which describes soil classes with percent sand, clay and loam given at different layers (Saskatchewan Soil Survey, 1992). All these maps make it possible to extend site based model results to landscape scales

## 6.4 Results and Discussion

### 6.4.1 Model Comparison

Using climate records and parameters derived for a specific site in GNP, the CENTURY and BIOME-BGC models predicted annual NPP which compared well with field observations (Table 6.1). However, CENTURY and BIOME-BGC showed a large deviation in 1995 and 2003, respectively. This was considered an acceptable deviation since the other annual productivity values compared well, and there was high uncertainty in the measured biomass and the aggregate parameterization used for the model prediction. Inter-comparison showed that two models

predicted NPP consistently along the year, when CENTURY predicted high NPP in 1986, 1991, and 1999, BIOME-BGC resulted in high NPP in these years accordingly. However, we can also observe the differences between predictions.

Table 6.9 Predicted and measured biomass

| Years | Biome-BGC (products/RE) | Century (products/RE) | Measured biomass ($g/m^2$) |
|---|---|---|---|
| 1995 | 55.9 / 17% | 82.8 / 74% | 47.6 |
| 2003 | 73.9 / 74% | 50.4 / 19% | 42.5 |
| 2004 | 65.4 / -8% | 62.2 / -13% | 71.4 |
| 2005 | 55.2 / 23% | 38.4 / -14% | 44.7 |

Note: 1995 data Source (Mitchell and Csillag, 2001)

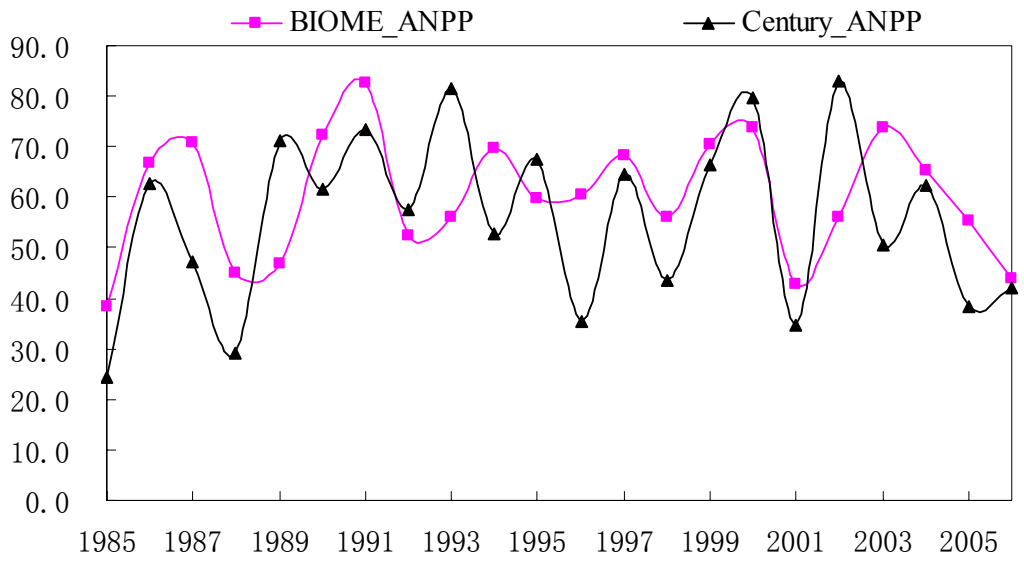


Figure 6.4 Simulated productivity from 1985-2006($g/m^2/yr$)

When NPP is plotted against precipitation and temperature, strong nonlinear relationships are evident in both models, but with intriguing differences (Figure 6.5).

BIOME-BGC has a weaker relationship with precipitation in comparison with CENTURY-precipitation relationship. The higher relationship between CENTURY and precipitation is reasonable since CENTURY was designed to relate NPP directly to environmental variables or indicators such as temperature, precipitation, available soil nitrogen, or other fertility factors, while the environmental variables influenced GPP and RA instead of NPP in the BIOME-BGC model. However, CENTURY temperature's relationship is weaker in comparison with BIOME-BGC temperature's relationship. This result may demonstrate that BIOME-BGC model is more sensitive to temperature than CENTURY.

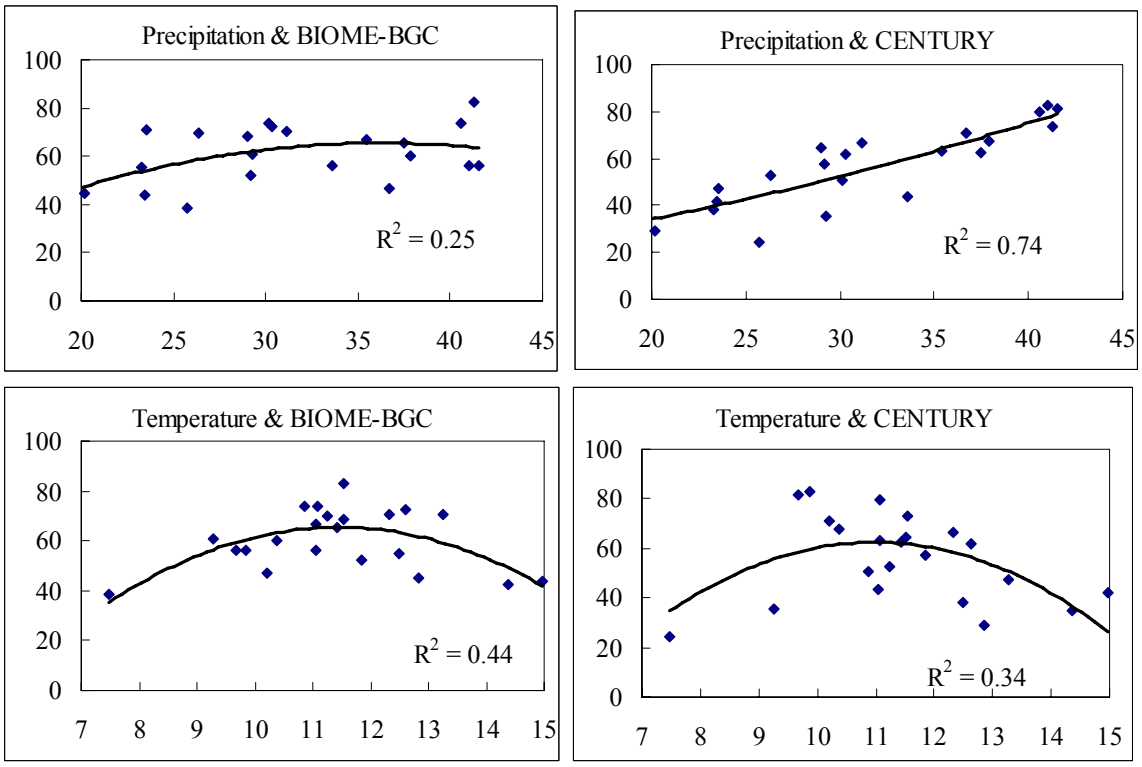


Figure 6.5 The relationships between climate data and simulated productivity (1985-2006)

We examined the NDVI-NPP relationship for the last 22 years (1985-2006) (Figure 6.6). The comparison of NPP vs. NDVI showed that the two parameters are correlated, and NDVI had

a greater correlation with BIOME-BGC over the years ($R^2$ is 0.5 with BIOME-BGC and 0.4 with CENTURY). The relationship between NDVI and NPP is not linear, and is steeper at low and high rates of NPP.

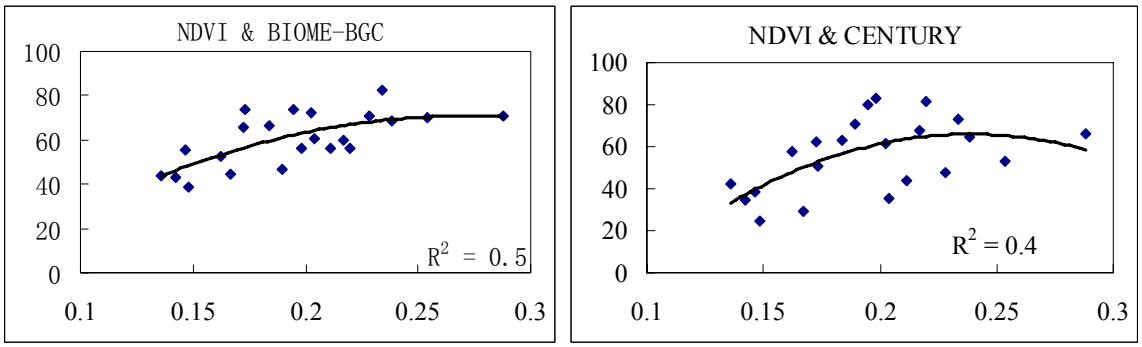


Figure 6.6 NDVI and simulated productivity (1985-2006)

Although the comparison shows that models can simulate productivity over years successfully, successful validation at specific sites does not guarantee successful simulation of spatial variability (Schimel et al., 1997). Both models (Century and BGC) have been extensively validated at specific sites (e.g., McGuire et al., 1993; Running, 1994); yet differ substantially in their simulation of spatial variability within vegetation types. Researchers (Schimel et al. 1985, 1991) presented a comparison of modeled and observed NPP along environmental gradients within the maritime coniferous vegetation type and the grasslands, and the results indicated the problems of using traditional site-specific data for spatial modeling. Few field studies have addressed variation of processes or state variables within vegetation types; this type of information is crucial for initiating and testing spatial ecosystem models. Therefore, we will introduce a remote sensing-based spatial model frame to minimize the above problems.

### 6.4.2 Remote Sensing-based Model Frame

Since the BIOME-BGC model needs less parameters and model outputs greatly correlate with NDVI data for the mixed grassland, we decided to develop a remote sensing-based process model frame by integrating remote sensing data with the site-specific BIOME-BGC model. As shown in Figure 6.7, the new model frame is not significantly different from other process models as it employs weather data, GIS data, and field data to initiate and drive the model as well. However, the difference is that the new model will also use remote sensing products, and therefore be able to scale up the model results to different spatial scales.

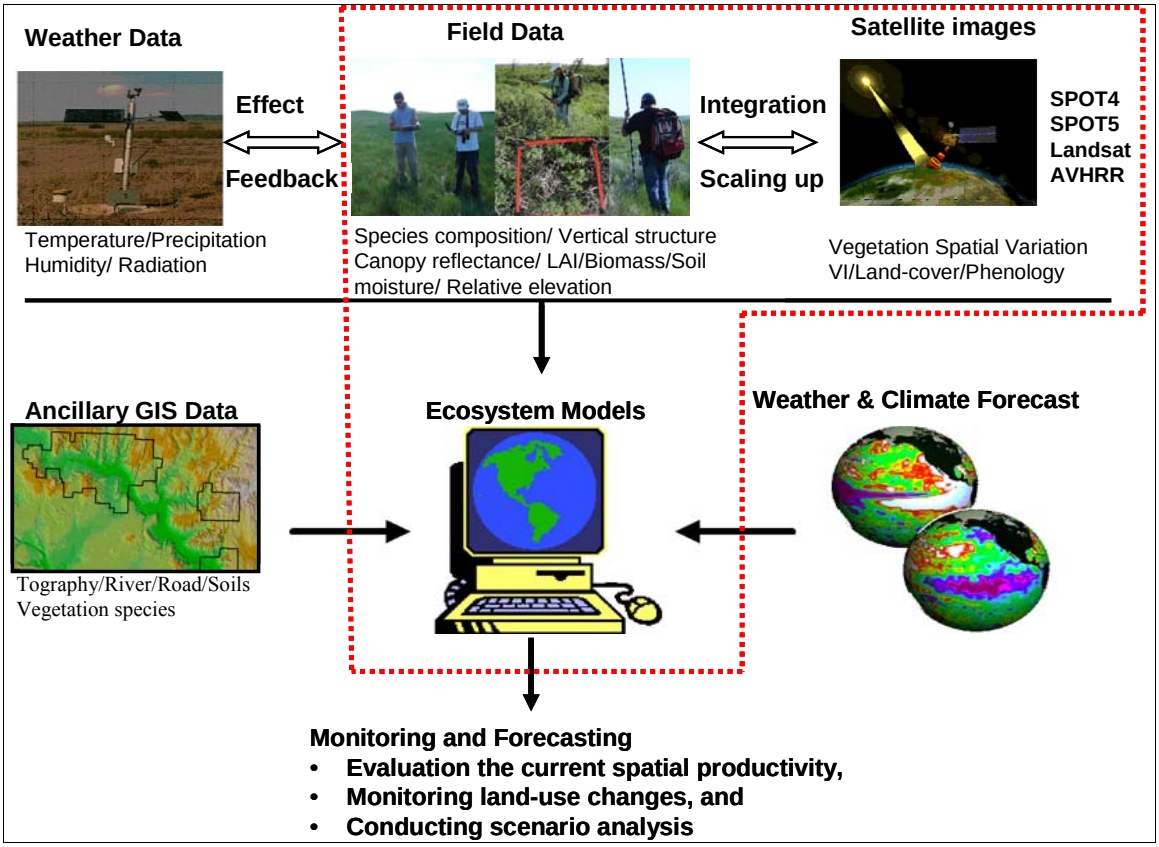


Figure 6.7 Proposed remote sensing data-based model frame

Figure 6.8 indicates that the new model frame can model productivity using different remote sensing products; this model structure is similar to the study conducted by Liu et al. (1997)

for the forest area. The remote sensing products used in this study are a 20 m land cover map, LAI map, dead material map, canopy height map, phenology map, and an elevation map, which were developed from previous chapters.

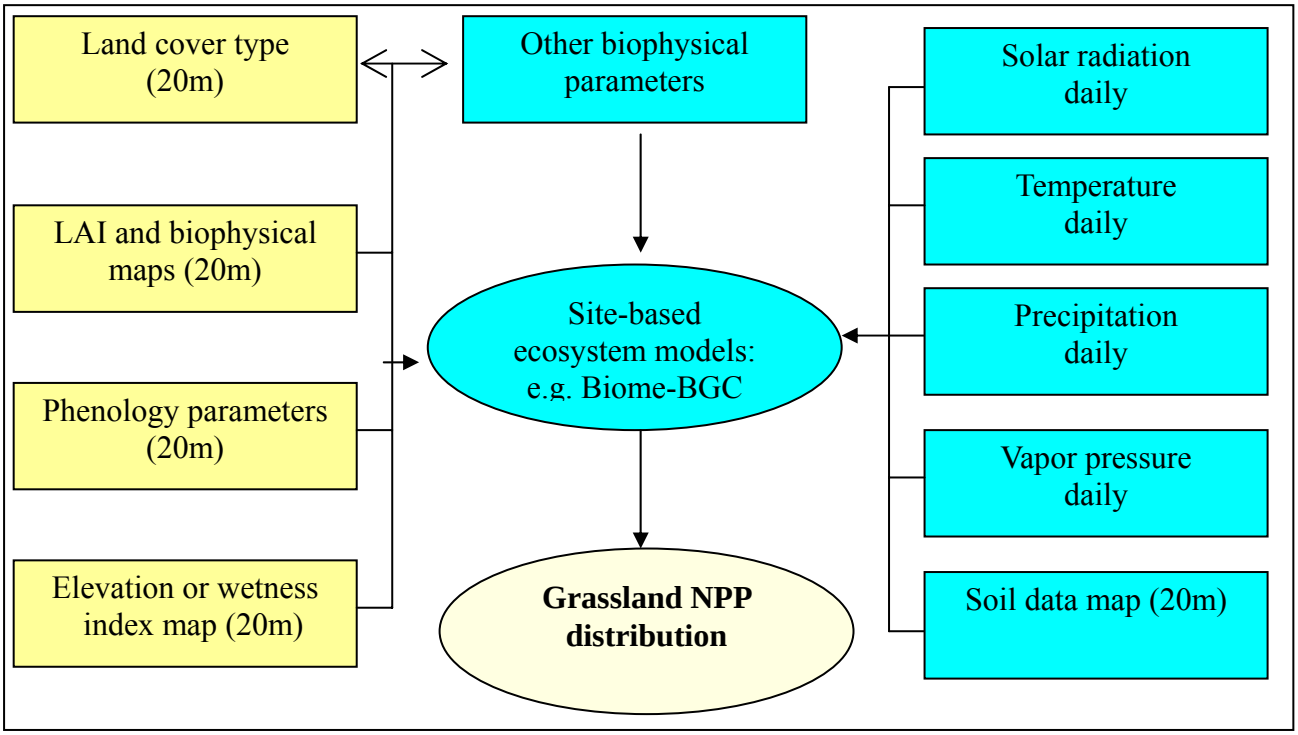


Figure 6.8 Detailed framework of remote sensing-based BIOME-BGC model, showing the major modeling steps, and input requirements, and the data spatial resolutions

To validate the new model, a case study was conducted for 2005 year in GNP. Using the developed maps as inputs, the above ground productivity (ANPP) was simulated with 20-m resolution for 2005 (Figure 6.9). The ANPP map was validated by the ground measurements, which was taken from the 30 sites, representing various grassland conditions in the west block of Grassland National Park. The corresponding pixels including the individual sites in the developed ANPP map were found. In order to ensure the sites are in the right locations, we selected a 5×5 pixel window to minimize the error from geometrical correction. The results showed that the

ANPP simulations and measurements at the locations compare well (average error = 9, and RMSE = 43). The map accuracy of 71% provides a critical validation to the model. The reason for the error between model results and observation might be from three sources: 1) inaccurate assignment of the other biological parameters in the model, as we used default parameters if they could not be obtained from remote sensing data; 2) error in remote sensing products. For example, the phenology map used in the model was downscaled from 1 km AVHRR product and is much larger than the resolution of LAI map and study sites. Further work is required to study this scaling effect, using high-resolution remote-sensing phenology map; 3) bias in the ground measurements. The ground measurements of productivity were calculated from the biomass collected from peak growing season based on the vegetation growth curve, whereas model ANPP represents the whole year. The annual ANPP values for various types in GNP with the remote sensing-based BIOME-BGC model are within the ranges of other results for the same area (Mitchell and Csillag, 2001). However, the proposed model provides much more detailed information with spatial resolution at 20 meters, which enables researchers to study grassland spatial heterogeneity and provides managers a better overview for each cover type.

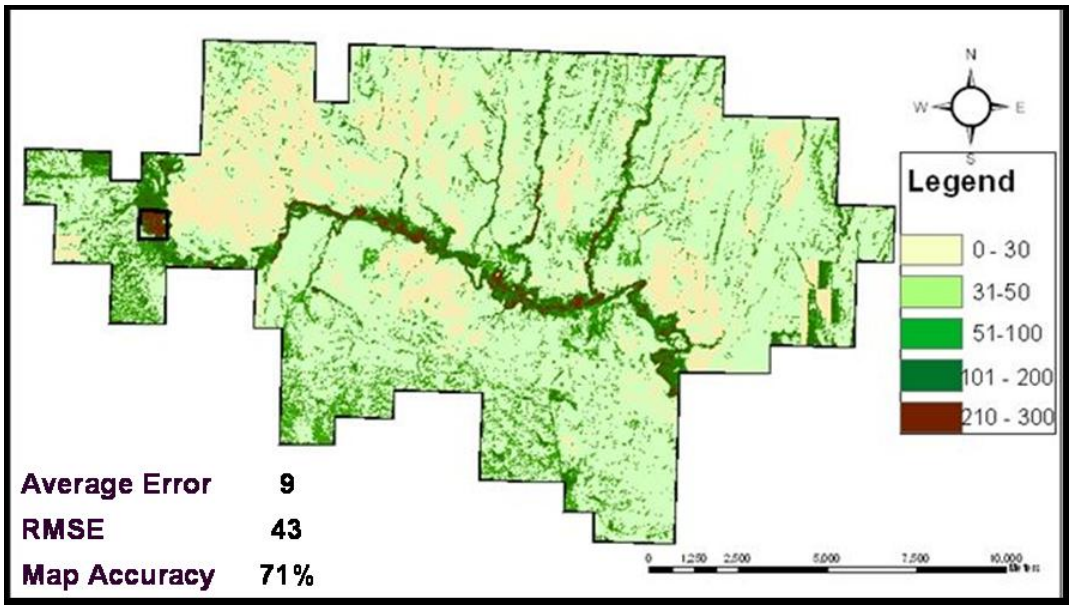


Figure 6.9 2005 Grassland ANPP Map (g/m$^2$/Yr)

## 6.5 Conclusions

The two site-specific ecosystem process models (BIOME-BGC and CENTURY) were compared for simulating productivity of the mixed grassland ecosystem. The results indicated that both models can simulate grassland productivity with an acceptable error. However, the models could not offer spatially distributed productivity for the study area, even though the study area is heterogeneous. To address this issue, a remote sensing-based model frame was proposed by integrating remote sensing products into site-specific BIOME-BGC model in order to simulate vegetation productivity in the landscape level. Using the developed model frame, we simulated a productivity map for GNP with 20 m resolution for 2005 based on remote sensing products proposed in previous chapters. The accuracy of simulated ANPP map is approximately 71%. Therefore, this modeling framework is a good tool to identify and quantify grassland productivity with spatial details.

## 6.6 Reference

Adams, B., White, A., and Lenton, T.M. 2004. An analysis of some diverse approaches to modeling terrestrial net primary productivity. Ecological Modelling. 177, 353–391.

Allen, J.D. 1990. A look at the remote sensing applications program of the National Agricultural Statistics Service. Journal of Official Statistics. 6, 393-409.

Asrar, G., Fuchs, M., Kanemasu, E.T., and Hatfield, J.L. 1984. Estimating absorbed photosynthetic radiation and leaf area index from spectral reflectance in wheat. Agronomy Journal. 76, 300–306.

Bouman, B.A.M. 1992. Linking physical remote sensing models with crop growth simulation models, applied for sugar beet. International Journal of Remote Sensing. 13, 2565–2581.

Boote, K.J., Jones, J.W., and Pickering, N.B. 1996. Potential uses and limitations of crop models. Agronomy Journal. 88, 704–716.

Bragg, T.B. 1995. Climate, soils and fire: the physical environment of North American grasslands. In: The Changing Prairie, K. Keeler and A. Joerns (eds.), Oxford University Press, New York.

Bruckler, L., and Witono, H. 1989. Use of remotely sensed soil moisture content as boundary conditions in soil–atmosphere water transport modelling. 2. Estimating soil water balance. Water Resources Research. 5, 2437–2447.

Burke, I. C., Kittel, T.G.F., Lauenroth, W.K., Snook, P., Yonker, C.M., and Parton,W. J. 1991.

Regional analysis of the central Great Plains. BioScience 41, 685–692.

Burke, I.C., and Lauenroth, W.K. 1993. What do LTER results mean? Extrapolating from site to region and decade to century. Ecological Modelling. 67, 19–35.

Cayrol, P., Kergoat, L., Moulin, S., Dedieu, G., Chehbouni, A. 2000. Calibrating a coupled SVAT-Vegetation growth model with remotely sensed reflectance and surface temperature—a case study for the HAPEX-Sahel grassland sites. Journal of Applied Meteorology. 39, 2452–2473.

Clevers, J.G.P.W., van Leeuwen, H.J.C., 1996. Combined use of optical and microwave remote sensing data for crop growth monitoring. Remote Sensing of Environment. 56, 42–51.

Coupland, R.T. 1950. Ecology of mixed prairie in Canada. Ecological Monographs. 20, 271–315.

Esser, G. 1986. The carbon budget of the biosphere—structure and preliminary results of the Osnabruck Biosphere Model. Ver offentlichungender Naturforschenden Gesellschaft in Emden von. 1814, 1–160.

Franks, S.W., and Beven, K.J. 1999. Conditioning a multiple-patch model using uncertain time–space estimates of latent heat fluxes inferred from remotely sensed data. Water Resources Research. 35, 2751–2761.

Fung, I.Y., Tucker, C.J., and Prentice, K.C. 1987. Application of advanced very high resolution radiometer to study atmosphere–biosphere exchange of CO2. Journal of Geophysical Research. 92, 2999–3015.

Genovese, G.. 1997. Yield Forecasting and operational approaches using Remote Sensing:

overview of approaches and operational applications in 1994 in the EU. Proceedings of the Seminar on Yield Forecasting, Villefranche sur Mer, 24-27 October 1994, ISBN92- 827-9451-2, pp. 79-86.

Geiger, D.R., and Servaites, J.C. 1994. Diurnal regulation of photosynthetic carbon metabolism in C3 plants. Annual Review of Plant Physiology and Plant Molecular Biology. 45, 235–256.

Goward, S.N., Markham, B., Dye, D.G., Dulaney, W., and Yang, J. 1991. Normalized difference vegetation index measurements from the Advanced Very High Resolution Radiometer. Remote Sensing of Environment. 35, 257–277.

Gillies, R.R., Carlson, T.N., Cui, J., Kustas, W.P., Humes, K.S. 1997. A verification of the 'triangle' method for obtaining surface soil water content and energy fluxes from remote measurements of the normalized difference vegetation index (NDVI) and surface radiant temperature. International Journal of Remote Sensing. 18, 3145–3166.

Guerif, M., and Duke, C.L. 2000. Adjustment procedures of a crop model to the site specific characteristics of soil and crop using remote sensing data assimilation. Agriculture, Ecosystems and Environment. 81, 57–69.

Hasager, C.B., Jensen, N.O. 1999. Surface-flux aggregation in heterogenous terrain. Quarterly Journal of the Royal Meteorological Society. 125, 1–28.

Holdridge, L.R. 1967. Life zone ecology. Tropical Science Center, San Jose, Costa Rica.

Houser, P.R., Shuttleworth, W.J., Famiglietti, J.S., Gupta, H.V., Syed, K.H., and Goodrich, D.C. 1998. Integration of soil moisture remote sensing and hydrological modeling using data

assimilation. Water Resources Research. 34, 3405–3420.

Kittel, T.G.F., Rosenbloom, N.A., Painter, T.H., Schimel, D.S., and VEMAP Modeling Participants. 1995. The VEMAP integrated database for modeling United States ecosystem/vegetation sensitivity to climate change. Journal of Biogeography. 22, 857–862.

Kimball, J.S., Thornton, P.E., White, M.A., and Running, S.W. 1997b. Simulating forest productivity and surface-atmosphere carbon exchange in the BOREAS study region. Tree Physiology. 17, 589–599.

Liu, J., Chen, J. M., Cihlar, J., and Park, W. 1997. A process-based Boreal Ecosystems Productivity Simulator using remote sensing inputs. Remote Sensing of Environment. 62,158-175.

Maas, S.J. 1988. Use of remotely-sensed information in agricultural crop growth models. Ecological Modelling. 41, 247–268.

Moran, M.S., Humes, K.S., Pinter, P.J. Jr. 1997. The scaling characteristics of remotely-sensed variables for sparsely-vegetated heterogeneous landscapes. Journal of Hydrology. 190, 337–362.

McGuire, A.D., Joyce, L.A., Kicklighter, D.W., Melillo, J.M., Esser, G., and Vorosmarty, C.J. 1993. Productivity response of climax temperate forests to elevated temperature and carbon dioxide: A North American comparison between two global models. Climatic Change. 24, 287–310.

Meyer-Roux, J., and King, C. 1992. European achievements in remote sensing: agriculture and forestry. International Journal of Remote Sensing. 13. 1329-1341.

Moulin, S., Bondeau, A., and Delécolle, R. 1998. Combining agricultural crop models and satellite observations: from field to regional scales. International Journal of Remote Sensing. 19, 1021–1036.

Mitchell, S.W., and Csillag, F. 2001. Ecological Modelling. 139, 101–121.

Nouvellon, Y., Moran, M.S., Seen, D.L., Bryant, R., Rambal, S., Ni, W., Be´gue´, A., Chehbouni, A., Emmerich, W.E., Heilman, P., Qi, J. 2001. Coupling a grassland ecosystem model with Landsat imgaery for a 10-year simulation of carbon and water budgets. Remote Sensing of Environment. 78, 131–149.

Potter, C.S., Randerson, J.T., Field, C.B., Matson, P.A., Vitousek, P.M., Mooney, H.A., and Klooster, S.A. 1993. Terrestrial ecosystem production: a process model based on global satellite and surface data. Global Biogeochemical Cycles. 7, 811–841.

Ranson, K.J., Sun, G., Knox, R.G., Levine, E.R., Weishampel, J.F., and Fifer, S.T. 2001. Northern forest ecosystem dynamics using coupled models and remote sensing. Remote Sensing of Environment. 75, 291–302.

Running, S.W., and Hunt, Jr. E.R. 1993. Generalization of a forest ecosystem model for other biomes, BIOME-BGC, and an application for global-scale models. Pages 141–158 in J. R. Ehleringer and C. B. Field, editors. Scaling physiological processes: leaf to globe. Academic Press, San Diego, California, USA.

Running, S.W. 1994. Testing Forest-BGC ecosystem process simulations across a climatic gradient in Oregon. Ecol. Appl. 4, 238–247.

Saskatchewan Soil Survey. 1992. Grasslands National Park Soil Survey. Unpublished report. University of Saskatchewan, Saskatoon, Saskatchewan, Canada.

Schmugge, T. 1998. Applications of passive microwave observations of surface soil moisture. Journal of Hydrology. 212/213, 188–198

Schimel DS et al. 1997. Continental scale variability in ecosystem processes: models, data, and the role of disturbance. Ecological Monographs. 67, 251–271

Schimel, D.S., Braswell Jr., B.H., Holland, E.A., Mc-Keown, R., Ojima, D.S., Painter, T. H., Parton, W.J., and Townsend, A.R. 1994. Climatic, edaphic, and biotic controls over carbon and turnover of carbon in soils. Global Biogeochemical Cycles. 8, 279–293.

Schimel, D.S., Kittel, T.G.F., and Parton, W. J. 1991. Terrestrial biogeochemical cycles: Global interactions with atmosphere and hydrology. Tellus. 43AB, 188–203.

Sellers, P.J. 1985. Canopy reflectance, photosynthesis and transpiration. International Journal of Remote Sensing. 6, 1335–1372.

Sellers, P.J., Berry, J.A., Collatz, G.J., Field, C.B., Hall, F.G. 1992. Canopy reflectance, photosynthesis and transpiration. III. A reanalysis using improved leaf models and a new canopy integration scheme. Remote Sensing of Environment. 42, 187–216.

Sellers, P.J., Heiser, M.D., Hall, R.G., Verma, S.B., Desjardins, R.L., Schuepp, P.M., MacPherson, J.I. 1997. The impact of using area-averaged land surface properties—topography, vegetation condition, soil wetness—in calculations of intermediate scale (aaproximately 10 km2) surface–atmosphere heat and moisture fluxes. Journal of Hydrology. 190, 269–301.

Thornton, P.E., and Running, S.W. 1999. An improved algorithm for estimating incident daily solar radiation from measurements of temperature, humidity, and precipitation. Agricultural and Forest Meteorology. 93, 211–228.

Thornton P. E., Running, S.W., and White, M.A. 1997. Generating surfaces of daily meteorological variables over large regions of complex terrain. J. Hydrol. 190, 214–251.

VEMAP Participants. 1995. Vegetation/Ecosystem modeling and analysis project (VEMAP): comparing biogeography and biogeochemistry models in a continental-scale study of terrestrial ecosystem responses to climate change and CO2 doubling. Global Biogeochemical Cycles. 9, 407–438.

Weiss, M., Troufleau, D., Baret, F., Chauki, H., Pre´vot, L., Olioso, A., Bruguier, N., and Brisson, N., 2001. Coupling canopy functioning and radiative transfer models for remote sensing data assimilation. Agricultural and Forest Meteorology. 108, 113–128.

White, J.D., Running, S.W., Thornton, P.E., Keane, R.E., Ryan, K.C., Fagre, D.B., and Key, C.H. 1998. Assessing simulated ecosystem processes for climate variability research at Glacier National Park, USA. Ecological Applications. 8, 805–823.

# CHAPTER 7 - SUMMARY

As highly synthesized quantitative parameters, vegetation productivity is the most important for characterizing the performance of an ecosystem (Liu et al., 1997). Vegetation productivity can be simulated by process models reliably because the foundation of the models is on the understanding of ecosystems. However, these models require many inputs and the application of such models to larger areas often depends on the availability of spatially distributed data. Many process models at the global scale are based on ecosystem-specific inputs, which assume that the vegetation is homogenous within the ecosystem at hand. In light of this shortfall, the overall objective of this research is to integrate remote sensing products to ecosystem process models. The hypotheses of this study are that: 1) remote sensing data, with different resolutions, can increase grassland productivity prediction accuracy at different levels; 2) remote sensing data, with mixed information in each individual pixel, can provide ecosystem process models with input parameters; 3) remote sensing data can be more effective in heterogeneous landscapes because of continues data acquisition in the coverage; and 4) remote sensing data can be used to monitor the ecosystem dynamics through process models because of the availability of high temporal resolution. Using ground hyperspectral data, medium resolution multiple-spectral satellite imagery (Landsat, and SPOT 4 &5), low spatial but high temporal resolution AVHRR imagery, and field biophysical data, this research validates all hypotheses by determining the optimum remote sensing resolution and classifiers. It also develops spatially distributed model parameters (including an LAI map, phenology map, and land cover map) from remote sensing data; compares commonly-used site-specific ecosystem models, and proposes a new remote sensing-based spatial ecosystem model for studying mixed grassland

prairie. The results show that it is feasible to integrate remote sensing products with a site-specific ecosystem model to represent spatially-distributed grassland productivity.

## 7.1 Conclusion

### 7.1.1 Scale of Vegetation Variation and Controlling Factors in the Mixed Grassland

This study revealed that variation in vegetation within the study area is controlled by soil moisture and topography. A strong correlation was found between LAI and soil moisture, and stronger correlations were found between LAI and topographic parameters. Among topographic parameters, the wetness index explained more of the total variation in LAI than both relative elevation and upslope length because the wetness index reflects the water storage in a location more strongly than other indicators. NDVI was significantly correlated with LAI and topography parameters, demonstrating that variation in LAI can be detected by remote sensing data and that imagery with 20 m resolution can reveal, to some extent, the effect of topography on grassland vegetation. The wetness index explained more of the total variation in NDVI than relative elevation and upslope length along the three transects.

Wavelet analysis showed that topographic factors are responsible for the majority of spatial variation of LAI at a large scale of approximatly 120 m. Therefore, following the sampling theorem (McGrew and Monroe, 2000), 20 to 30 m (one fourth of a period, 120 m) would be an optimum pixel size to detect potentially important patterns associated with topography in our study area. For example, landscape patterns of LAI, biomass, photosynthetic flux and evapotraspiration of vegetation within the study region can likely be described effectively using this fundamental pixel size.

Wavelet analysis also showed spatial variation of soil moisture at scales of 20 m and 40 m, closely associated with the spatial scales of LAI (20 m and 40 m). Since there is a wide variety of soil types in GNP (Csillag et al., 2001), the two small scales of LAI may result from an integrated effect of other environment factors (soil texture, depth, and chemical and physical properties) on soil moisture. The smaller scales also suggest that imagery resolutions larger than 20 m may not be able to identify all spatial variability resulting from soil moisture in our study area.

Heterogeneity of the broadband NDVI along two 2560 m transects demonstrated that vegetation variation at the large scale 120 m can be detected by satellite imagery with a 20 m resolution. This result largely confirmed the conclusion that the NDVI variation is also related to topography at the landscape scale (Brosofske et al., 1999) and that the appropriate resolution imagery can examine the spatial characteristics associated with topography for landscape level ecosystem studies (Gamon et al., 1993). In addition, the NDVI has a significant spatial scale of 50 m and 40 m in two transects, which must be a result of spatial variation from soil moisture. Both global features of the NDVI along the two extensive transects did not show spatial variation at the 20 m scale (associated with soil moisture), which was identified by the ground biophysical data. This result indicates that some small features that create heterogeneity (such as soil moisture) may not be identified at broader scales.

In conclusion, the implications of this study are that: (1) in investigating grassland variation, one should consider the effect of both soil moisture and topography, not only at a fine scale but also at a coarse scale; (2) to estimate grassland productivity, applying the appropriate topographical parameters is important; (3) the wavelet approach is useful for revealing both localized and global features of soil moisture and topography that exert significant effects on grassland vegetation; (4) remote sensing data can reveal the variation of grassland biophysical

properties and monitor the effect of topography on grassland vegetation by performing wavelet approach, and (5) 20 to 30 m (one fourth of a period, 120 m) would be an optimum pixel size to detect potentially important patterns associated with topography in our study area.

### 7.1.2 The Performance of Remote Sensing VI for Modeling Vegetation Properties in the Mixed Grassland

Using ground-based hyperspectral, biophysical, and satellite data, this study compared the predictive capabilities of VIs for estimation of grassland LAI. The relationships between grassland LAI and selected VIs are significant. Among the biophysical indices, ratio-based VIs and soil-line-related VIs are better than chlorophyll-corrected VIs in LAI estimation. The performance of RDVI, ATSAVI, and MCRAI2 at estimating LAI are slightly better than that of other VIs within the groups of ratio-based, soil-line-related, and chlorophyll-corrected VIs, respectively.

The litter-corrected ATSAVI (L-ATSAVI) appeared to be the best indicator in estimating LAI. L-ATSAVI could explain 55% of grassland LAI and improved LAI estimation capability in our study area by about 10% compared with other selected VIs. Our results indicated that previous vegetation indices have limitations in removing the effect of litter and that incorporating CAI into ATSAVI can improve the ability of LAI estimations in the study area.

Although the current study utilizes a dataset collected along a transect with high vegetation variability, the results of this study are confined to our study site, one mixed grassland ecosystem. Future research should test the feasibility of these vegetation indices through radiative transfer models or ground truth data from different study sites with different vegetation types, and also apply the improved vegetation index, L-ATSAVI, to remotely sensed imagery.

### 7.1.3 Remote Sensing Vegetation Biophysical Properties Developed for Modeling Grassland Productivity

We developed the LAI map based on the relationship between LAI and two indices, ATSAVI and RDVI. A detailed assessment of the accuracy of the regression models indicated that ATSAVI was likely better in estimating and mapping LAI than the RDVI for the mixed grassland ecosystem. The accuracy of the LAI map, derived from ATSAVI, was calculated to be 66.7% and this map represents the spatial distribution of vegetation for the study area.

The significant relationships found between measured LAI and the biophisical data (i.e. green biomass, dead biomass, and canopy height) solves the difficulty for mapping biophysical information due to insufficient sampling coverage for GNP. Biophysical maps (green biomass map, dead biomass map, and canopy height map) were developed from the LAI map using the regression models between biophysical data and measured LAI. A careful examination of these maps showed that, in general, the three maps accurately represent the biophysical information as explained for the LAI map. Statistical results indicated that the canopy height map resulted in the highest map accuracy, followed by green biomass, while the least accurate is dead biomass.

### 7.1.4 Remote Sensing Land Cover Map and Vegetation Phonology Developed for Modeling the Mixed Grassland Productivity

Through extracting spectral signals from different land cover types, we concluded that SPOT 4 20 m data sets have a high enough spectral, spatial, and temporal resolution to be able to classify 7 major land cover areas with an overall accuracy of 87%, and to classify eight finer classes with an overall accuracy of 85%. This study also showed that multi-temporal remotely sensed data are critical in grassland classification. However, a successful classification map is not

only based on a better classification algorithm, but is also dependent on the careful selection of training sites and the image acquisition date. Among classification algorithms, the object-oriented classification showed the best results. It is clear that the higher resolution images (SPOT4) offer an advantage over Landsat TM in classifying finer classes.

Using high temporal resolution imagery (AVHRR NDVI), we found it is possible to identify vegetation phenology. Generally, in mixed grass prairie, early May is the green up of forb and shrub species, and some grass species such as crested wheatgrass. The second green up period extends from June 11st until June 21th, indicating the green-up of native grass species. The peak growing season appeared in late June and the end of growth season occurred in early October.

### 7.1.5 Model Comparison and the Development of Spatial Ecosystem Process Model Frame

The two site-specific ecosystem process models (BIOME-BGC and CENTURY) were compared for simulating productivity for the mixed grassland. The results indicated that both models can simulate grassland productivity with an acceptable error. However, the models could not offer spatially distributed productivity for the study area. To address this issue, a remote sensing-based model frame was proposed by integrating remote sensing products into site-specific BIOME-BGC model, in order to estimate productivity in the landscape level. Using the developed model frame, we simulated the productivity map for GNP at 20 m resolution for the year 2005, based on remote sensing products developed in previous chapters. The simulated ANPP map accuracy is about 71%. Therefore, this modeling framework is a good tool to identify and quantify grassland net primary production with spatial details.

## 7.2 Potential Applications

There are three potential application of this research; that are of scientific, ecological, and economic applications. Scientifically, the research addressed a critical gap in modeling spatially-distributed productivity for the mixed grassland ecosystem. The results from this research identified the most optimum spatial resolution, most suitable spectral vegetation indices, and an efficient model frame in measuring distribution of grassland productivity. Considering the large number of mixed grassland ecosystems in North America, which are not analyzed in this study, and taking into account the existence of other grasslands across Europe and Asia, many more ecosystem properties and processes could be readily identified by using the methodology employed in this study.

As for ecological applications, many of the biophysical measures developed for GNP can be taken not only to monitor changes in the vegetation community itself, but also to understand the influence of vegetation changes on the associated faunal community. The new model framework can be applied to grassland management by providing high spatial resolution productivity, and thus assure sustainable development of northern mixed grasslands. Furthermore, output of this study will contribute to other studies such as climate change, carbon sequestration, sustainable ecosystem development, and grassland ecology.

The economic application of this study is that it will generate in a cost-effective and efficient way to accurately measure grassland productivity at a range of spatial scales; it will provide a tool for stakeholders, park managers, and ranchers to make better decisions regarding conservation planning, grassland management, and sustainable grazing intensity. Indeed, GNP is moving forward to incorporate the developed maps and modelframe in aid of spatial fire fuels

modeling, and habitat modeling for species at risk and biomass monitoring for a reintroduced herd of plains bison.

### 7.3 Limitations

This research addressed the gap in the current site-specific process models by using remote sensing products. However, there are still some limitations that need to be addressed in future studies.

(1) Accuracy of Remote Sensing Products

The accuracy in remote sensing products (e.g. LAI) strongly affects most components of the models, including radiation absorption, transpiration, photosynthesis, respiration, and soil water balance. Therefore, reliable remote sensing products are a prerequisite for regional application of a process model. However, the remote sensing products, especially those derived from vegetation indices, offer only reasonable first-order estimates of biophysical variables based on an empirical relationship. Consequently, the analysis for the RE demonstrated that the proposed maps derived from empirical relationships should be treated carefully in areas of higher or lower vegetation cover. To avoid this type of problem in future experiments, more samples from areas with higher or lower vegetation cover should be measured to ensure that observations are representative. Furthermore, some error propagation may exist when using derived maps as input for modeling grassland productivity, even if there is a significant relationship between satellite data and field biophysical data.

(2) Availability of Remote Sensing Products

Even though remote sensing data can be used to estimate vegetation properties in diverse temporal and spatial scales, optical sensors that provide a spatially comprehensive overview at a finer spatial resolution (for example, 20-30 m) for heterogeneous grasslands can not provide an adequate update for daily or monthly time-step models. Conversely, high-temporal resolution imagery (such as AVHRR) can be used to offer daily inputs for models or used to identify vegetation phenology. However, the coarse spatial resolution (AVHRR is 1.1 km) might not be able to capture spatial details for the mixed grassland, and thus increases model uncertainty. For ecosystem models, it could be argued that an ideal system would utilize data to estimate variables that have spatial and temporal scales comparable to those required by the ecosystem model. Unfortunately, with current technology, the design of a sensing system requires a balance between the spatial and the temporal.

In addition, the developed hyperspectral vegetation index (L-ATSAVI) was found to be the best remote sensing index in estimating vegetation biophysical properties while minimizing the effects of litter and soil background. However, a lack of hyperspectral imagey for the study area made this index incapable of functioning.

(3) Study the Responses of Models on Disturbance

All of the ecosystem models are sensitive, implicitly or explicitly, to disturbance in their productivity simulation. Both the effects of disturbance (human and natural) and spatial data describing disturbance regimes are critical aspects of spatially-distributed ecosystem models. This study did not test the response of models to disturbance because the study area (GNP) has been protected from grazing and large human activities over years and there is no significant

disturbance in the GNP. Considering disturbance responses is a key ‘‘next step’’ for the proposed spatial ecosystem models by using the data from outside of GNP.

## 7.4 References

Brosofske, K.D., Chen, J., Crow, T.R., and Saunders, S.C. 1999. Vegetation responses to landscape structure at multiple scales across a northern Wisconsin pine barren landscape. Plant Ecology. 143, 203-218.

Csillag, F., and Kabos, S. 2002. Wavelets, boundaries, and the spatial analysis of landscape pattern. Ecoscience. 9, 177-190.

Gamon, A., Field, C.B., Roberts, D.A., Ustin, S.L., and Valentini, R. 1993. Functional patterns in an annual grassland during an AVIRIS overflight. Remote Sensing of Environment. 44, 1-15.

Liu, J., Chen, J. M., Cihlar, J., and Park, W. 1997. A process-based Boreal Ecosystems Productivity Simulator using remote sensing inputs. Remote Sensing of Environment. 62, 158-175.

McGrew, J. C., and Monroe, C. B. 2000, An introduction to statistical problem solving in geography (2nd ed.) (Boston: McGraw-Hill) pp. 110.

APPENDIX A –FIELD DATA COLLECTION FORM

**Date:** **Time:** **Recorder:**

| **Plot Series:** | | **Rel. elev.:** | **Lat.:** | **Long.:** | | **Soil core:** |
|---|---|---|---|---|---|---|
| **Quad rat** | **Series** | | | | | |
| | **Aspect** | | | | | |
| | **Slope** | | | | | |
| **Cover-top layer** | **Grass** | | | | | |
| | **Forb** | | | | | |
| | **Shrub** | | | | | |
| | **Standing dead** | | | | | |
| **Cover-Low layer** | **Litter** | | | | | |
| | **Moss** | | | | | |
| | **Lichen** | | | | | |
| | **Rock** | | | | | |
| | **Bare ground** | | | | | |
| **Height** | **Litter depth** | | | | | |
| | **Average height** | | | | | |
| | **No. of hits: 0-10** | | | | | |
| | **10-20** | | | | | |
| | **20-30** | | | | | |
| | **30-40** | | | | | |
| | **40-50** | | | | | |
| **Cover of grass \forb\shrub species** | **Needle & thread** | | | | | |
| | **Blue gramma** | | | | | |
| | **June grass** | | | | | |
| | **Western wheatgrass** | | | | | |
| | **Northern wheatgrass** | | | | | |
| | **Awned wheatgrass** | | | | | |
| | **S lender wheatgrass** | | | | | |
| | **Green needle grass** | | | | | |
| | **Sedge** | | | | | |
| | **Salt grass Prairie sage** | | | | | |
| | **Pasture sage** | | | | | |
| | **Sage brush** | | | | | |
| | **Cactus** | | | | | |
| | **Unidentified grasses** | | | | | |
| | **Unidentified forb** | | | | | |
| | **Unidentified shrub** | | | | | |
| **Soil moisture** | | | | | | |
| **Soil temperature** | | | | | | |
| **Biomass** | | | | | | |

**Note** (location description, community, etc.):

APPENDIX B – INSTRUMENTS GUIDES DEVELOPED FOR FIELDWORK

## 1. ASD Spectroradiometer

**What you should know:**

1. Hardware: instrument body (power button, battery status indicator, parallel port, power supply jack, battery check, fiber optic cable, pistol grip), laptop, cables, white reference, power chargers.
2. Fiber optic cable: coiled loosely
3. Power sequence:
   Turn on —first instrument, then laptop. Warm up 15 minutes later before measurement.
   Turn off ---first laptop, then instrument.
4. Battery status indicator light:
   Off : No battery connected or running on battery power.
   Solid yellow: Charging
   Green: Fully charged
   Yellow flash: Standby or battery out of temperature range.
   Red: Error

**Operation procedures:**

Preparing:

- ✧ CHARGE both instrument and laptop indoor every night.
- ✧ Remember to wear black clothes, especially when measuring shrub spectra.
- ✧ Set up the field quadrads.
- ✧ Watch the sky. If it is clear day and time is between 10:00am-2:00pm, then ready for following steps:

1. Take out the laptop and connect with instrument.
2. Turn on the instruments and warm up 15 minutes.
3. Install the fiber carefully, do not stretch the fiber or pull it.
4. Turn on the laptop and carry everything with you (reference and fiber optic cable in hands).
5. Click SW in the screen.
6. Select the menu at the top of screen called ***Spectrum Save*** （**Alt+c**）.
   - ✧ Path name: D:\2006fielddata\date
   - ✧ Base name: sitename
   - ✧ Starting Spectrum #: 000
   - ✧ Number of files to save: 999
7. Point the pistol to the white reference.
8. **Ctrl+o** ----- optimization (look at right corner in the panel till ‘optimization completed’)
9. **F4** ----- Collect a white reference

- ✧ If a straight line spectrum appears on the screen, hold it there for 3 - 5 seconds to make sure the atmospheric conditions are stable.
- ✧ If not a straight line, go back to step 7.
- ✧ Redo step 7-10 at least every 10 - 15 minutes if atmospheric conditions change.

10. Point the pistol to the sample surface, remember to keep the pistol completely vertical (using leveling bubble on top**)**
11. **Space bar** ----- Save spectra data.

**2. LAI 2000 Plant Canopy Analyzer**

**What you should know:**

1. Use your shadow to avoid direct sun when measuring both above and below reading.
2. Make sure the fish eye points to open area when you take above readings.
3. Use leveling bubble when taking measure on flat area.
4. Make your sensor parallels to the slope when measuring sloped area.

**Operation procedures:**

1. Connect the sensor (connector is n your left as you view the front panel keypad).
2. Pow on (on)
3. Oper ---Set Op Mode: MODE = 1 sensor x---Seq=1 above and several below readings, Reps=1
4. Set Promps (FCT 1 2): Prompt 1=Site, Prompt 2=Quad
5. Log: Promt 1=Site name, Prompt 2=Quad name, then take the readings.
6. Power off (FCT 0 9)
7. Download data ---Two formats: save as, and export

**3. HH2 Moisture Meter and ThetaProbe**

**What you should know:**

**1. Hardware: Meter, Probe, connectors, robs, ML-INK1 insertion kit, battery**

- ✧ Do not remove the cross-head sealing screws.
- ✧ Do not remove the ThetaProbe from soil by pulling on the cable.
- ✧ Do not attempt to straighten the measurement rods while they are still attached to the probe body.
- ✧ Clean the guide block with fresh water and mild detergent.
- ✧ Clean rods with a fine oil based lubricant.
- ✧ Disconnect the sensor immediately on receiving the low battery warning, or you will lose data.
- ✧ Ensure the HH2 is sleeping before changing the battery (Do we have enough battery?).
- ✧ You have 30 seconds to replace the battery before all stored readings are lost. If possible, download data first.
- ✧ 1 battery can take approximately 2000 readings.
- ✧ Memory: 227-2186 readings
- ✧ **Erase: yes only when you want to erase stored data.**

**2. Measurements:**

- ✧ Be very careful when removing and re-inserting the probe into a previous location, because the presence of air pockets around the rods will reduce the value of soil moisture content measured.
- ✧ If soil is heterogeneous, it will be necessary to take measurements from at least three closely-spaced locations.

APPENDIX C – FIELD PLAN FOR LAND COVER CLASSIFICATION IN GNP

## 1. Objective:

The objectives are to: 1) investigate the biophysical and spectral characteristics of 18 land cover communities; and 2) provide a map of current land cover communities within Grasslands National Park to aid in creating an effective management plan for the park.

## 2 Data Collection

### 2.1 Sampling sites selection

Supervised and object-oriented classifications require field work prior to image classification, in order to identify field sites for training data. Sample sites were chosen based on the current database for GNP (GEMS Project Report #3, John Wilmshurst). The 20 land cover communities are showed in Table 1. Since we can identify road, track and river clearly from the satellite imagery, and we had enough sites for the Crested Wheat grass based on Tara's field work and enough thorny buffalo berry sites from last year's field work, we do not need to visit the sites for these five land cover types. The land cover communities that we should visit are reduced to be **15** now.

Ideally, we would like to choose 30 sites for each land cover community, in which 15 sites will be training data and the rest 10 sites will be used for post classification accuracy assessment. Study sites are selected which are within park boundaries, mostly in the west block, as the focus was to map species invasion within the park area. To determine 30 sites for visiting, we first extract all the points for each type of communities based on the state classes map (GEMS Project Report #3, John Wilmshurst). Then the purpose based sampling method will be used to choose 30 sites for each community. If some communities do not have enough points, such as Prairie Dog community, we will visit all the points we extract from the map.

The purpose based sampling is drawn solely on the operator's judgment and is deliberate in selecting representative sites (McCoy, 19, 2005). This method of sampling is defensible in areas with limited accessibility or where the operator is working with a phenomenon which they are familiar with. Although, there is always operator bias which renders accuracy and level of confidence statements in the final map statistically invalid because random sampling was not used (McCoy, 19, 2005).

Table 1: List of state classes in the GNP. (GEMS Project Report #3, John Wilmshurst). We can identify road, track and river clearly from the satellite imagery, and we had enough sites for Crested Wheatgrass based on Tara's field work and enough thorny buffalo berry sites from last year's field work. Therefore, we do not need to visit the sites for these five land cover types.

| Land Cover | Land Cover Code |
|---|---|
| Speargrass-BlueGrama | 6001 |

| | |
|---|---|
| Creeping Juniper-Speargrass | 6004 |
| Pasture Sage-Speargrass-BlueGramaGrass | 6005 |
| Alkali Grass-Nuttail's Salt Meadow Grass | 6006 |
| SageBrush-W Wheatgrass-Opuntia | 6007 |
| Disturbed-Smooth Brome | 6008 |
| Rose-Winter Fat | 6009 |
| Willow-BuckBrush | 6010 |
| Rose-BuckBrush | 6011 |
| Saskatoon-ChokeCherry-Canada GooseBerry | 6012 |
| Disturbed: Russian wild Rye | 6013 |
| Shrubby Cinquefoil - Rose | 6014 |
| Thorny Buffaloberry | 6015 |
| Speargrass-Western Wheatgrass | 6020 |
| Crested Wheatgrass | 6023 |
| Prairie Dog | 6024 |
| Exotic | 6027 |
| River | 6099 |
| Road | 8000 |
| Track | 8001 |

## 2.2 Sampling Design

A sampling scheme was produced to collect biophysical data within the sites. Five 0.5 $m^2$ quadrats were positioned within 60 x 60 meter study sites to collect data for each study site. The first quadrat was randomly placed at one corner of the plot, the second quadrat was placed 60 meters north of the first quadrat, the third quadrat was placed 60 meters west of the second quadrat, the fourth quadrat was located 60 meters south of the third quadrat, and the final quadrat was placed in the centre of the site. This sampling scheme is designed to represent a sample from four different pixels from Landsat imagery and 9 different pixels from SPOT 4 imagery. McCoy suggests an equation for determining the area of a sample site as:

$$A = P \times (1 + 2L)$$

Where A is minimum site dimension, P is image pixel dimension, and L is vocational accuracy. So with Landsat ETM+ data of pixel dimension 30 meters and locational accuracy of at least 0.5 pixels the minimum sample site size should be 60 x 60 meters.

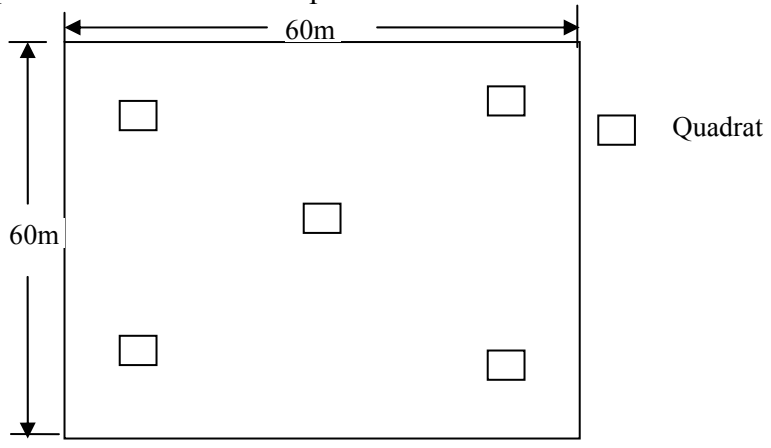

Figure The sampling scheme for the data collection

**2.3 Instruments and collected variables**

For each site, we are going to collect:

- Locational information
- A picture of the site
- LAI
- Dominant Species
- Green Cover
- Dead Cover

Instruments used for data collection include the following: a Garmin GPSMap 76S Global Positioning System (GPS), Li-Cor LAI-2000 Plant Canopy Analyzer, a digital camera, and a 50*50cm quadrat. GPS readings were taken for locational positioning. The LAI-2000 was used to collect Leaf Area Index (LAI) for quadrat level. The digital camera will take a picture for the site. The quadrat will be used to measure green and litter cover. Cover was estimated to the nearest 5% for cover values ranging from 10% to 90% and to the nearest 1% for cover values less than 10% and greater than 90% in green cover and litter (bare ground if it dominates the quadrat). Main species were identified for each site.

**3. Work load estimation**

Expected sites are as followed:

| Land Cover | Land Cover Code | Expected sites |
|---|---|---|
| Speargrass-BlueGrama | 6001 | 30 |
| Creeping Juniper-Speargrass | 6004 | 30 |
| Pasture Sage-Speargrass-BlueGramaGrass | 6005 | 30 |
| Alkali Grass-Nuttail's Salt Meadow Grass | 6006 | 7 |
| SageBrush-W Wheatgrass-Opuntia | 6007 | 30 |
| Disturbed-Smooth Brome | 6008 | 28 |
| Rose-Winter Fat | 6009 | 23 |
| Willow-BuckBrush | 6010 | 30 |
| Rose-BuckBrush | 6011 | 30 |
| Saskatoon-ChokeCherry-Canada GooseBerry | 6012 | 13 |
| Disturbed: Russian wild Rye | 6013 | 5 |
| Shrubby Cinquefoil - Rose | 6014 | 0 |
| Speargrass-Western Wheatgrass | 6020 | 30 |
| Prairie Dog | 6024 | 13 |
| Exotic | 6027 | 10 |
| Total | | **309** |

- GPS readings and Pictures: 309
- LAI measurements: 309*5
- Dominant Species: 309
- Green and litter cover measurement: 309*5

**4. Reference:**

McCoy, R. M. (2005) Field *Methods in Remote Sensing*. New York: The Guildford Press.

APPENDIX D –FIELD PLAN FOR LAI INSTRUMENTS COMPARISON

## 1. Objectives:

- ✧ Comparing indirect measurement of leaf area by two commercially available instruments, AccuPAR and the LAI-2000, with direct destructive measurements of leaf area.

## 2. Data collection:

### 2.1 Instruments and other stuff

- ✧ ASD Spectroradiometer /Soil moisture meter /LAI 2000 /AccuPAR /GPS
- ✧ High accurate scale (error +-0.0001)
- ✧ Four tent pegs and string to make 120*120cm$^2$ for measurement
- ✧ 5*5&10*10cm$^2$ Bristol boards with scale on to measure direct leaf area
- ✧ 0.1m$^2$ hoop and 0.1m$^2$ square frame
- ✧ Hand shear, plastic bag and flag

### 2.2 Sites location

LAI measurement will be measured within about 20 sites, which will encompass the range of grass density:

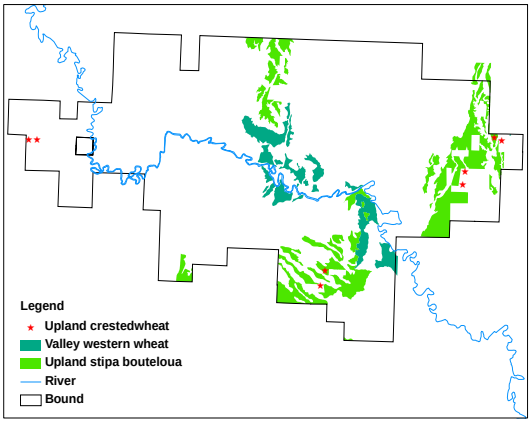


- ✧ 5 valley brome sites (high density)
- ✧ 5 valley sagebrush / western wheatgrass sites (not including the shrubs though for ease of interpretation)(medium to high density)
- ✧ 5 upland crested wheatgrass (medium to high density)
- ✧ 5 upland stipa / bouteloua sites (typically low density)

### 2.3 Samples and measurements within a site:

For our study area, we use the leaf removing method for comparison (e.g. Wihelm, 2000). After obtaining removed leaf sample per site, Leaf area is measured on a sub-sample of leaves and related to green mass (e.g. via specific leaf area, *SLA*, m2 g–1). Finally, the total mass of leaves

collected within a known ground-surface area is converted into *LAI* by multiplying by the *SLA*.

- ✧ remove the non-grass species in the sites before any measurements
- ✧ take spectral measurements (4 for each site )
- ✧ take soil moisture measurements (4 for each site)
- ✧ LAI measurements:
  - ✓ Use two LAI meters to measure LAI (named as LAI 1) for a site.
  - ✓ Clip grass (by hand shear) in four green circles within the site.
  - ✓ Remove grass from the site and put into plastic bag.
  - ✓ Weigh the clipped grass
  - ✓ Use two LAI meters to measure LAI (named as LAI 2).

    Direct LAI = sum (4 clipping area)

    Indirect LAI = LAI 1- LAI 2

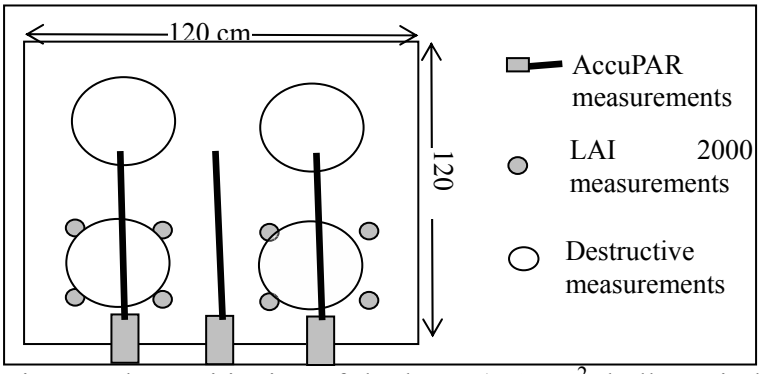


Figure. The positioning of the hoop (0.1 $cm^2$, hollow circles) where the grass is cut in each site, and the positioning of the sensors where under-canopy LAI readings were taken with the LAI 2000 (small grey circles) and AccuPAR (the bold line). The positioning of the sensors was shown for only one side of a site. In the field, we measured optically estimate LAI for four sides of each site with the instruments and average all the measurements to represent LAI for this site.

**3. Work load estimation**

Field work: 20 sites, so we have----

- ✧ 80 samples to clip, weigh, sort
- ✧ 20 Accupar readings and 40 LAI-2000 readings (1 above and 8 below, two measurements for each site)

Home work: 20 sites, for each site----

- ✧ Measure 10cm*10cm leaf area for each site and weigh them ($G_1$ g) ---stored in a refrigerator at $3^0$C and measuring has been done within 24h (Johnson and Pierce, 2004).
- ✧ Calculate total true leaf area index for the site:

  Specific leaf area: SLA= 100 ($cm^2$) / $G_1$ (g) = 0.01 /$G_1$ ($m^2$/ g)

  Weight per 4 circles in a site = $G_0$ (g)

  Leaf area per site = $G_{0*}$ SLA = 0.01$G_0$/ $G_1$ ($m^2$)

  LAI per site= [0.01$G_0$/ $G_1$ ($m^2$)]/0.4($m^2$)=0.025 $G_0$/ $G_1$
- ✧ Download 20 Accupar readings and 40 LAI-2000 readings and transfer
- ✧ Dry subsample and total sample biomass

**4. Reference:**

Wilhelm, W. W., Ruwe, K. and Schlemmer, M. R. 2000. Comparison of three leaf area index meters in a corn canopy. Crop Sci. 40: 1179-1183.

APPENDIX E –SPOT IMAGE ORTHORECTIFICATION PROCEDURES

Orthorectification is the process of using a rigorous math model and a digital elevation model (DEM) to correct distortions in raw images. SPOT scene products derived from SPOT 1, 2, 3, and 4 satellites are provided in the CAP format. Alternatively, SPOT 5 images are provided using the newly developed DIMAP format. The DIMAP format was introduced in mid-2002 with the launch of the SPOT 5 satellite and since its release the new data format has also been available with SPOT 4 images. The orthroctification method for CAP and DIMAP is different. Following we introduced the methods about how to orthorectify two formats of SPOT image individually.

## 1. Orthorectification SPOT (CAP format)

### (1) Pre_Orthorectification: Add orbit information to raw image

- Go to the **EASI** command prompt and run "s **CDSPOT**" from there
- To read in the RAW data using CDSPOT, place RAW files in a directory called SCENE01 and use this directory as the CDDIR directory. Be sure all RAW files reside within this directory and CDSPOT will automatically read the files it needs to create the output FILE. The output file cannot be written to the same path as your SCENE01 directory.
- In CDSPOT command prompt typing:

**CDDIR = "D:\SCENE01**
**FILE = "D:\Spot_Out.pix"**
**CDIC = 1,2,3,4**
**TEX1 =**
**SPFILE =**
**REPORT =**

*Typing ' **s CDSPOT** ' to view the parameters. I have included my EASI parameters that I was able to the data in with here:*
*CDSPOT CD SPOTIMAGE SPOT Format*
*CDDIR - CD Directory :D:\SCENE01*
*FILE - Database File Name : D:\Spot_Out.pix*
*CDIC - CD Input Channel List } 1 2 3 4*
*TEX1 - Database Descriptive Text 1 :*
*SPFILE - Scene Parameter File :*
*REPORT - Report Mode: TERM/OFF/filename :TERM*

*Notice: Some things to check when assigning your parameters:*
*1.) That your 'FILE' parameter is a different directory than your 'CDDIR' directory*
*2.) There should be no spaces in any of the directory paths*
*3.) CDDIR must end in with the '\' character. So c\SCENE01 will not work but c:\SCENE01\ will*
*4.) All RAW files you sent me must reside in the SCENE01 folder*
*5.) The directory that your output file must already exist.*

*6.) Prior to running CDSPOT the output file cannot already exist, CDSPOT will create the output file*

- Run CDSPOT to add orbit information:

  EASI>**r cdspot**
  Type <CR> for Scene information > **CR**
  Type <CR> for Imagery File Descriptor > **CR**

**(2) Orthorectification**

- Project Setup
- Data input -----"read PCIDSK file" : the image has been added the orbit information
- Generate DEM map

  OrthoEngine panel----Import&Built DEM (Under Processing Step) ----DEM from TIN
- Collect GCPs for Orthorectification based on Geometric corrected image
- Orthorectified correction

  OrthoEngine panel----Ortho Generation (Under Processing Step) ----Schedule ortho generation (Note: Browse DEM image)

## 2. Orthorectification SPOT (DIMAP format)

**(1) Start a project:**

- Start OrthoEngine, and start a new project. Give your project a file name.
- Select Satellite Orbital Modeling as the math modeling method. Under Options, choose Toutin's Model, and click Accept..
- Enter the appropriate projection information for your project.

**(2) Data Input**

For rigorous modeling with Geomatica OrthoEngine, you will need to order **Spot 5 Level 1A data**. Products higher then level 1A already have some level of correction applied, and therefore are not suitable for orthorectification. **DIMAP** (tiff) format is supported for Spot 5 orthorectification. DIMAP is a metadata format developed by SPOT Image, which uses GeoTIFF as the primary interchange layer. The data will come in a directory with an .XSL file, a metadata file (METADATA.DIM), a tiff imagery file IMAGERY.TIF), and some preview JPEG files. **Note:** OrthoEngine requires the imagery file and the metadata file to be located in the same directory.

- To import Spot 5 data for orthorectification, select Data Input under Processing Steps, and select Read Data From CD-ROM.
- Set CD Format: to SPOT 1-5(DIMAP)
- Set Requested channels 1 for panchromatic data, and Requested channels 1-4 for multispectral data. Supply an output file, a scene description, and a report file name.

**(3) Collect GCPs and Tie Points**

- Select the GCP/TP Collection processing step.
- GCPs can be collected using many methods. Select Geocoded Image if a previously corrected image is available.
- Select DEM. Identify the location of the related DEM
- Once you have collected your GCPs, run the model calculation and proceed to the residual report panel (under the Reports processing step) to review the initial results.

**(4)Generating Ortho Images**

- The final step is to set up your Ortho Image Production. Proceed to the Ortho Generation processing step.
- Select the files to be processed, select the DEM file to be used, and set your processing options. Click Generate Orthos.

# APPENDIX F–SPOT AND LANDSAT IMAGERY ATMOSPHERIC CORRECTION PROCEDURES

ATCOR2 is atmospheric correction and haze removal software used to correct changes in the spectral reflectance of materials on the earth's surface. ATCOR2, is used for atmospheric correction in images of relatively flat terrain, and can be applied to data from a number of sensors. The input for ATCOR2 is a geometrically corrected image contained in a single PCIDSK (.pix) file. ATCOR2 output is a scaled reflectance image.

SPOT and Landsat are generally the same with a few exceptions: Tilt, Calibration file (ie gain and bias)

## IMAGE PROCESSING STEPS

The first step in performing the atmospheric correction is to create a single file of the Landsat or SPOT bands for input to ATCOR2. Sensor input information required by ATCOR2 are image acquisition date, layer band assignment, scale factors, sensor type, pixel size, and calibration file. Atmospheric input includes solar zenith angle, model for solar and thermal region, visibility, and ground elevation. The majority of the parameters are straightforward and require basic information about the image origin, acquisition details and sensor information. Other parameters require a more detailed discussion.

### Calibration Files

The unit of electromagnetic radiation is [mW cm-2 sr-1 μm-1]. That is, the rate of transfer of energy (MicroWatt, mW) recorded at a sensor, per square centimeter on the ground, for one steradian (sr) (three dimensional angle from a point on Earth's surface to the sensor), per unit wavelength being measured. This measure is referred to as the **spectral radiance**. Prior to the launch of a sensor, the relationship between measured spectral radiance and DN is determined. This is known as the sensor calibration. Satellite data usually do not come in this (comparable and defined) unit. The reason is that the measured signal depends on the sensitivity and storage capacity of the detector (i.e. 8-bit, 16-bit etc.). Therefore the data is re-scaled so that the signal received by the sensor fits into a defined range using a function which is described by an **Offset** (also called Bias) and a **Gain**. In most remotely sensed images a linear model relates the digital value (DN) of an image pixel to the intensity of reflected radiant energy (Wm-2 sr-1mm-1). These scaled values are then stored as integers (for example 8-bit or 0 to 255 for Landsat ETM+).

ATCOR re-scales the DNs of the image into the true "radiance at sensor" employing a reverse operation. In order to calculate the radiance for a given pixel in a spectral band the calibration gain and offset must be known. The scaling and therefore the offset and gain are different for each sensor and are often adjusted over time as the sensor begins to deteriorate. The gain and

offset used in each image is recorded in the image metadata and is used by ATCOR in the form of a calibration file. Calibration files differ between sensors and images.

The standard calibration files are in the cal folder under the ATCOR folder where Geomatica is installed (for example, C:\Program Files\Geomatica_V100\atcor\cal).

**Gain and Bias (Landsat)**
The calibration file contains a table of the bands, the gain value for each band, and the bias for each band. ATCOR uses mW/cm-2 sr-1 micron-1 as the radiance unit for each band, except the thermal band which uses mW m-2 sr-1 micron-1. Since the sensors may use a different radiance unit, you may need to convert the values.

To create your own file, enter the values found in the metadata into a new file: The Bias or Offset as c0 and the Gain as c1. Make sure to use the correct units [mW cm-2 sr-1
µm-1] or [W m-2 sr-1 µm-1].

**Example of an ATCOR *.cal file (etm_new.cal), values are from the example above:**

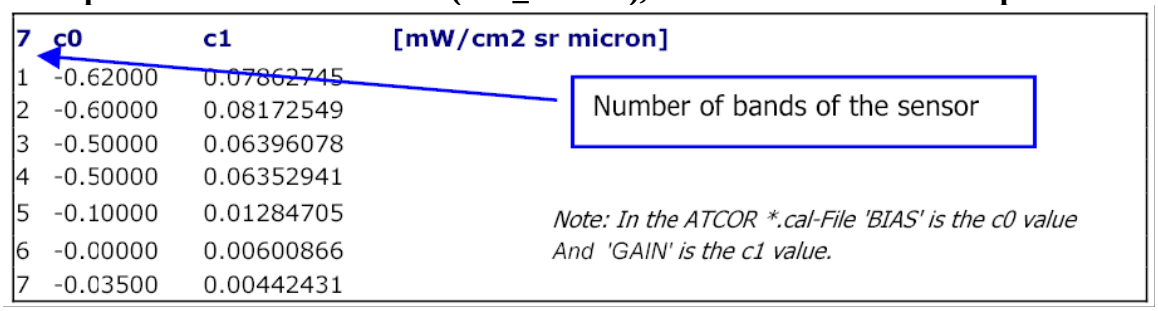


ATCOR employs the unit [mW cm-2 sr-1 micron-1]. For each channel the at-sensor radiance L(i) and digital number DN(i) are related by
L(i) = c0(i) + c1(i)*DN(i)
where c0(i) and c1(i) are the offset (bias) and slope (gain) of the linear calibration equation. The metadata files of different sensors use different units, so care has to be taken to convert these numbers into the ATCOR radiance unit. The c0, c1 coefficients (with unit mW cm-2 sr-1 micron-1) are specified in a "sensor.cal" file.

**Gain and Bias (SPOT)**
The **SPOT** calibration coefficient (Absolute Calibration Gain) A(i) is specified in the metadata file as: DN(i) = A(i) * L(i)
The conversion of the Spot count values to irradiances is performed as follows:

L(i) = DN(i) / A(i)

The A(i) coefficients (with unit [m2 sr micron W-1]) enter the ATCOR calibration file and c0(i)=0. ATCOR **converts** the A(i) **internally** as c1(i) = 0.1 / A(i) to obtain the required unit [mW cm-2 sr-1 micron-1].

**Band Setup**
If you did not use a CD read algorithm to import your images, you may need to match the sensor band numbers to the correct image channel numbers. To set up the channels, click Band Setup.

When you prepared the PCIDSK (.pix) file for atmospheric correction, the band numbers may not match the channel numbers. For example, band 1 from the sensor may not necessarily be in channel 1 in your file. You need to match the sensor band numbers to the correct image channel numbers.

**Tilt**
The calculations for atmospheric correction will depend on the sensor view angle. For sensors without tilt capability this parameter will not appear. There are two categories for sensors that do have tilt capability: 1) sensors with East/West tilt capability and 2) sensors with East/West and North/South tilt capabilities (also known as omni tilt sensors). The satellite elevation, or the elevation above the horizon, is used to determine the magnitude of the tilt. The tilt magnitude will either be Nadir (no tilt), 10, 20 or 30 degrees. The sun azimuth and satellite azimuth are used to determine the tilt direction. The tilt direction is defined by ATCOR's discrete azimuth grid. Tilt angles are specified in the metadata and may be prefixed with (L)eft or (R)ight. Left indicates an East angle while Right represents West angle.

**East/West Tilting Sensors:** Cartosat PAN, IRS-1C/D PAN, MSU-E, SPOT
**Omni Tilt Sensors:** Ikonos, OrbView, QuickBird

**Running Atmospheric Correction**
When you perform the atmospheric correction, Focus adds a thematic raster metalayer to the Maps tree. The metalayer contains the image being corrected, the Haze bitmap mask layer, the Cloud bitmap mask layer, the visibility layer, and a layer with the Value-Added Data. **To execute** the Atmospheric Correction the metalayer must be accessed and **Run Atmospheric Correction** must be selected.

**Scaled Surface Reflectance**
The result of the atmospheric correction is a scaled surface reflectance image with a range of 0 to 255 for 8-bit data and 0 to 65535 for 16-bit data. If you want unscaled values or percent reflectance values, divide the scaled values by 4 for 8-bit data and by 10 for 16-bit data. For example, 150 divided by 10 equals 15% reflectance for a 16-bit image.

The **accuracy** of the method depends on several factors:

- radiometric calibration accuracy of the sensor (typically 3-10%)
- radiative transfer code : accuracy of MODTRAN 4 better than 5 % in the atmospheric window regions
- correct choice of atmospheric input parameters : up to user
- For near nadir view angles (off-nadir angle < 10 degree), a flat terrain, and avoiding the specular and backscattering regions, an accuracy of the retrieval of surface reflectance of +/-0.02 (reflectance < 0.10) and +/-0.04 (reflectance > 0.40) is possible. For larger off-nadir view angles bidirectional effects can play a strong role.